NOVEL β' and α'/β' SIALON CERAMICS

A thesis submitted for the degree of

DOCTOR OF PHILOSOPHY

of the University of Warwick

by

CARL ADRIAN JASPER

Senior Materials Scientist
British Gas PLC
Solihull

May 1990

For my parents

PREFACE

This thesis describes original work which has not been submitted for a degree at any other University.

The investigations were carried out in the Centre for Advanced Materials at the University of Warwick under the supervision of Professor M.H. Lewis and in the Technical Department at Lucas Cookson Syalon Limited, Solihull, under the supervision of Dr A. Szweda and Dr W.I. Wilson, during the period October 1985 to September 1989.

This thesis describes the production of β'-sialon ceramics pressureless-sintered with a neodymium oxide additive, and the production of new α'+β' sialon materials, the mechanisms of formation and transformation, with the aim of developing improved engineering materials.

ACKNOWLEDGEMENTS

I would like to thank Professor M.H. Lewis, Dr. A. Szweda and Dr. W.I. Wilson for their advice and guidance during the supervision of this project.

I would also like to thank:

Dr. D.P. Thompson and Dr. K. Liddell in the Crystallography Laboratory, University of Newcastle upon Tyne, for the use of, and help with, the Hägg-Guiner X-ray diffraction camera;

Mr. G. Smith and Mr. S. York, University of Warwick, for help with the electron microscopy;

Many colleagues, past and present, especially Dr. R.J. Lumby, for their invaluable help, stimulating discussion and encouragement;

Delta Rods Ltd., West Bromwich, for their cooperation in evaluating components;

Lucas Cookson Syalon Ltd., and British Gas PLC for the financial assistance;

and finally Sandra Beaufoy and Hayley Gilder for typing this script.

ABSTRACT

β'+glass sialon materials are prepared with an Nd_2O_3 sintering additive. These materials exhibit similar property characteristics to equivalent Y_2O_3-based compositions. With the absence of an Nd phase equivalent to YAG, phase relationships in the Nd-Si-Al-O-N system are examined to identify alternative grain boundary devitrification products. Materials in which the residual glass after sintering is recrystallised to give a mixture of Nd-N-α wollastonite and $NdAlO_3$ are shown to exhibit high temperature property characteristics comparable to the conventional β'+YAG sialon materials. The glass forming region in the Nd-sialon system is more extensive than for yttrium and new phases have been identified within the expanded volume. These also offer potential as fully crystalline matrix devitrification products. The most significant of these has the composition $Nd_3Si_3Al_3O_{12}N_2$. β'+$Nd_3Si_3Al_3O_{12}N_2$ materials are prepared and found to exhibit excellent properties up to ~ 1300°C.

The preparation of pure α' and α'+β' sialon materials by transient liquid phase sintering is particularly sensitive to starting composition. The fabrication of α'+β'+glass materials allows greater flexibility but high temperature properties are still sensitive to the chemistry and concentration of the liquid sintering additives and to post sintering heat treatments. α'+β'+glass materials are developed with a very minor amount of residual glass of a composition which allows full devitrification to form mainly YAG. Upon annealing, the α' species is particularly receptive to the non-stoichiometric elements which results in removal of the intergranular residual glass and subsequently increased solid/solid contact. To alleviate the interfacial energy anisotropy the YAG crystals are diffusively rearranged to an isolated equiaxed morphology. The limitations on high temperature use are mitigated by the discontinuous nature of this YAG phase. Component field trials and the potential of this new range of generic sialon materials are discussed.

CONTENTS

GLOSSARY OF ABBREVIATIONS

YAG	Yttrium aluminium garnet	$Y_3Al_5O_{12}$
YAP	Yttrium mono-aluminate	$YAlO_3$
YAM	Yttrium aluminate	$Y_4Al_2O_9$
N-YAM	Yttrium silicon aluminum oxynitride Range of composition	$Y_4Al_2O_9 \rightarrow Y_4Si_2O_7N_2$

CHAPTER I. INTRODUCTION

1. Engineering Ceramics

Engineering Ceramics can be defined as inorganic materials consisting of metallic and non-metallic elements bonded together to give a product that exhibits excellent mechanical properties which are often retained at elevated temperatures. Most of these materials have a high degree of covalent bonding and it is the very nature of these strong directional bonds which gives them their great strength and durability. They include the carbides, nitrides and oxides of the metals silicon, aluminium, boron and beryllium, and certain transition metals such as titanium and zirconium. Table I.1 shows typical properties of this range of materials with values for mild steel included for comparison.

Fabrication of ceramic components from these compounds involves forming the powdered starting materials into the required shape followed by some sort of high temperature firing cycle to get the particles to coalesce, either by solid state diffusion or by liquid formation at the particle interfaces, which then allows liquid phase sintering to occur. In practice, the mechanical behaviour of the product depends as much on the final microstructure of the material as on the intrinsic properties of its constituents.

The ideal engineering ceramic, for applications such as in gas turbine engines, must be able to perform in regimes well beyond those accessible by the conventional nickel-based super-alloys (>1100°C).

The requirements for such a material therefore, are that it must have a high melting or decomposition temperature, excellent oxidation and creep resistance combined with good thermal shock properties, and a high elastic modulus to specific gravity ratio.

Table I.1 Typical properties of the potential high temperature engineering materials

Material	Melting or decomposition temperature (°C)	Specific modulus MPa	Thermal expansion coefficient x 10^{-6} $°C^{-1}$ (20 - 1000°C)	Thermal conductivity Wm^{-1} K^{-1} (at specified temp, °C)
Al_2O_3	2050	90	8.5	6.3 (1000)
AlN	2450	103	4.9	20 (800)
BeO	2530	124	9.0	20.3 (1000)
BN	2700	48	0.8[a], 7.5[b]	12.1[a], 26.8[b] (1000)
C (Graphite)	3500	39	2.2	600 (1000)
SiC	2600	172	4.3	70 (400)
Si_3N_4	1830	117	3.0	36 (1000)
TiN	2930	43	9.3	29.3 (20)
ZrO_2	2700	212	10.0	2 (700)
Mild Steel	1500	38	11.0	40 (20)

[a] Normal to c-axis
[b] Parallel to c-axis

Source: ASM Engineered Materials Reference Book

Also desirable is high chemical stability, low electrical conductivity, and a low coefficient of friction.

Selection of the most suitable material must take into account all of these factors. There is no benefit having a material which will withstand extreme temperatures if its thermal conductivity is so low that slight changes in temperature result in thermal gradients which in turn produce strains greater than the critical strain necessary for failure. Of the materials outlined above many are fallible in a number of areas: - Al_2O_3 has poor thermal shock properties, graphite and TiN have very poor oxidation resistance, AlN is prone to hydrolysis, BeO is highly toxic, and BN is difficult to fabricate. This leaves the silicon-based ceramics as the most likely candidates.

2. Silicon Nitride Ceramics

Silicon nitride has been recognised as a potential high temperature material for over twenty-five years, but unlike the traditional silicate and alumino-silicate ceramics (porcelain, pottery, china, etc.) the activation energy for self-diffusion is very high (because of the strong covalent Si-N bonds) and fully dense, pure Si_3N_4 ceramics cannot be formed by a simple firing method. Instead some oxide agent has to be added to catalyse the sintering reaction and much of the development work has been in refining the starting compositions and optimising the sintering techniques. Today, these ceramics are commercially available, fabricated by a pressureless-sintering route with 5-10 wt.% sintering additive.

Unfortunately, these additives have to be chemically very pure to retain the desired properties, hence they require careful processing and are expensive. The most commonly used additive, Y_2O_3

now costs 5-6 times as much as the raw silicon nitride powder itself and strategic location factors are becoming increasingly important as demand rises.

3. Broad Objectives

The broad objectives of the present research were to develop a range of silicon nitride based ceramics, comparable with the existing Y_2O_3-fluxed materials, pressureless-sintered with Nd_2O_3 as the additive. Nd_2O_3 currently costs around £15 per kg compared with £90 per kg for Y_2O_3 and is more widely available. The initial compositions were to be centred upon the Y_2O_3 based ceramics, sintered using the same temperature cycles, with the aim of generating a family of equivalent materials which could be fabricated without incurring any additional cost. The final materials were to be achieved by optimising the heat treatments as necessary, after assessment of the preliminary results. Little work has been carried out on Nd_2O_3 as a sintering additive for silicon nitride ceramics, but the market constantly demands cheaper raw materials which now makes this exploration worthwhile.

There is also a great demand for improved high temperature materials, hence the existing Y_2O_3 based variants were examined with a view to incorporating the initial additive into the silicon nitride structure itself so that the final material exhibits more of the properties associated with the Si-N bonds rather than the constraints imposed by the microstructure. It was hoped that this would eventually lead to a material with better high temperature capabilities again prepared using standard processes i.e. without increasing the overall cost.

CHAPTER II. SILICON NITRIDE CERAMICS - STRUCTURE AND PROPERTIES

1. Silicon Nitride

Silicon nitride exists in two crystallographic forms, α and β. Hardie and Jack (1957) showed that both polymorphs are hexagonal of similar a unit cell dimension, but with the c parameter for α almost twice that of β (a_α = 7.748Å, c_α = 5.617Å; a_β = 7.603Å, c_β = 2.907Å). The crystal structures determined by Wild et al. (1972a) are presented schematically in Figures II.1 and II.2. β-Si_3N_4 is built up of a 3-D array of planes of SiN_4 tetrahedra joined at the corners in such a way that each nitrogen atom is common to 3 tetrahedral units. The α form has similar structural units but the layers are stacked ABCD... as opposed to the AB... stacking sequence found in the β. The β form contains long vacant channels parallel to the c-axis and the different stacking arrangement of the α form causes these to break up into large holes repeated at regular intervals throughout the lattice. The unit cell contents were found to be Si_6N_8 for the β form and $Si_{12}N_{16}$ for the α, with 2 of these holes per unit cell in the latter.

Hardy and Jack (1957) also found that the α structure was slightly distorted from the idealised form and suggested that it was in fact an oxynitride with a range of composition:

$$Si_{11.4}O_{0.3}N_{15} - Si_{11.5}O_{0.5}N_{15}$$

electrical neutrality being maintained by some of the Si sites becoming vacant; in effect generating a defect structure. Kohatsu et al. (1974) and Kato et al. (1975) disputed these findings and showed that although α-silicon nitride could accommodate oxygen atoms this was not essential for stabilization. Instead they formulated that α

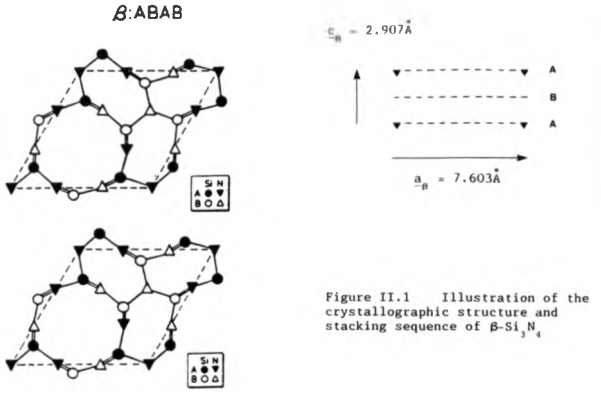

Figure II.1 Illustration of the crystallographic structure and stacking sequence of β-Si_3N_4

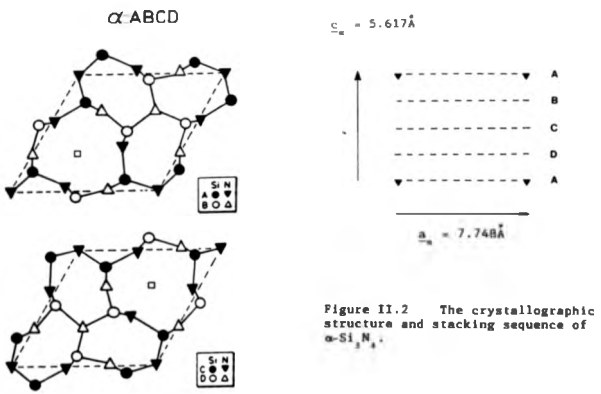

Figure II.2 The crystallographic structure and stacking sequence of α-Si_3N_4.

□ denotes possible sites for modifier cations for example as in Y α'-sialons.

was a pure nitride and that the oxygen was present as a thin surface film of silica on the Si_3N_4 particles. Jack (1983) further proposed the possibility of having lower valency silicon ions, Si^{2+} or Si^{3+}, in the interstices to reduce the overall positive charge and allow partial replacement of the nitrogen atoms with oxygen. Hampshire et al. (1978) support this hypothesis and conclude that α-silicon nitride has a range of composition:

$$Si^{2+}_{0.2}\ Si^{4+}_{11.9}\ N^{3-}_{16} \quad - \quad Si^{2+}_{0.2}\ Si^{4+}_{11.8}\ O^{2-}_{0.5}\ N^{3-}_{15.5}$$

The presence of a surface oxide layer is now generally accepted and the ability to accommodate a small amount of oxygen into the structure recognised, although the actual method by which it is incorporated still remains conjecture.

2. Sialons

The discovery that α-silicon nitride could accommodate oxygen atoms concurrently led Oyama and Kamigaito (1971) and Jack and Wilson (1972) to discover that the crystal chemistry could be modified further so that Al^{3+} ions could replace Si^{4+} if at the same time O^{2-} ions replaced N^{3-}. This was possible because of the similarity of the Si-N and Al-O bond lengths, 1.74Å and 1.75Å respectively. Jack (1973) gave this new type of materials the generic term 'sialon', an acronym derived from the chemical symbols of the constituent elements. The resultant materials, α'-sialon and β'-sialon are thus solid solutions of aluminium and oxygen in silicon nitride, iso-structural with their α-Si_3N_4 and β-Si_3N_4 counterparts, but with slighly expanded unit cell dimensions depending on the level of substitution. Lumby et al. (1975) showed that the β'-phase has a range of homogeneity extending

between Si_3N_4 and Al_2O_3N maintaining a constant metal:non-metal atom ratio of 3:4, according to the formula:

$$Si_{6-z}\,Al_z\,O_z\,N_{8-z} \qquad \text{(II.i)}$$

where z is the compositional factor with a maximum value of approximately 4.2 at 1750°C. The variation in unit cell dimensions with increasing substitution levels has been widely studied since the original Jack and Wilson (1972) version; e.g. Hohnke and Tien (1983) and Slasor (1985). Figure II.3 shows the most recent determination by Liddell (1986).

Jack and Wilson (1972) also discussed the feasibility of having metal cations in the interstices of the α' structure with an appropriate partial replacement of Si-N bonds with Al-N to compensate for the imbalance in valency. This was verified by Jama et al. (1975) who revealed the existence of an expanded α' when $LiSi_2N_2$ was reacted with Al_2O_3. In general α' sialons are represented by the formula

$$M_x(Si,Al)_{12}(O,N)_{16} \qquad \text{(II.ii)}$$

where M is the modifier cation and x is the number incorporated into the unit cell. Theoretically, x has a range of value from 0 to 2; 0 representing the unimplanted α'-sialon structure with 2 being the maximum number of vacancies available per unit cell. In practice M can be any positively charged ion provided its ionic radius is small enough to be accommodated within the interstitial hole and it forms a complex oxide.

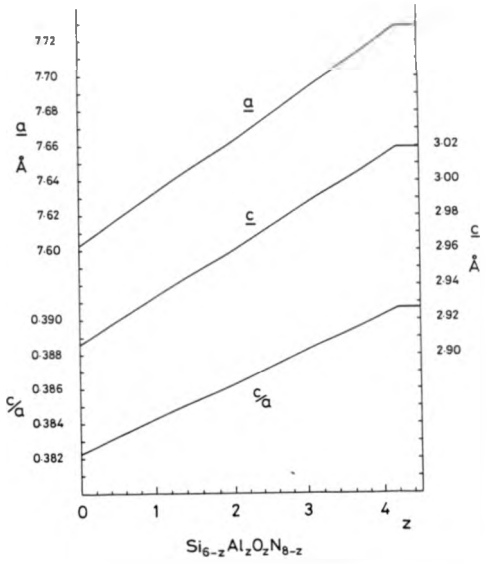

Figure II.3 Variation in unit cell dimensions of β' - sialon with Al and O substitution (after Liddell, 1986)

Note that the curves reach a plateau at z ~ 4. The lattice has become fully expanded. Additional Al and O atoms are accommodated in the few remaining interstitial holes.

3. The Sintering of Silicon Nitride-based Ceramics

Funke and Samsonov (1958) found that pure silicon nitride could not be sintered by a simple heat treatment. For thermally activated diffusion processes to take place the material had to be heated to well above 1600°C and appreciable decomposition occurred. The first silicon nitride articles of near theoretical density were prepared by Deeley et al. (1961) by hot-pressing with 5 wt.% MgO as an additive, and Lumby and Coe (1970) showed that significant improvements in strength could be obtained with 1 wt.% MgO and a high proportion of the α-Si_3N_4 phase. Wild et al. (1972b) and Colquhoun et al. (1973) established that the MgO reacted with the surface silica on the silicon nitride to form a liquid, and suggested that this promoted densification by allowing liquid phase sintering to occur. Upon cooling, all of the initial α-Si_3N_4 had been transformed to the β form and the liquid phase remained in the final product as an intergranular glass.

Liquid phase sintering was first described by Price et al. (1938), who investigated the densification processes in W-Ni-Cu alloys and concluded that the densification mechanism involved a solution-reprecipitation process. Kingery (1959) suggested that in the presence of a liquid phase the driving force for densification was connected to the capillary forces acting between the particles and proposed that three distinct stages were involved in the overall densification cycle (Figure II.4). These consist of an initial rearrangement stage which occurs when the liquid is first formed and is drawn to the contact points between individual particles by capillary action. This viscous flow process draws the particles closer together to form a more tightly packed structure. The second stage is a solution-reprecipitation process and involves atomic

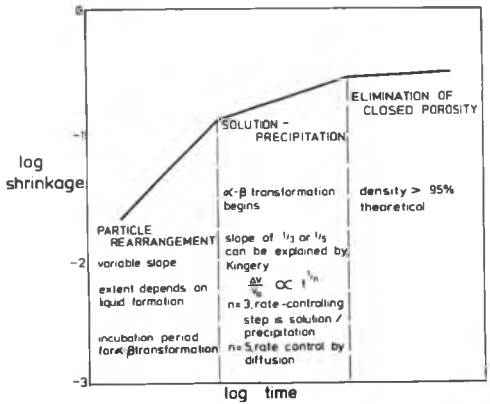

Figure II.4 Model plot of the 3 successive stages involved in liquid phase sintering of nitrogen ceramics

transport or diffusion through the liquid medium followed by reprecipitation at various sites. Here, the driving force is related to the increase in solubility brought about by the compressive stresses which result from the inter-particle capillary attraction. The third and final stage of densification is identified as the elimination of closed porosity. This involves the growth of grains within the structure to an extent which prevents further material transport via the liquid phase from taking place and is normally associated with a reduction in the densification rate (Lenel, 1948).

The conditions for liquid phase sintering are that the solid phase must be soluble within the liquid and that the liquid must wet the matrix. Wild et al. (1972b) found that the glass in their hot-pressed materials could be devitrified to enstatite ($MgSiO_3$) and silicon oxynitride (Si_2N_2O) and so confirmed some partial solubility of nitrogen within the liquid, and Terwinger and Lange (1974) showed that $MgSiO_3$ (m.p. 1545°C) wets a silicon nitride substrate very effectively. They concluded that the liquid would allow transport of silicon and nitrogen but did not consider that the $\alpha \rightarrow \beta$ transformation was necessary for densification to occur. The simple 3-stage Kingery view of sintering was thus substantiated, but the chemical intricacy of the Si-Al-O-N system required additional factors to be considered to take into account complex grain morphologies and phase transformations. Hampshire (1980) has shown that the Kingery model can be successfully applied to the densification of sialon compositions but it can not give an accurate value of the rate controlling coefficient. Brook et al. (1977) have now described the densification processes using a Coble model and have shown that both the densification and the $\alpha \rightarrow \beta$ transformation are controlled by grain

boundary diffusion processes, although full densification can occur without the transformation becoming complete.

4. Methods of Producing Silicon Nitride-based Components

The earliest successful attempts at fabricating solid components followed from a natural extension of the nitriding process involved in synthesis of the Si_3N_4 powder itself. In reaction bonding, the raw silicon powder is first formed into the required shape using conventional forming techniques (e.g. isostatic pressing, slip casting, or injection moulding), then the compact is nitrided between 1150°C and 1400°C to give a bonded mixture of α and β-Si_3N_4 as the reaction product (i.e. Reaction bonded silicon nitride - RBSN). The main advantage of this method is that only slight shrinkage occurs which allows fairly complicated shapes to be fabricated, with reasonable tolerance, quite cheaply. Unfortunately, it is difficult to nitride thick sections and the product always contains 15-30% porosity which reduces its mechanical strength, although much of this strength is retained to temperatures in excess of 1400°C and the absence of any amorphous intergranular phase affords it excellent oxidation resistance.

As outlined earlier, hot-pressing with an oxide additive provides a means of forming solid components with Si_3N_4 as the starting powder. Compacts consisting mainly of α-Si_3N_4 with 1-2 wt% metal oxide are heated typically for 3-5 hours at 1600-1800°C under pressures of 20-30 MPa to give a product which contains mostly β-Si_3N_4 with a very minor intergranular glass phase. This material has excellent room temperature properties, but at about 1000°C the glass starts to soften which drastically reduces its performance. Much development work has concentrated on modifying the composition of the

final glass and minimising its volume, but without impeding densification. Gazza (1975) found that with Y_2O_3 additives the materials produced had improved high temperature strength and creep resistance, and ascribed these improvements to the formation of more refractory grain boundary phases. Huseby and Petzow (1974) and Buang (1979) have since showed that CeO_2, BeO_2, La_2O_3 and ZrO_2 can be useful in hot-pressing Si_3N_4 and Dodsworth (1980) obtained good results with Sc_2O_3, but neither offered any particular advantage over yttria. The melting point or liquidus eutectic of the secondary phase still remains the limiting factor. In addition the process is restricted to simple shapes and requires expensive diamond machining. Today hot-pressed silicon nitride (HPSN) is only reserved for a few minor applications.

It was soon realised that by increasing the volume and fluidity of the liquid phase, silicon nitride ceramics could be sintered without the application of pressure, the reduction in surface area providing the driving-force for densification (sintered silicon nitride - SSN). This process allows much more intricate shapes to be fabricated, but the greater volume of liquid generated subsequently results in more residual glass, which is undesirable. Tsuge et al. (1975) showed that further improvements could be achieved by recrystallising the glass to form yttrium silicon oxynitride phases, but the starting composition had to be controlled very precisely to ensure sufficient devitrification to be effective.

The evolution of sialon ceramic alloys opened up the possibility of reducing or eliminating the grain boundary phase by incorporating its elements within the Si_3N_4 framework. This alloying process also demands less stringent control of the starting composition because of the large range of solid solubility of the products. The use of Al_2O_3

and AlN as additives, in addition to a metal oxide, allows fully dense materials to be pressureless-sintered with a minimal amount of liquid phase. The liquid itself, and subsequently the derived residual glass, contains dissolved nitrogen which can be varied to achieve more desirable properties. (In general, the higher the N/O ratio the more stable the glass due to the higher degree of covalent bonding associated with the nitrogen). Alternatively, the starting composition may be tailored to generate a residual glass which may be completely devitrified to give an essentially two phase material with high temperature properties comparable to HPSN.

5. The Si-Al-O-N System

Phase diagrams are of particular importance in understanding the behaviour of nitrogen ceramics since they are an interpretation of the reactions which may occur within a particular system and it is the reactions between the constituent phases which determine the equilibrium composition and ultimately the final material properties. The use of a reciprocal salt diagram to represent compositions within the 4-component Si-Al-O-N system has been comprehensively explained by Jack (1978). In short any sialon composition may be plotted as a point within a square whose corners correspond to the components Si_3N_4, SiO_2, AlN, and Al_2O_3 expressed in molecular equivalents i.e. Si_3N_4, Si_3O_6, Al_4N_4, and Al_4O_6. (The assumption that one mole of silicon nitride has the formula Si_3N_4 rather than say Si_6N_8 is arbitrary but once chosen automatically fixes the formula for one mole of the other components). Any point on the plane represents 12 positive and 12 negative valencies although the actual number of atoms in each composition changes with position across the diagram. (It is convenient to consider the compounds in ionic terms even though the interatomic bonding is predominantly covalent).

Hot-pressing appropriate mixtures of Si_3N, AlN, Al_2O_3, SiO_2 and Si_2N_2O allowed Gaukler et al. (1975) and Jack (1976) to establish the main phase assemblages which occur in the Si-Al-O-N system and formulate an initial Si-Al-O-N behaviour diagram (Fig. II.5). Further work by Layden (1976) and Roebuck (1978) and more recently by Wells and Slasor (1984), to accurately determine the phase solubility limits has characterized a number of necessary refinements to generate the present behaviour diagrams at 1700°C and 1800°C shown in Figure II.6.

As well as β'-sialon a number of other phases have been reported. O'-sialon (Jack 1976) is a solid solution of silicon oxynitride with a limited range of composition extending from Si_2N_2O towards Al_2O_3 along the 2M:3X line. Its structure is isomorphous with that of silicon oxynitride, based on an orthorhombic unit cell with dimensions a = 5.498Å, b = 8.877Å and c = 4.853Å and consisting of layers of Si-N atoms joined by Si-O-Si bonds to form a network of SiN_3O tetrahedra.

X-phase was first reported by Oyama and Kamigaito (1971) and Jack and Wilson (1972) as a minor phase formed when reacting α-Si_3N_4 and Al_2O_3 at 1700°C. Drew and Lewis (1974) showed that two modifications, "high" and "low" X-phase, could be formed depending on whether cooling from a melt at 1800°C or by heating to a lower temperature - 1600°C. Korgul et al. (1983) found that "low" X-phase is in fact a more ordered form of "high" X-phase and that both have a triclinic structure with the composition being close to $Si_3Al_6O_{12}N_2$. Towards the aluminium nitride corner of the behaviour diagram six phases were observed by Jack (1973) and Gauckler et al. (1975) each with a range of homogeneity along lines of constant metal: non-metal atomic ratios, $M_m:X_{m+1}$ where $4 \leq m \leq 10$. These have since been characterized by Thompson (1977) and Roebuck and Thompson (1977) as

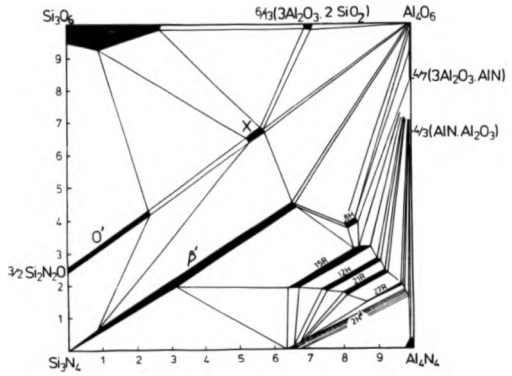

Figure II.5 Early representation of the Si-Al-O-N behaviour diagram (after Jack, 1976)

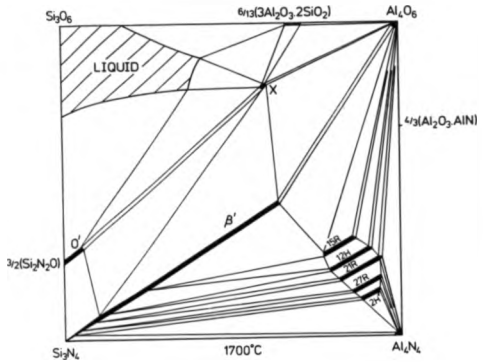

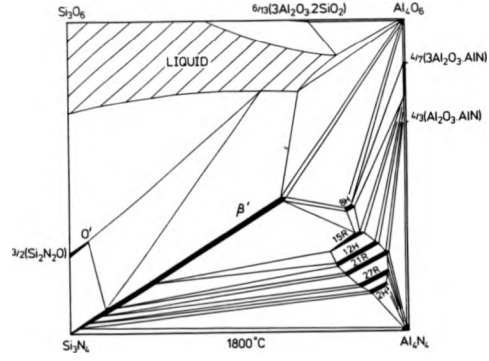

Figure II.6 The Si-Al-O-N behaviour diagrams at 1700°C and 1800°C (after Walls and Slasor, 1984)

"polytypoids" based on the Wurzite-like aluminium nitride structure but with stacking sequences related to their composition. They have either hexagonal (H) or rhombohedral (R) unit cells and are described by the Ramsdell (1947) notation as 8H, 15R, 12H, 21R, 27R, and $2H^{\delta}$ with compositions 4M:5X, 5M:6X, 6M:7X, 7M:8X, 9M:10X and > 9M:10X respectively.

Despite having 4 binary compounds the Si-Al-O-N system itself is ternary and no more than 3 phases may exist together at equilibrium. This is especially important when considering the phases present in a material after reaction.

6. M-Si-Al-O-N Systems

The addition of another metal in the form of an oxide to facilitate densification has necessitated the study of phase relationships in the five component M-Si-Al-O-N systems. Representation of compositions in a 5-component system consisting of 3 metal and 2 non-metal atoms (i.e. a "quaternary system of the third kind"; Zernicke (1955)) is best performed by use of the Janecke triangular prism representation, after Janecke (1907), where all the sides are of equal length and the vertices represent the metal oxide and nitride equivalents. Any composition may then be expressed in terms of valency equivalents and represented as a point within the prism; Jack (1978). Figure II.7 shows the representation of the general M-Si-Al-O-N system based on the standard Si_3N_4-Al_4N_4-Si_3O_6-Al_4O_6 plane. The front and rear triangular faces represent the nitrides and oxides respectively and the three square faces are all reciprocal salt diagrams. Being quaternary up to 5 phases may exist in a material at the same time at equilibrium.

ax = by = cz = 12

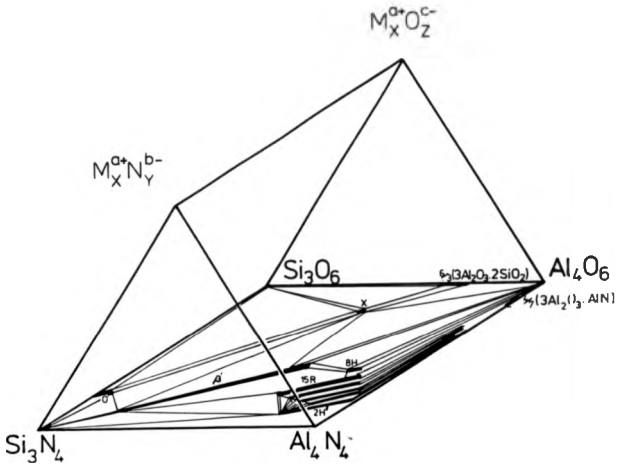

Figure II.7 Jänecke prism representation of the general M-Si-Al-O-N systems (after Jänecke, 1907)

6.1. The Y-Si-Al-O-N System

Yttria has been the most widely used, and studied, densification additive in the preparation of sialon ceramics. Consequently, phase relationships in the Y-Si-Al-O-N system are the best understood. In describing the overall behaviour diagram however, it is pertinent to first consider the Si_3N_4-Si_3O_6-Y_4O_6-Y_4N_4 plane then extend from this into the 3-D Janecke prism. The phase relationships in the Y-Si-O-N system determined by Rae (1976) are shown in Figure II.8. Ito and Johnson (1976) noted a number of yttrium silicates along the Y_2O_3-SiO_2 join and these have recently been characterised by Liddell and Thompson (1986) as a whole series of temperature dependent polymorphs of yttrium disilicate ($Y_2Si_2O_7$). There are 4 yttrium silicon oxynitride phases:

(i) N-melilite $Y_2O_3.Si_3N_4 \rightarrow Y_2Si_3O_3N_4$

Tetragonal with unit cell dimensions a = 7.597 Å, c = 4.908 Å, (Rae et al., 1975).

(ii) N-α-wollastonite $Y_2O_3.Si_2N_2O \rightarrow YSiO_2N$

Monoclinic with unit cell dimensions a = 7.012 Å, b = 12.186 Å, c = 18.202 Å, β = 90.76°, (Lange et al., 1977).

(iii) N-apatite $Y_{10}(SiO_4)_6N_2$

Hexagonal with unit cell dimensions a = 9.360 Å, c = 6.770 Å (Gaukler et al., 1980).

(iv) N-YAM $2Y_2O_3.Si_2N_2O \rightarrow Y_4Si_2O_7N_2$

Monoclinic with unit cell dimensions a = 7.558 Å, b = 10.446 Å, c = 10.818 Å, β = 111.0° (Morgan, 1977).

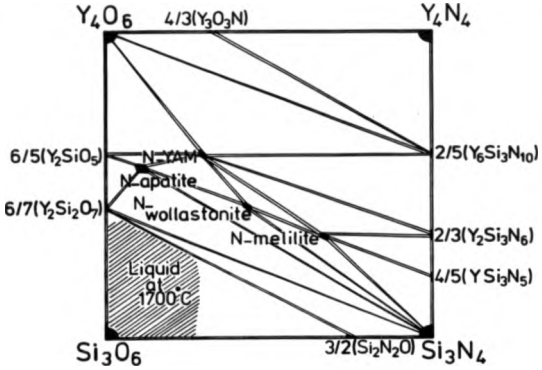

Figure II.8 Phase relationships in the Y-Si-O-N system (after Rae, 1976)

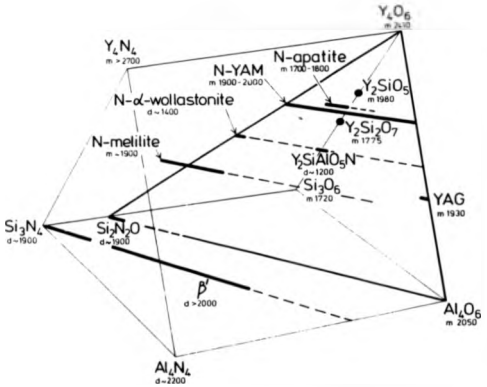

Figure II.9 The limits of solid solubility of the Y-Si-O-N phases in the Y-Si-Al-O-N system (after Jack, 1981)

and Jameel (1984) has characterised 3 yttrium silicon nitrides along the Si_3N_4-YN join: $Y_6Si_3N_{10}$, $Y_2Si_3N_6$ and YSi_3N_5.

All of the yttrium silicon oxynitride phases in the Y-Si-Al-O-N system have some range of solubility extending along the appropriate line of constant M:X ratio towards the aluminium corner of the diagram. Figure II.9 shows the limits of penetration into the Janecke prism, after Jack (1981). It can be seen that N-α-wollastonite has only a very small range of homogeneity with YAP ($YAlO_3$) occurring at the Al-rich end of its tie line. N-apatite allows slightly more aluminium substitution and N-melilite has an extensive solubility range, but only the N-YAM phase extends right across the diagram to its yttrium aluminate, YAM ($Y_4Al_2O_9$), analogue. Rae (1976) also outlined a yttrium silicon aluminium oxynitride, termed B-phase, Y_2SiAlO_5N, on the $YAlO_3$-wollastonite tie line. Subsequent work by Tanaka et al. (1979) and Spacie (1984) has shown that this too has a small range of homogeneity but it is only stable from approximately 1050°C to 1200°C. Also along the Y_2O_3-Al_2O_3 join is the 3:5 Y:Al yttrium aluminium garnet phase, YAG. Lewis and Barnard (1980) suggested that this too had some range of partial solubility of Si and N, and this is now generally taken to be correct but the actual compositional limit is believed to be very restricted (see also Spacie (1984) and Sun et al. (1988)).

When considering the yttrium phases for a refractory grain boundary matrix YAG appears the most suitable. N-α-wollastonite becomes unstable above 1400°C and the other oxynitride phases, especially N-melilite, readily oxidise. The yttrium disilicates offer good oxidation resistance but their inability to accommodate the aluminium and nitrogen species gives little freedom with regard to compositional control.

Lewis et al. (1980) first reported YAG in connection with β'-sialon ceramics as a devitrification product obtained upon heat treating appropriate β'+glass materials. The devitrification process was explained with reference to the behaviour diagram by Lewis & Lumby (1983). To achieve a perfect two-phase β'+YAG ceramic it is necessary that the bonding phase composition moves out of the glass forming region to YAG and as it does so the excess components diffuse into the β' or precipitate as more β' of modified composition. This is indicated in Figure II.10 by the arrows at the end of the tie lines passing through the average composition C. The flexibility in phase composition to achieve this equilibrium state is of particular importance.

With the exception of the above, the only other phase in the Y-Si-Al-O-N system is Y-α', a structural modification of α-Si_3N_4 (section II.2) described by the formula $Y_x(Si,Al)_{12}(O,N)_{16}$ that lies on the Si_3N_4-4/3(Al_2O_3N)-YAl_4N_4 plane (Figure II.11). Jameel (1984) observed its range of homogeneity and showed that the minimum and maximum solubility limits for α' along the Si_3N_4-YAl_3N join are 0.3 and 1.1 atoms per unit formula respectively, and that the upper limit of Al solubility extends along a line of constant Si:Al ratio of 2.53:1, giving the α' region a small roughly triangular appearance. Slasor (1988) has recently determined the phase relationships for the whole plane and concludes that it is extremely difficult to form dense pure single phase α' without some melilite or glass or both present due to excess oxygen, or residual polytypoid due to too little. The α' region is limited to the width of the Si_3N_4-4/3(Al_2O_3N)-YAl_4N_4 plane and any small deviations in the starting mix result in a composition either above or below it. Wells (1986) has shown that this also applies to α'+β' materials. A composition which lies in the α'+β' region is highly sensitive to the estimation of surface oxides on the

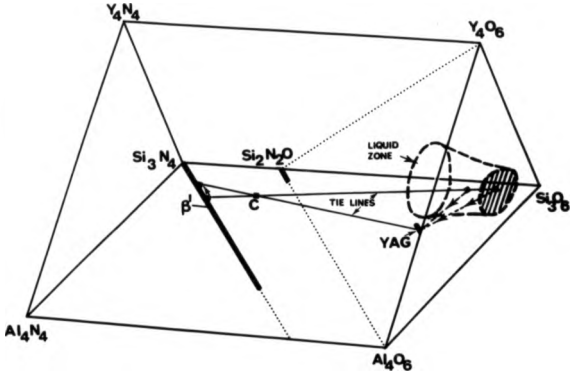

Figure II.10 Janecke prism representation of the Y-Si-Al-O-N system indicating possible changes in the β' and matrix composition during recrystallisation (after Lewis and Lumby, 1983)

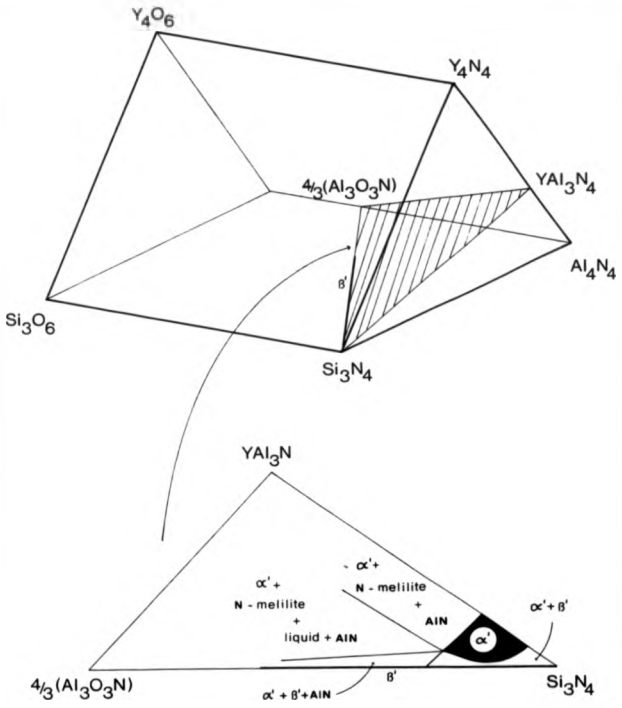

Figure II.11 Phase relationships in the Si_3N_4 - YAl_3N - $4/3(Al_3O_3N)$ plane showing the extent of the α' region and position of the plane within the Jänecke prism

nitride powders, material pick-up during milling, and weight loss on firing.

In order to form dense products an excess of liquid is required and this can be used to generate either α'+glass or α'+β'+glass materials. Unfortunately, restrictions on the position of the α'-YAG plane with respect to the glass composition and the phase fields through which it passes make it difficult to form pure two phase α'+YAG materials but the preparation of fairly good α'+β'+YAG materials has been carried out; Walls (1986).

6.2 The Nd-Si-Al-O-N System

The phase relationships in the Nd-Si-Al-O-N system have been reported by Spacie et al. (1985). Synonymous with the yttrium system, neodymium forms a corresponding series of silicate and oxynitride phases but there are a few major differences. Firstly, there is no neodymium variant of the yttrium aluminium garnet phase, although $NdAlO_3$ forms much more readily and is stable over a wide range of temperatures. Neither is there a low temperature phase equivalent to the B-phase (Y_2SiAlO_5N) identified by Rae (1976). There is however an additional phase Nd_2O_3:AlN, reported by Marchand (1976), (tetragonal with lattice parameters a = 3.702Å, c = 12.536Å: melting point 1620°C), with no analogue in the Y-Al-O-N system, and whilst a complete range of solubility exists from N-YAM ($Y_4Si_2O_7N_2$) to YAM ($Y_4Al_2O_9$) in the Y-Si-Al-O-N system, only the end points have been established for neodymium. All of the neodymium phases have expanded unit cell dimensions compared to their yttrium counterparts, undoubtedly due to accommodation of the increase in ionic radii: 0.89Å for Y^{3+}; 0.98Å for Nd^{3+}. The lowest eutectic temperatures in the Nd_2O_3-SiO_2 and Nd_2O_3-Al_2O_3 binary systems are lower than in the

equivalent Y_2O_3-SiO_2 and Y_2O_3-Al_2O_3 ones: 1600°C (Figure II.12, Toropov, 1960a) and 1750°C (Figure II.14, Toropov and Kiseleva, 1961) respectively as opposed to 1660°C (Figure II.13) Toropov, 1960b) and 1760°C (Figure II.15, Toropov et al. 1964). In the ternary Y_2O_3-SiO_2-Al_2O_3 system (Figure II.16, Bondar and Galakhov, 1963) the lowest eutectic occurs at ~1360°C and for the corresponding Nd_2O_3-SiO_2-Al_2O_3 case this minimum is expected to be even lower. How this affects the Nd-phases and sintering characteristics of Nd-sialons is not as simple as might be expected. For example the Nd-N-α wollastonite phase is stable to 1700°C compared with only 1400°C for the yttrium variant. The extent of the neodymium glass forming region is known to be larger than for the yttrium case. Indeed, neodymium glasses with up to 30 equivalent % of nitrogen have been claimed by Fernie et al. (1990). Liddell (1987) also points out that instead of a β'-sialon and liquid phase field, as with yttrium, there is an extensive β'+melilite+liquid region so large that it intersects the β'-$NdAlO_3$ plane thus making it impossible to obtain a 2-phase β'+neodymium aluminate material free from melilite, by recrystallising. (cf. β'+YAG in the yttrium system, see section IV.2).

7. Mechanical Properties and Thermal Behaviour

Whilst an understanding of the phase relationships is essential in forming 'ceramic alloys', the final material properties depend as much on the generated microstructure as on the intrinsic properties of its constituents. There is now a good understanding of the deformation and fracture mechanisms, and hence of the principles for the 'ideal' ceramic microstructure, but these are rarely achieved in practise. Microstructural morphology is constrained by the

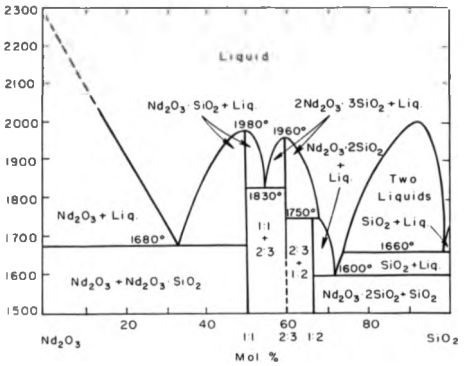

Figure II.12 Binary phase diagram of the Nd_2O_3 - SiO_2 system (after Toropov, 1960a)

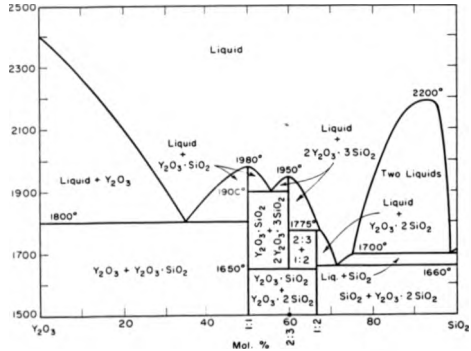

Oxide ratios of compounds are given as Y_2O_3: SiO_2

Figure II.13 Binary phase diagram of the Y_2O_3 - SiO_2 system (after Toropov, 1960b)

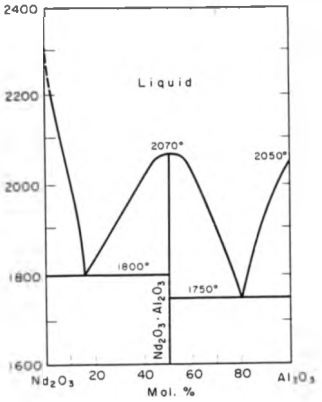

Figure II.14 Binary phase diagram of the Nd_2O_3 - Al_2O_3 system (after Toropov and Kiseleva, 1961)

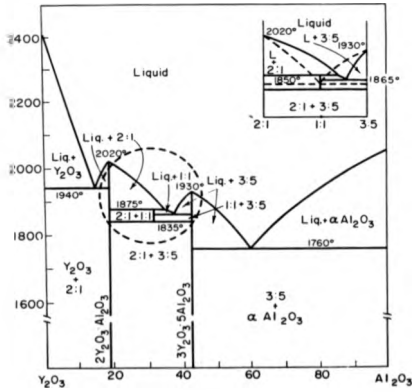

Figure II.15 Binary phase diagram of the Y_2O_3 - Al_2O_3 system (after Toropov et al., 1964)

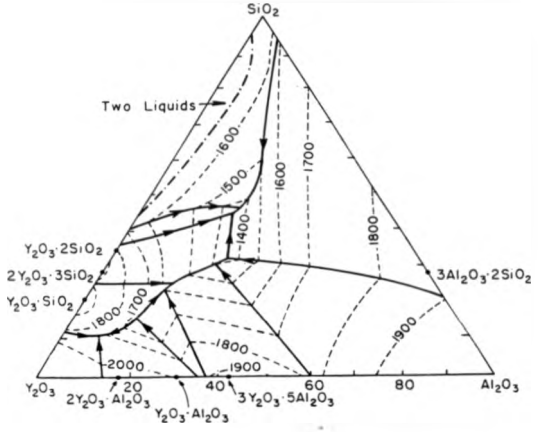

Figure II.16 Ternary phase diagram of the Y_2O_3 - SiO_2 - Al_2O_3 system (after Bondar and Galakhov, 1963)

conflicting requirement for ease of fabrication and the restrictions imposed by the reactions and transformations which can occur during simple processing procedures.

At low temperatures Si_3N_4-based ceramics are inherently brittle and undergo sub-critical crack growth to failure. Their resistance to crack propagation is termed the fracture toughness (K_{Ic}) of the material, which also forms the basis for its mechanical strength. Figure II.17 (after Lewis et al., 1988) illustrates the established toughening mechanisms which can offer resistance to this sub-critical crack growth behaviour within a stressed ceramic element.

'Micro-cracking' at grain or particle interfaces can shield the main crack from the influence of the applied stress (Faber and Evans, 1983). The origin of this effect is believed to result from anisotropy in the thermal expansion of the grains in a monophase ceramic or differential expansion between the grains and surrounding matrix in a multiphase version. For this to occur there is necessarily a critical range of particle size, above which general cracking occurs and below which micro-cracking may not be initiated. Unfortunately, to produce such a structure demands careful control of the process heat treatments and the effect is most likely to be lost due to relaxation of the microscopic stresses at elevated temperatures.

'Crack-deflection' toughening is applicable over a wide range of temperature and stems from the reduced stress intensity at the crack-tip when the crack deviates from the plane normal to the axis of the applied stress, and from repeated bifurcation of the main crack fronts. Faber and Evans (1984) showed that a twist deflection is the most effective, and most prolific with more than 10 vol.% acicular grains, saturating at an aspect ratio (l/w) of ~ 10.

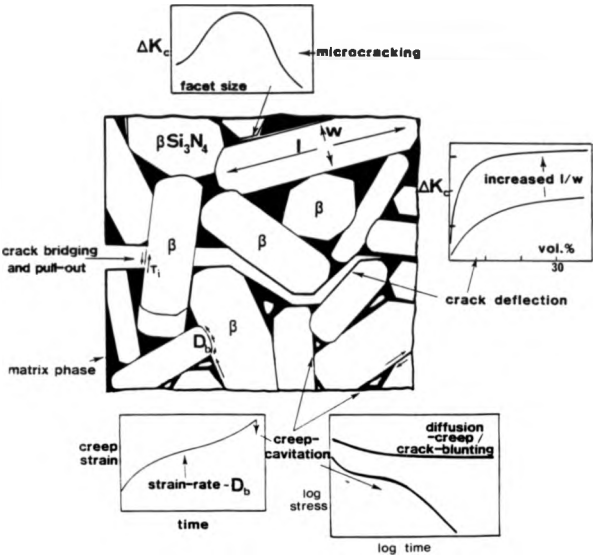

Figure II.17 Illustration of the relationship between microstructural parameters and the mechanisms for increasing fracture toughness, creep and creep-rupture resistance (after Lewis et al., 1988)

'Crack-bridging' by elongated grains in the wake of a sub-critical crack also offers improvements in fracture resistance over a wide range of temperatures. Here the mechanism relies on the formation of crack-resistant grains which have relatively weak interfacial cohesion. The energy for 'pull-out' is associated with the interfacial shear stress (τ_i) and sliding friction, and hence the interface area and volume fraction are important parameters.

At elevated temperatures time-dependent (creep) deformation, creep rupture and oxidation are the most important factors. It is now recognised that in the high temperature regime the performance of Si_3N_4-based ceramics is governed by the inertness of their secondary intergranular phases. The onset of oxidation and creep degradation coincides with 'glass softening' and even though this may offer an increase in K_{Ic} via 'crack-blunting' by viscous deformation, any benefit is far outweighed by these considerations.

Kingery et al. (1960) have identified 3 distinct creep mechanisms:

(i) Primary or transient creep which stems from the viscoelastic response of the vitreous intergranular phase when the stress is applied.

(ii) Grain boundary diffusional or Coble creep (Coble, 1963; 1970) which is normally dominant over long periods of time, with the applied stress well below that necessary for brittle failure, and

(iii) Tertiary creep which is normally associated with very high stresses and/or temperatures resulting in cavitation in the glassy intergranular channels during grain boundary shear.

In reality the creep process is the superposition of all 3 components and may be described by the general creep equation

$$\dot{\varepsilon} = A\sigma^{n} \exp(-Q/RT) \qquad \text{(II.iii)}$$

where $\dot{\varepsilon}$ = strain rate

σ = stress

Q = the activation energy

A is a constant related to the boundary diffusion coefficient and the average grain size, and n is the rate controlling stress exponent which is determined by the underlying creep mechanisms taking place (n=1 for pure steady state diffusional creep).

Oxidation begins with the formation of a superficial silicate film formed by oxygen reacting with the Si_3N_4 species, which leads to the release of nitrogen, and proceeds with preferential attack of the intergranular vitreous phase which is more reactive. Oxygen permeates inwards towards the bulk and the nitrogen migrates towards the outer surface. A chemical potential gradient is created which induces outward diffusion of the metal cations, some of which then react with the oxide layer to form more complex oxides (Babini et al., 1984) (See Figure II.18). Generally below 1300°C the initial layer is protective and impedes further rapid oxidation, limiting it mainly to diffusion and ion transport processes. At higher temperatures the evolution of large nitrogen bubbles at the oxidation front causes parts of the protective skin to flake or spall off when they burst and the oxidation mechanism proceeds as before albeit more rapidly due to the lower viscosity associated with the higher temperature and consequent increase in cationic mobility. Obviously, any other factors which reduce the viscosity of the glass at elevated temperatures, for

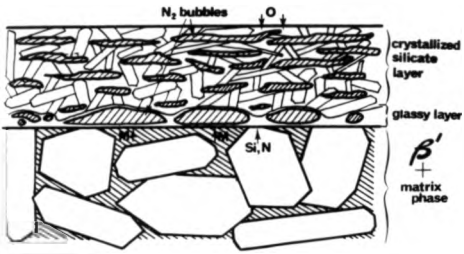

Figure II.18 Schematic of atmospheric oxygen and matrix metallic ion diffusion processes in the oxidation of bi-phase β'-sialon materials
(after Lewis and Barnard, 1980)

example impurity elements lowering the liquidus eutectics, will have a dire effect upon the oxidation rate. In porous materials, like reaction-bonded silicon nitride, gaseous infusion of oxygen into the bulk through interconnecting channels is another important parameter.

Porosity also affects the mechanical strength of the material. Modulus of rupture (MOR) values are dictated by K_{1c} via the relationship

$$MOR = \frac{1}{Y} K_{1c}\, c^{-1/2} \qquad \text{(II.iv)}$$

where Y is a geometrical constant and c the critical flaw size. As porosity increases generally so does the effective flaw size.

The hardness of dense silicon nitride based ceramics is dependant upon the Burgers vectors associated with dislocation motion in the direction parallel to the applied stress. Again porosity destroys the properties, this time by affording less bulk resistance to plastic deformation.

B. Overview

Identification of the mechanisms for toughening and for high temperature creep and creep-rupture resistance has led to the formulation of model ceramic microstructures. The ideal monolithic ceramic should be fully dense, entirely crystalline, with all phases stable to elevated temperatures, and nominally consist of small acicular grains randomly interspersed in a bulk of smaller more uniform grains, all of which are well bonded together. A good knowledge of the phase relationships in a particular system allows an understanding of the reactions and transformations which may occur in

order to approach this idealised state, but in practise this is rarely achieved. Instead, the materials developed have to be a compromise of the best properties obtainable with fairly simple process routes. For Si_3N_4-based materials in particular this includes promoting the formation of a liquid so that liquid phase sintering may occur and adapting the final microstructure to accommodate or modify the liquid residues as best as possible. Fortunately, with silicon nitride, inter-solution of some of the added oxide species to form sialon permits a greater degree of flexibility to enable retention of more of the pure nitride properties and such materials have now reached a stage of commercial availability within their development.

The Lucas Syalon* ceramics exemplify the current range of sialon materials. Pressureless-sintered with a yttria additive, 3 versions are available:

Syalon 101 - a β'+glass material with excellent properties up to about 1000°C

Syalon 201 - a β'+YAG material formed by a heat treatment re-crystallisation process, and

Syalon 501 - a spark machinable version of 101 with 50 wt.% TiN added.

The level of performance that the monolithic materials have now reached in relation to the structural ceramic development objectives, to fulfill applications such as in gas turbines, outlined in the 1970's is illustrated in Figure II.19. It is evident that in the high

---

* Syalon is a registered trade-mark of Vesuvius Zyalons Midlands Ltd (formerly Lucas Cookson Syalon Ltd.).

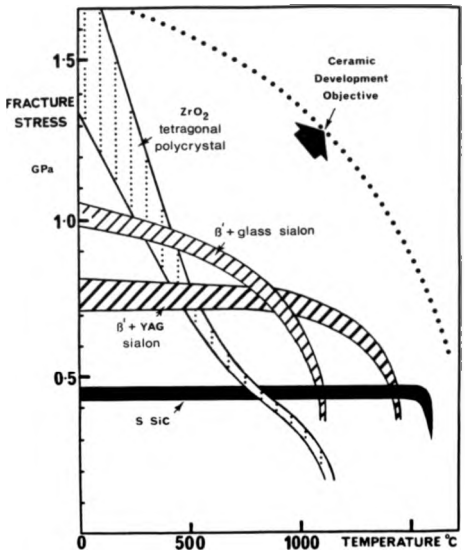

Figure II.19 Comparison of the strength-temperature relationships for various monlithic ceramics and the development objectives outlined in the 1970's
(after Lewis, 1987)

stress/high temperature regime sialon materials are still incapable of performing satisfactorily. The residual intergranular phases still remain the inhibiting factor. Even for Syalon 201, at 1300°C in an oxidizing environment the silica layer formed at the surface reacts with the YAG causing it to revert back to a liquid and then the normal catastrophic processes ensue. Any developments which can further reduce the liquid volume fraction and/or incorporate it into the Si_3N_4 structure itself must be seen as productive in trying to improve the usefulness of these materials in this upper operating region.

9. Specific Objectives

The specific objectives of the present research were:

1. To produce a β'+glass material with properties comparable to Syalon 101 prepared with Nd_2O_3 as the sintering additive
2. To develop an Nd_2O_3-based material for use at temperatures above 1000°C.
3. To improve the performance of the existing high temperature sialon materials by incorporating as much of the sintering liquid as possible into the silicon nitride structure to form α'+β' materials.
4. To examine the feasibility of producing such materials on a commercial basis.
5. To evaluate these materials in industrial applications alongside those currently used.

CHAPTER III. MATERIALS, PREPARATION AND EXPERIMENTAL PROCEDURES

1. Powder Specifications

The compositions investigated contained mixtures of Si_3N_4, 21R polytypoid and Al_2O_3 powders with either Y_2O_3 or Nd_2O_3 as the densification additive. The powder suppliers, particle sizes, and impurity contents are listed in Table III.1. Where the particle sizes needed to be measured this was performed using a Microtrac Laser Particle Size Analyser.

The Nd_2O_3 powder was calcined at 1000°C for 3 hours before use and stored in a desiccator containing silica gel. All of the other powders were kept in the plastic containers in which they arrived.

2. Preparation of Compositions

The starting compositions were calculated taking into account the amount of surface oxide on the silicon nitride and polytypoid powders claimed by the manufacturers. For the Nd_2O_3 substituted Syalon-equivalent materials the increase in molecular weight was also taken into consideration. The powders were weighed to an accuracy of ±0.01g. Small batches of 100g were ball-milled for 72 hours in 0.5 litre capacity rubber pots using 1.08kg of 5mm diameter Syalon 101 grinding media with 310 ml of isopropanol as the mixing medium. For the trial components larger batches of 1.4kg were prepared in 5 litre polyethylene tubs with 6kg of media and 2.5 litres of isopropanol, again milling for 72 hours. In both cases the tubs were rotated at 60 rpm. Measurements before and after tumbling showed that media 'pick-up' was typically around 0.5% of the powder charge weight and that contamination from the vessels was negligible (<0.1%). After

Table III.1 Raw Powder Specifications

Powder	Supplier	Av Particle size (μm)	Phases Present and Impurities
Si_3N_4 grade 1002	Cookson plc	0.6	α > 95% β < 5% O < 2.0% Fe < 0.01%
Si_3N_4	Kennametal Inc Pennsylvania	1-2	α > 95% α β < 5% O < 2.0% Fe < 1.0% Al < 0.53% C < 0.4% Ca < 0.07%
Si_3N_4 grade LC10	H.C Starck GMBH Berlin	<1.5	α > 95% β < 5% O < 2.1% Fe < 0.3% C < 0.2% Fl < 0.1% Unreacted Si < 0.5%
Si_3N_4 grade BS	Denka Japan	1.4	α < 10% β > 90% O < 1.0%
21R polytypoid (milled 72 hr)	Cookson plc	<1	O < 4.0% Unreacted Si < 1.0%
Y_2O_3 'ultrafine'	Rare Earth Products	0.6	Si < 10 ppm Al < 7ppm Ca < 5ppm Pb < 3ppm Mg < 1ppm
Nd_2O_3 99.9%	BDH	2-6	~ 50% $Nd(OH)_3$ La_2O_3 < 100 ppm Other rare earth oxides < 100 ppm
Al_2O_3 grade CT 3000	Alcoa	0.6	Na_2O < 0.09% SiO_2 < 0.02% Fe_2O_3 < 0.02%

mixing, the slurry was passed through a 45μm sieve and dried in a fan-assisted oven for 24 hours at 110°C. Finally, the powder, which had now become agglomerated, was forced through an 850 μm sieve before being isostatically pressed to 20,000 psi in sealed rubber bags.

3. Pressureless-sintering and Heat Treatments

The compacts were lightly sprayed with a 50/50 BN/SiO_2 mixture, to provide a protective coating and inhibit SiO_2 loss during firing, then placed in a Syalon-lined graphite pot and sintered in 1 atmosphere of pure nitrogen in a Wentgate VF0808 microprocessor controlled carbon resistance sintering furnace.

Post-sintering heat treatments were carried out following a similar routine except that the billets were not sprayed before being loaded into the furnace. Also the cooling rate was controlled where necessary. Typical sintering and annealing temperature cycles are shown in Figure III.1.

Preforms for the components were pressed in large rubber bags in the same way as before and partially fired to give more 'green state' strength. This allowed them to be machined nearer to the final shape, using conventional techniques, before sintering in the normal way. This process, known as 'bisque-firing', is common practise in the porcelain ceramics industry and its use has been adapted for Syalon ceramics to minimise the amount of final diamond machining required.

4. Density Measurements

Densities were determined using the bouyancy method outlined in British Standards BS 1902-308 (1989). The samples were weighed in air (W_A), and suspended in water (W_W), and the density (ρ) calculated

Fig. III.1 Schematic Representations of
Typical Sintering and Annealing Cycles

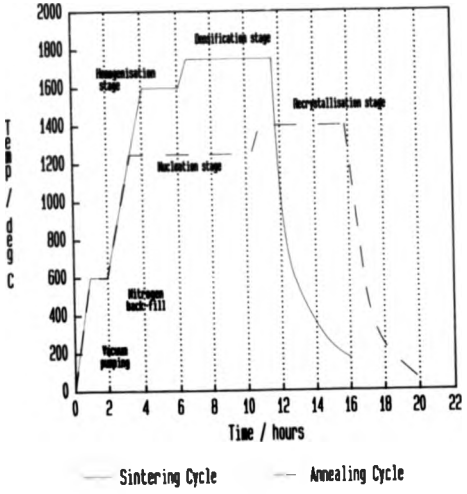

according to

$$\rho = \frac{W_A}{W_A - W_W} \rho_W \qquad \text{(III.i)}$$

where ρ_W is the specific density of the water at the ambient temperature.

For more porous specimens with a continuous network of porosity, for example as with the as-pressed or partially fired billets, the dry weight was first noted (W_A) then the specimens boiled for 1 hour in de-ionised water. After cooling, the suspended weight (W_W) was measured followed by the saturated or damp weight (W_D), with the excess water carefully wiped off the surface, and the bulk density (ρ_B) obtained from

$$\rho_B = \frac{W_A}{W_D - W_W} \rho_W \qquad \text{(III.ii)}$$

Finally, the results were compared with an estimate of the maximum theoretical densities calculated using the method of mixtures.

5. Microstructural Characterisation

5.1 X-Ray Techniques

The crystalline phases in the materials were identified using X-ray powder diffraction techniques. Diffraction spectra were obtained with a Phillips PW 1700 X-ray Diffractometer using copper Kα radiation of wavelength 1.54184Å over a 2θ range of 8° to 84° (Debye-Scherrer technique). The phases were identified by reference to the JCPDS (1975) powder diffraction index. For the Nd phases which were not listed the spectra were compared with those of the yttrium compounds. In general, the Nd phases have the same structure as the

corresponding yttrium ones: the peaks have similar intensities but the larger Nd atoms result in slightly expanded unit cells and the peaks are shifted to larger d-spacings, accordingly, and hence 2θ values.

The relative proportions of the α and β species were determined from the two most intense peaks using the relationship determined by Grand et al. (1979):

$$\frac{\beta}{\alpha} = \frac{I_{101}(\beta) \div I_{210}(\beta)}{I_{102}(\alpha) \div I_{210}(\alpha)} \qquad \text{(III.iii)}$$

The amount of Y_2O_3, Al_2O_3 and 21R polytypoid remaining in the samples was estimated by comparing the relevant peak heights with those of traces of the 'as-mixed' compositions. The amount of other phases present was estimated from their respective peak heights in conjunction with their apparent abundance when viewed under the microscope (estimated accuracy $\pm$ < 10%).

Accurate unit cell dimensions (±0.002Å) were obtained with a Hägg-Guinier focusing camera. Again monochromatic Cu Kα radiation was used to produce diffraction spectra from which the positions of the X-ray reflections were measured and the d-spacings determined.

In all cases the samples were crushed using a ballistic Tema Mill and the powders contained small traces of WC from the chamber lining.

5.2 Electron Microscopy, Diffraction and Microanalysis

Samples for SEM analysis were mounted in conducting bakelite resin and diamond polished to a 1μm surface finish. A thin coating of carbon was evaporated onto the surface, using an Edwards vacuum coating machine, to prevent 'charging'.

Microstructural analysis was carried out using a Cambridge Stereoscan 250 Scanning Electron Microscope, in both the secondary electron and back scattered imaging modes, in conjunction with a Link Systems 860 Energy Dispersive X-ray Analyser (EDAX).

Transmission specimens were prepared by cutting thin slices (0.2mm thick) from test bars (see section III.6) using a Capco annular diamond saw. These were then ground to ≈50μm thickness and finally diamond polished to a 1μm surface finish on both sides. After mounting on brass rings the sections were thinned in an argon-ion beam thinner, with the beam at an incident angle of 20°, to produce an electron transparent region. Again, a thin carbon coating was applied to prevent 'charging'.

Electron diffraction and microstructural analysis were conducted using a Jeol 2000 FX Transmission Electron Microscope, and a Jeol 100C instrument fitted with a scanning (STEM) attachment and an EDAX 9100 Energy Dispersive X-ray Analyser for semi-quantitive composition analysis. (Accuracy of results typically ± 2-3%.)

6. Mechanical Property Testing

All of the mechanical property measurements were carried out on test bars machined from the bulk of fully dense billets. 7mm x 4mm rectangular bars for the fracture toughness tests and 4mm x 4mm for modulus of rupture were cut from the length with a diamond saw, then a further 0.5mm was ground off each face to ensure squareness. Finally, the bars were polished to 10μm finish to remove any major surface flaws which the machining processes may have introduced.

6.1 Fracture Toughness

Fracture toughness measurements were carried out at room temperature using the single-edge notched beam (SENB) technique described by Srinivasan and Seshadri (1981). The specimens were 'notched' to a depth of 1.75mm (30% of the bar height) with the Capco saw (blade width 0.45mm) before being polished. The samples were fractured in a specially constructed 4-point jig (inner span 10mm, outer span 20mm) using an Instron 1122 unit with a crosshead speed of 0.5mm min^{-1}. The K_{Ic} values were determined from the load at failure using the equation

$$K_{Ic} = \frac{3P(L-l)}{2bd^2} a^{\frac{1}{2}} \left\{ 3.86 - 6.15 \frac{a}{d} + 21.7 \left(\frac{a}{d}\right)^2 \right\}^{\frac{1}{2}}$$

where

P = applied load L = outer span

b = specimen width l = inner span

d = specimen height a = notch depth

after Brown and Srawley (1966).

6.2 Modulus of Rupture

MOR tests were conducted using the 3-point bend technique (support span 20mm). Room temperature tests were carried out using the Instron 1122 unit (crosshead speed 0.5mm min^{-1}) interfaced to a Hewlett-Packard HP85 computer for automatic fracture stress data tabulation. 16 results were obtained for each sample type and the associated Weibull modulus determined.

High temperature MOR tests were performed on an Instron 4301 unit fitted with a SiC resistance furnace. The samples were allowed

to 'soak' at temperature for 15 minutes before being broken as before. The fracture stress (σ) was calculated from the load at failure (W) following the simple beam theory derivation.

$$\sigma = \frac{3}{2}\frac{Wa}{bd^2} \qquad \text{(III.v)}$$

where a is the support span, b is the specimen width and d the specimen height.

6.3 Hardness

Hardness tests were carried out on the broken pieces of room temperature MOR bars using a Rockwell Hardness Tester (A scale; 60kg load using a ball indenter). Whilst this method was quick and required no extra material or preparation, the hardness of sialons is right at the top of this scale and the technique really serves more to rank these materials rather than to provide quantitative values. For a more informative comparison the values were converted to equivalent Vickers micro-hardness (kg mm^{-2}).

Some of the indentations were examined to determine how the materials had deformed under the applied load. Unfortunately this was not as successful as hoped. The indent produced with a 60kg load was generally in the form of a crater, 300-400 μm across (cf 2.1 μm average grain size), with a surrounding disrupted zone which showed little or no evidence of surface cracking.

6.4 Creep Testing

Tensile creep tests were performed at temperatures of up to 1327°C using the 4-point bending mode (inner span 25.4mm outer span 50.8mm) with a constant stress of 77 MPa. Loading was achieved by a lever system which amplified the load at the specimen by 5 times. The deflection between the inner support points was measured via an alumina rod connected to a transducer and used to calculate the % strain induced. The furnace was taken up to temperature and the bar allowed to 'seat-in' for 24 hours under a preload of 100g prior to testing.

6.5 Oxidation Resistance

Oxidation tests were carried out for a period of up to 1000 hours at 1300°C. Broken pieces from MOR bars were placed on an iridium sheet inside an air oven and removed at time intervals. The specimens were then sliced and examined in the SEM after preparing in the normal way. Sections from the creep bars were also examined for comparison.

CHAPTER IV. THE Nd-Si-Al-O-N MATERIALS

The Nd-sialon compositions investigated are listed in Table IV.1 together with sintering temperatures, firing times, and reaction products.

1. Material Processing

Initial attempts at fabricating sialons with H.C. Starck LC 10 grade silicon nitride powder resulted in materials of low density (< 3.10 g cm^{-3}). A 101-type sialon (composition 3 Table IV.1) was prepared with 7.7 equivalent wt.% Nd_2O_3 and sintered using the normal temperature cycle for yttrium-based Syalon 101. Weight loss on sintering was quite high at 2.3% and close examination of a fracture surface showed that the material contained areas of high porosity, consistent with some gas evolution during the warm-up process (Figure IV.1) XRD analysis showed that the raw Nd_2O_3 powder was approximately 50% neodymium hydroxide, $Nd(OH)_3$. Neodymia is hygroscopic and once open to the atmosphere hydrolyses completely over a period of about 1 month. Thermogravimetric analysis showed that the hydroxide was converted to the monohydrate (NdOOH) above 340°C and returned to its pure oxide form above 550°C (figure IV.2). The pale mauve 'as-received' powder turned bright turquoise-blue during this burn-out process. The weight losses measured in each step corresponded accurately with those calculated for the removal of water molecules according to the equations

$$2Nd(OH)_3 \rightarrow 2NdOOH + 2H_2O \uparrow \qquad \text{(IV.i)}$$

and

$$2NdOOH \rightarrow Nd_2O_3 + H_2O \uparrow \qquad \text{(IV.ii)}$$

Table IV.1 The Nd-sialon compositions investigated

Comp No.		Wt.% Constituents Si_3N_4	21R	Nd_2O_3	Al_2O_3	Sinter Cycle °C/hrs	Density g cm^{-3}	Crystalline Reaction Products after Sintering	z value β′
1	K	80	–	20[a]	–	1700/5	2.84	β′ + melilite + wollastonite	–
2	S	85	–	11	4	1600/2 1750/5	3.24	β′	–
*3	S	82	3	11[a]	4	1600/2 1750/5	3.08	β′	0.42
4	S	82	3	11	4	1600/2 1750/5	3.28	β′	–
5	S	82[b]	3	11	4	1600/2 1750/5	3.29	β′	–
6	C	82	3	11	4	1600/2 1750/5	3.31	β′	–
7	K	82	3	11	4	1600/2 1750/5	3.31	β′	0.43
8	K	79	6	11	4	1600/2 1750/5	3.33	β′	–
9	K	76	9	11	4	1600/2 1750/5	3.32	β′ + melilite (tr)	–
+10	K	79	8	9	4	1600/2 1750/5	3.28	β′	0.62
11	K	80	8	9	3	1600/2 1750/5	3.29	β′ + melilite (tr)	–
12	K	81	8	9	2	1600/2 1750/5	3.26	β′ + melilite (tr+) + α (tr –)	–
13	K	82	8	9	1	1600/2 1750/5	3.15	β′ + melilite (tr++) + α (tr)	–
14	K	83	8	9	0	1600/2 1750/5	3.14	β′ + melilite + α (tr+)	–
15	K	76	8	12	4	1600/2 1750/5	3.38	β′ + melilite (tr++) + wollastonite (tr)	–
16	K	78	8	12	2	1600/2 1750/5	3.37	β′ + melilite (tr+++)	0.61
17	K	79	8	12	1	1600/2 1750/5	3.27	β′ + melilite	–
18	K	80	8	12	0	1600/2 1750/5	3.14	β′ + melilite + $NdAlO_3$ (tr) + α (tr)	–
19	K	81	8	11	0	1800/5	3.35	β′ + melilite + $NdAlO_3$ + α (tr+)	–
20	K	82	8	10	0	1800/5	3.35	β′ + melilite + $NdAlO_3$ + α (tr)	–
21	K	83	8	9	0	1800/5	3.33	β′ + melilite + $NdAlO_3$ + α (tr)	–
22	K	84	8	8	0	1800/5	3.30	β′ + melilite + $NdAlO_3$ + α (tr)	–
23	K	78	10	12	0	1800/5	3.34	β′ + melilite + $NdAlO_3$ (tr++)	–

a Untreated powder
b Heat treated 1600°C/3hrs

K Kennametal Si_3N_4
C Cookson Si_3N_4
S H.C. Starck Si_3N_4

* Syalon 101 – type composition
\+ Syalon 201 – type composition

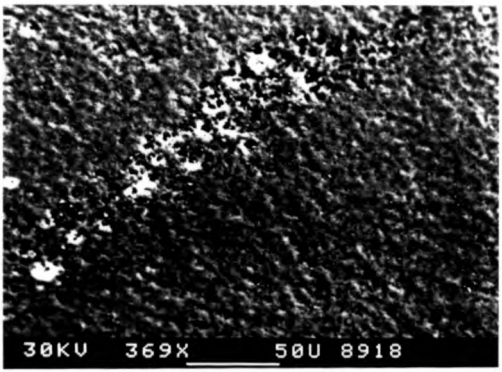

Figure IV.1 Areas of high porosity in the Nd Syalon 101-type material consistent with gas evolution during warm-up

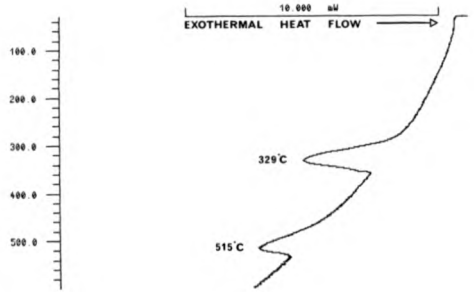

Figure IV.2 Thermal analysis trace of the as-received Nd_2O_3 powder illustrating the 2-stage decomposition of the hydrolysed species back to the pure oxide form

As a result all the Nd_2O_3 powder was calcined by heating at 1000°C for 3 hours before use. (It was found that powder treated in this way could be stored in a desiccator for several months with no deleterious effects). This greatly improved the density (3.28 g cm^{-3}) although some small areas of porosity still remained. Heat treating the Si_3N_4 powder for a few hours at 1600°C further improved matters but only changing to Cookson or Kennametal silicon nitride completely alleviated the problem.

Starck silicon nitride always contains some fluorine, believed to originate from a cleaning process in which the silicon powder is leached with HF to remove excess oxygen prior to nitriding. It appears that this reacts with the water or hydrogen given off by the hydroxide to form a weak acid which volatilizes as the billet is heated up and 'out-gasses' leaving the holes. All further compositions were made up using either Cookson or Kennametal silicon nitride powder.

Other problems were observed upon early microstructural examination of the materials. Large neodymium-rich areas along with substantial glass deficient regions were discovered indicating poor dispersion during mixing. This was attributed to the rather large grain size of the Nd_2O_3 powder. Microtrac tests showed the particles to be of the order of 2-6 μm which formed agglomerates 2-3 times this size during the burn-out treatment. By milling the as-received powder the average particle size could be reduced to approximately 1 μm which subsequently gave rise to a more homogeneous material reflected by an increase in mechanical properties (see later Section VI.2).

2. Microstructure of the As-sintered Materials

Upon microstructural examination, it was clear that the transmission specimens did not thin evenly during the preparation

stage resulting in 'hillocks' or regions of varied thickness in the images (Figure IV.3). This made the study of large areas difficult.

The general microstructural appearance of the as-sintered materials was very similar to that of equivalent yttrium based compositions except that neodymium atoms are more strongly electron absorbing and this gives rise to better contrast in the transmission electron microscope. The bulk microstructure consisted mainly of hexagonal β-sialon grains set in a neodymium glass matrix (Figure IV.4). As in their yttrium β'-glass counterparts the grains themselves have an essentially bi-modal size distribution. Large prismatic crystals, typically 1 μm across the basal plane and up to 10 μm in length, form a primary framework with smaller crystals, up to 2 μm in size, filling the bulk of the intersticies. The larger crystals nucleate early on in the reaction and grow rapidly when the liquid becomes available, often trapping the pore or particle upon which they initiated. Much evidence of these 'pre-cursors' appears as clusters of encapsulated Nd-rich globules or droplets indicating that the β'-grains had grown around small crystals of an intermediate phase which had precipitated from the liquid during warm-up and re-melted with some of the soluble constituents diffusing into the grain later on (Figure IV.5). This elongated grain growth behaviour stops once the grains impinge upon one another. All grains then continue to precipitate and grow fairly steadily until full density is achieved.

Some grains 80-100 μm in length were also visible, especially in the early materials. These are often seen in the yttrium sialons but were in much greater abundance here. They are believed to stem from large liquid-rich regions which develop either because of poor mixing, agglomeration of the Nd_2O_3 powder when the slurry was dried, or uneven heating.

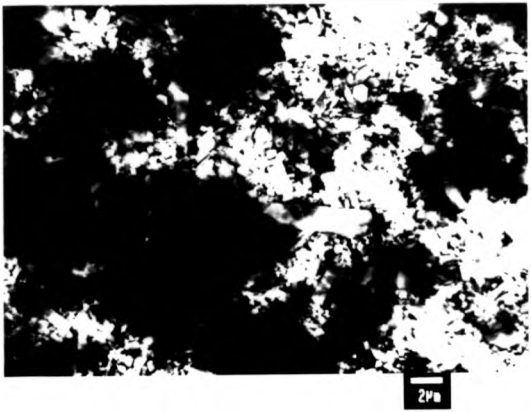

Figure IV.3 Example of uneven ion-beam thinning, characteristic of the Nd-based materials

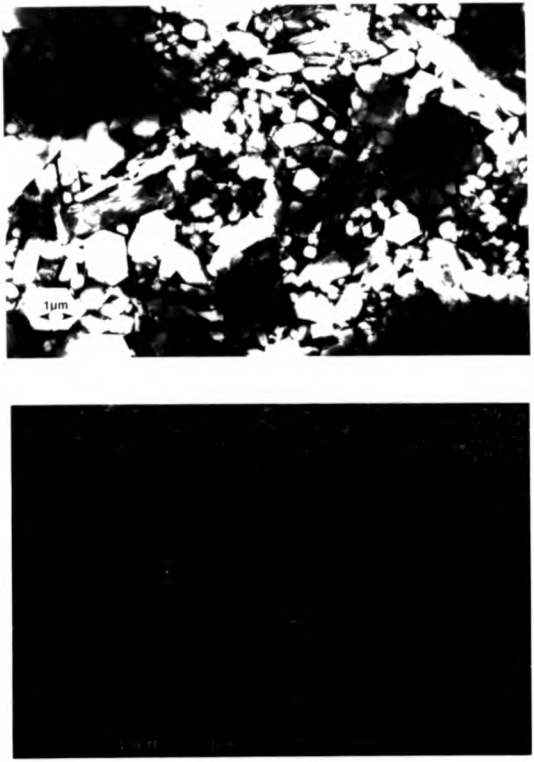

Figure IV.4 General microstructure of the Nd β′+glass materials:
a) TEM image b) SEM image

Figure IV.5 Example of β' nucleation on intermediate phases formed during the warm-up cycle and subsequent entrapment with rapid grain growth

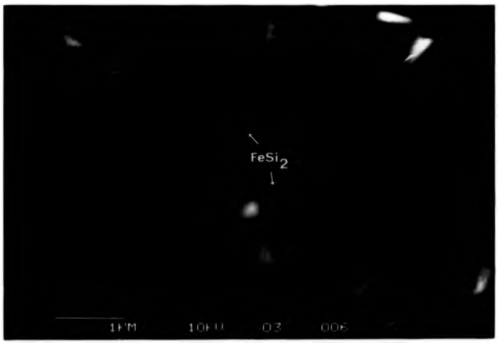

Figure IV.6 Small areas of crystalline Iron Silicide ($FeSi_2$) in the matrix glass resulting from iron impurities in the raw Kennametal silicon nitride powder

There were also numerous small areas (1-2 μm) of matrix phase in the Kennametal silicon nitride based materials, of lighter contrast than the glass, which were found to be Iron Silicide ($FeSi_2$) (Figure IV.6). These probably result from iron impurities introduced during the manufacturing process; - Kennametal are known to use steel balls to mill the raw silicon powder before nitriding.

EDAX analysis of the β'-crystals gave the aluminium substitution levels outlined in Table IV.1 (end column). The values obtained are in good agreement with those obtained for equivalent yttrium-based compositions. In general, increasing the amount of 21R polytypoid in the starting composition led to an increase in the z-value of the sialon. The glass composition was also found to depend on polytypoid level; materials with low additions tended to have glasses which were silicon rich, with roughly equal amounts of Nd and Al, whereas increasing the polytypoid content, solely at the expense of Si_3N_4, gave a glass which contained proportionately more aluminium and nitrogen, although the actual amount of glass present appeared to decrease. In current understanding of the Y-Si-Al-O-N system, the primary role of the polytypoid is in forming high z β'-sialon. Once the Y_2O_3-Al_2O_3-SiO_2 eutectic liquid has formed a number of typical reactions which may proceed are as follows:-

The 21R polytpoid may dissociate to form β' according to the equation:

$$\underbrace{6AlN.SiO_2}_{\text{21R polytypoid}} \xrightarrow[\text{in situ}]{-\ 1450^{\circ}C} 4AlN + 0.5\ \underbrace{(Si_2Al_4O_4N_4)}_{\beta'\ \ z\ =\ 4} \qquad \text{(IV.iii)}$$

AlN may react with silica to form more high z β':

$$4\ AlN + 2SiO_2 \rightarrow \underbrace{Si_2Al_4O_4N_4}_{\beta'\ z = 4} \qquad \text{(IV.iv)}$$

or the silicon nitride may dissolve and react to give β' via the relationship

$$Si_3N_4 + AlN + Al_2O_3 \rightarrow \underbrace{Si_3Al_3O_3N_5}_{\beta'\ z = 3} \qquad \text{(IV.v)}$$

(see phase diagram representations Figure IV.7).

In reality the sintering process is a mixture of these and many other competing reactions, the mechanisms of which are still conjecture, but the overall view is that as the individual reactions proceed the high z β' is effectively diluted by solution and reprecipitation of the bulk Si_3N_4 until equilibrium is reached. It appears that similar reactions occur in the Nd-Si-Al-O-N system; increasing the polytypoid content leads to a higher overall z value with a reduced final glass volume.

The materials with low Al_2O_3 content always contained some Neodymium-nitrogen-melilite ($Nd_2O_3.Si_3N_4$). Reducing the amount of Al_2O_3 further or increasing the amount of Nd_2O_3 resulted in more melilite being formed and left some unreacted α-Si_3N_4. It had already been seen that Nd_2O_3 reacts readily with Si_3N_4 to form melilite (Composition 1 Table IV.1) but its formation during the firing of these compositions is contrary to that observed with yttria. As outlined in Section II.6.2, Liddell (1987) has shown that there is an extensive β'+melilite+liquid region in the Nd-Si-Al-O-N system and

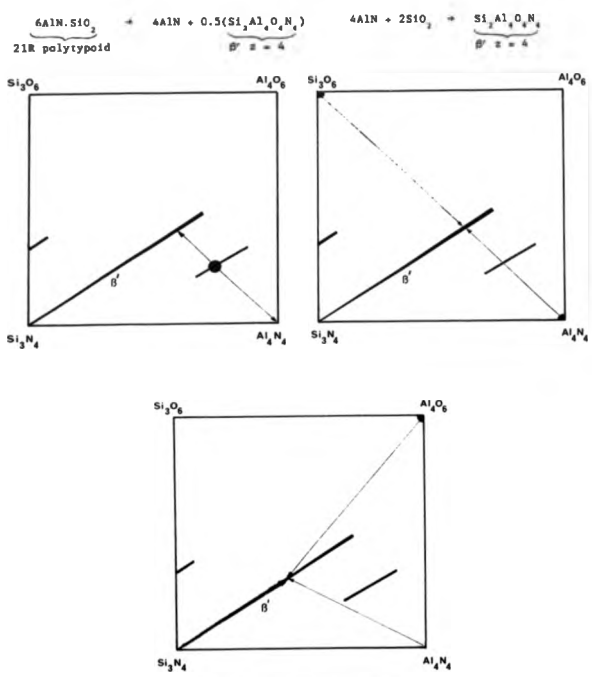

Figure IV.7 Illustration of some of the possible reactions for generating high z β' - sialon

these compositions must simply lie within this phase field (see Figure IV.8). The 201-type composition (8 wt% polytypoid, 6 equiv. wt% Nd_2O_3 and 4 wt% Al_2O_3) formed only β'+glass and must lie close to the edge of this 3-phase region, since increasing the amount of Nd_2O_3 slightly pushes the composition over the boundary line to where the precipitation of melilite is favoured; in a similar way decreasing the amount of Al_2O_3 produces the same overall effect.

In the case of varying only the polytypoid level the description is a little more obscure. The melilite only occurred in materials with 8 wt% polytypoid or more and where the amount of Nd_2O_3 or Al_2O_3 had been modified as above. It appears that the polytypoid provides a certain amount of nitrogen for the liquid, below which melilite precipitation cannot take place, the composition is shifted too far from this phase field in the quaternary diagram (see Figure IV.9) The inevitable formation of melilite, when trying to obtain higher z β' or prepare compositions on the β'-$NdAlO_3$ plane, must simply reduce the amount of liquid available thus preventing the full α-Si_3N_4 → β'-sialon transformation from taking place.

3. Annealed Materials

Post-sintering heat treatments were carried out isothermally for 5 hours or using the standardised annealing cycle for Syalon 201; 1250°C/7 hrs followed by 1400°/5 hrs (see Figure III.1). The samples were then allowed to cool naturally or with a controlled linear decrement over a timed period. X-ray diffraction techniques were used to identify any secondary crystalline phases present. The results from the range of varying polytypoid materials heat-treated with the standard cycle are presented in Table IV.2 and the data from fixed compositions with different annealing cycles in Table IV.3. Some

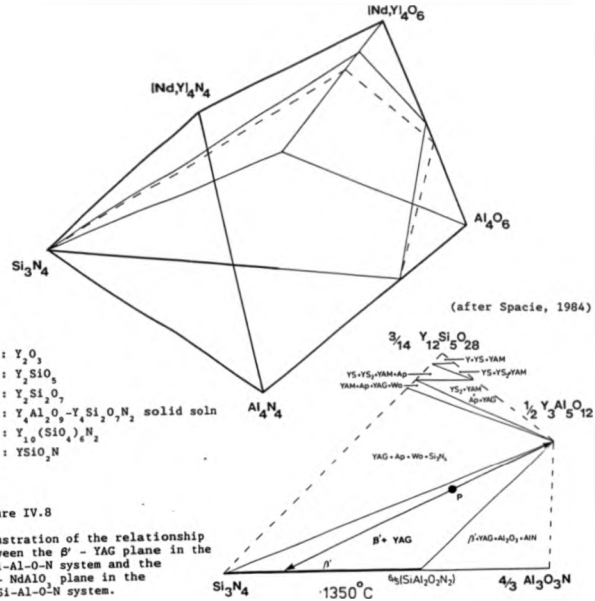

Figure IV.8

Illustration of the relationship between the β' - YAG plane in the Y-Si-Al-O-N system and the β' - $NdAlO_3$ plane in the Nd-Si-Al-O-N system.

At 1350°C a glass of composition such as at P in the β' - YAG plane devitrifies to give β'+YAG (as indicated by the arrows). In the β' - $NdAlO_3$ plane Nd-N melilite interupts the simple β'+liquid field such that upon heat treatment a glass of composition, such as at Q, gives Nd-N melilite and $NdAlO_3$, and no β'. Hence, forming a pure 2-phase β'+$NdAlO_3$ material is not possible.

12H - 12H polytypoid
15R - 15R polytypoid
A - apatite
L - liquid
M - melilite
Y - Nd YAM
N - Nd_2O_3

(after Liddell, 1987)

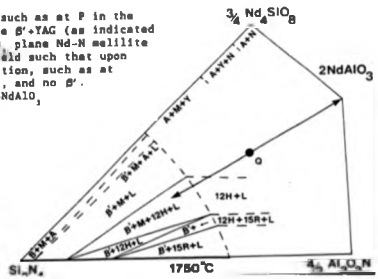

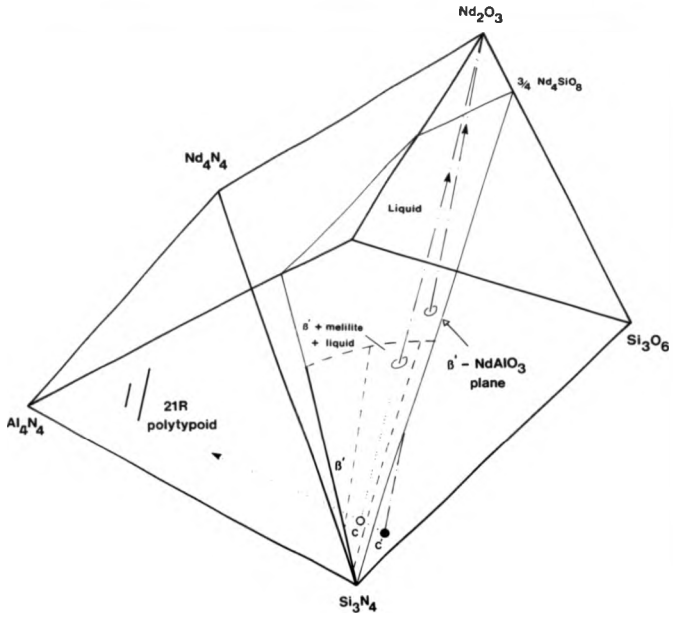

Figure IV.9 Illustration of how increased Nd_2O_3 content shifts the average composition C into the β'+Nd-N melilite phase field. With insufficient polytypoid, C', melilite precipitation is avoided.

Table IV.2 Crystalline phases identified in the Nd-sialon materials after annealing (standard cycle)

Composition No. (Ref Table IV.1)		Crystalline phases present after sintering	Crystalline phases identified after annealing
2	zero 21R	β′	β′ + apatite (v)
7	7.7 eq.% Nd_2O_3	β′	β′ + $NdAlO_3$ (ms) + apatite (tr)
8	4 wt.% Al_2O_3	β′	β′ + $NdAlO_3$ (s)
9	Increasing 21R	β′ + melilite (tr)	β′ + $NdAlO_3$ (vs)
10	9 wt % Nd_2O_3	β′	β′ + $NdAlO_3$ (ms)
11	8 wt % 21R	β′ + melilite (tr)	β′ + $NdAlO_3$ (m) + melilite (vw)
12	decreasing Al_2O_3	β′ + melilite (tr+) + α (tr-)	β′ + $NdAlO_3$ (W) + melilite (w) + α (tr-)
13		β′ + melilite (tr++) + α (tr)	β′ + $NdAlO_3$ (vw) + melilite(m) + α (tr)
14	Zero Al_2O_3	β′ + melilite (w) + α (tr+)	β′ + melilite (ms) + α (tr+)
15	12 wt % Nd_2O_3	β′ + melilite (tr++) + wollastonite (tr)	β′ + $NdAlO_3$ (ms) + wollastonite (tr)
16	8 wt % 21R	β′ + melilite (vw)	β′ + $NdAlO_3$ (m) + melilite (tr)
17	decreasing Al_2O_3	β′ + melilite (w)	β′ + $NdAlO_3$ (w) + melilite (tr+)
18	Zero Al_2O_3	β′ + melilite (m) + $NdAlO_3$ (tr) + α (tr)	β′ + $NdAlO_3$ (vw) + mel (tr++) + α (tr)
19	8 wt % 21R	β′ + melilite (ms) + $NdAlO_3$ (w) + α (tr)	β′ + $NdAlO_3$ (m) + wollastonite (m)
20	zero Al_2O_3	β′ + melilite (ms) + $NdAlO_3$ (w) + α (tr)	β′ + $NdAlO_3$ (m) + wollastonite (w)
21	decreasing Nd_2O_3	β′ + melilite (ms) + $NdAlO_3$ (w) + α (tr)	β′ + $NdAlO_3$ (w) + mel (tr) + wol (tr)
22		β′ + melilite (ms) + $NdAlO_3$ (vw) + α (tr+)	β′ + $NdAlO_3$ (w) + mel (m) + wol (tr)

Peak intensities vs-very strong s-strong ms-medium strong m-medium
w-weak vw-very weak tr-trace

Table IV.3 Crystalline phases identified in the Nd-sialon materials after annealing (various cycles)

Comp (Ref Tab IV.1)	Anneal Cycle °C/hrs	Crystalline phases identified
2		(85 wt.% Si_3N_4; 7.7 eq.% Nd_2O_3; 4 wt.% Al_2O_3
		Contained only β′ after sintering)
	1000/5	β′
	1050/5	β′
	1100/5	β′ + $Nd_2Si_4Al_2O_4N_4$ (tr+)
	1150/5	β′ + $Nd^1Si^1Al^3O^1{}^2N^1$ (tr++) + unknown (tr)
	1200/5	β′ + $Nd^1Si^1Al^3O^1{}^2N^1$ (vw) + apatite (vw)
	1250/5	β′ + $Nd^1Si^1Al^3O^1{}^2N^1$ (vw) + apatite (vw)
	1300/5	β′ + $Nd^1Si^1Al^3O^1{}^2N^1$ (vw) + apatite (vw)
	1350/5	β′ + Nd-N-apatite (w)
	1400/5	β′ + Nd-N-apatite (w)
7		(82 wt.% Si_3N_4; 3 wt.% 21R; 7.7 eq.% Nd_2O_3; 4 wt.% Al_2O_3
		Contained only β′ after sintering: Syalon 102 equivalent)
	1000/5	β′ + $Nd_2Si_4Al_2O_4N_4$ (v)
	1000/10	β′ + $Nd^1Si^1Al^3O^1{}^2N^1$ (m)
	1050/5	β′ + $Nd^1Si^1Al^3O^1{}^2N^1$ (m)
	1100/5	β′ + $Nd^1Si^1Al^3O^1{}^2N^1$
	1150/5	β′ + $Nd^1Si^1Al^3O^1{}^2N^1$
	1200/5	β′ + $Nd^1Si^1Al^3O^1{}^2N^1$
	1250/5	β′ + $Nd^1Si^1Al^3O^1{}^2N^1$
	1300/5	β′ + $Nd^1Si^1Al^3O^1{}^2N^1$ (m) + apatite (tr)
	1350/5	β′ + Nd-N-apatite (vw) + $NdAlO_3$ (vw)
	1400/5	β′ + Nd-N-apatite (vw) + $NdAlO_3$ (vw)
10		(79 wt.% Si_3N_4; 8 wt.% 21R; 6 eq.% Nd_2O_3; 4 wt.% Al_2O_3
		Contained β′ only after sintering: Syalon 201 equivalent)
	1000/5	β′ + wollastonite (m)
	1050/5	β′ + wollastonite (m) + $Nd_2Si_4Al_2O_4N_4$ (vw)
	1100/5	β′ + wollastonite (m) + $Nd^1Si^1Al^3O^1{}^2N^1$ (w)
	1150/5	β′ + wollastonite (m) + $Nd^1Si^1Al^3O^1{}^2N^1$
	1200/5	β′ + wollastonite (m) + $Nd^1Si^1Al^3O^1{}^2N^1$
	1250/5	β′ + wollastonite (m) + $Nd^1Si^1Al^3O^1{}^2N^1$
	1300/5	β′ + wollastonite (m) + $Nd^1Si^1Al^3O^1{}^2N^1$
	1350/5	β′ + $NdAlO_3$ (s)
	1400/5	β′ + $NdAlO_3$ (s)
20		(82 wt.% Si_3N_4; 8 wt.% 21R; 10 wt.% Nd_2O_3
		Contained β′ + melilite + $NdAlO_3$ + α (tr) after sintering)
	1250/7 1400/5	β′ + $NdAlO_3$ (m) + wollastonite (w)
	1400/10	β′ + $NdAlO_3$ (m) + wollastonite (m)

phases existed in such small quantities that peaks on the diffractometer traces were only just detectable.

3.1 Microstructure of the Annealed Zero Polytypoid Materials

XRD analysis of bulk samples of the materials with no polytypoid added to the starting mix revealed small traces of a new phase of composition $Nd_3Si_3Al_3(O,N)$ (discussed later in Section IV.3.2.), after annealing for 5 hours at 1100°C. After 5 hours at 1150°C slightly more was detectable together with minor traces of an unidentified phase. At 1200°C a small amount of Nd-N-apatite ($Nd_{10}(SiO_4)_6N_2$) was recrystallised. This was found to be highly segregated, only occuring in rather large glassy areas adjacent to the 80-100 μm β'-grains, and usually as single crystals 2-6 μm in size (Figure IV.10). nearest neighbours were typically 5-15 μm away with no evidence of similar long-range orientation. This isolated behaviour is believed to be the result of micro-inhomogeneity. Much of the liquid which develops during sintering is absorbed by the growth of the β' crystals, but on a microscopic scale the rate of removal of the stoichiometric elements from the surrounding matrix may vary from grain to grain. In particular, studies of the reaction sequences in the Y-Si-Al-O-N system have shown that the Si_3N_4 → β'-sialon reaction starts to occur at a lower temperature than the 21R → high z β' reaction during warm-up (see section V.3). The β'-grains which form in the first 'pockets' of liquid to appear must obtain their Al and O directly from the eutectic liquid rather than from the dilution of high z β'. As these early crystals grow, the liquid at their interfaces must become aluminium deficient and eventually be unsuitable for more β' precipitation. Even though there may be some inter-diffusion later on, many of these regions remain large enough and significantly

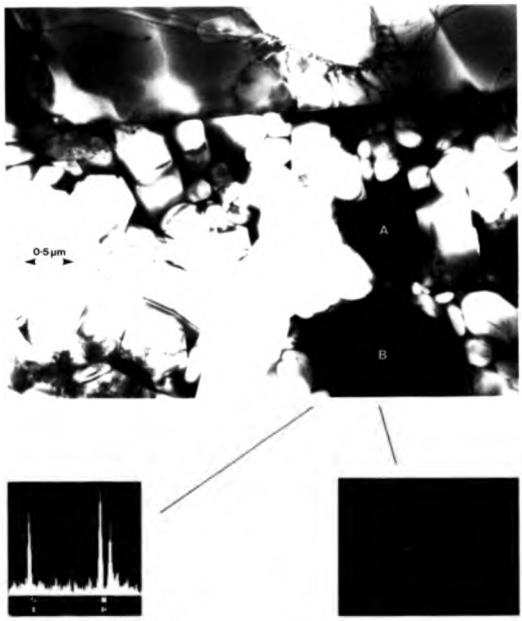

Figure IV.10 Inhomogeneous precipitation of the Nd-N apatite phase. A and B are single Nd-N apatite crystals.

different in composition for Nd-N-apatite to be favoured as a product of crystallisation from the resultant glass upon annealing.

This timing of competing reactions may also explain the evolution of more 80-100 μm grains in Nd-containing materials than in the corresponding yttrium sialons. The solution reprecipitation reaction may only require the presence of a liquid to proceed, say above 1300°C; whereas the 21R reactions may be constrained until enough thermal energy is supplied for activation, whether there is liquid present or not. If this were the case the lower eutectic temperatures in the Nd-system would allow the first reactions more time to occur before the 21R reactions could start. Also, increasing the temperature during the interim stage may provide additional kinetic energy for grain growth.

The apatite peaks on the diffractometry traces were shifted slightly indicating larger d-spacings than expected. Semi-quantitative EDAX analysis showed that the apatite phase contained approximately 3.5 At% aluminium although there seemed to be a fair degree of variation from grain to grain, again suggesting some non-uniformity. By contrast, in the yttrium system Y-N-apatite ($Y_{10}(SiO_4)_6N_2$) has a range of composition extending towards $2Y_2O_3.3SiO_2$ and is known to accommodate some Al and O in place of Si and N with a corresponding change in lattice parameter.

The two phases were found to co-exist, always with some residual glass upon annealing between 1200°C and 1350°C. Increasing the temperature tended to result in more apatite but with the same amount of new phase. When annealed at 1400°C, regardless of hold time or cooling rate, only glass and an increased amount of apatite remained. It would appear that the thermodynamic potential for the formation of Nd-apatite is high. Whilst some apatite precipitates at the lower

temperatures more thermal energy is required to speed up the rate of recrystallisation in order to obtain significant amounts within the 5 hour annealing cycle. It is likely that when the annealing temperature is increased to above 1350°C the new phase melts or dissociates and re-dissolves to form more glass. This must change the composition of the existing glass such that the evolution of more apatite occurs, which in turn shifts the glass composition probably by making it Nd deficient so that the re-precipitation of the new phase becomes unfavoured upon cooling.

3.2 Microstructure of the Annealed 3 wt% Polytypoid Materials

In the materials with 3 wt% 21R polytypoid added to the starting mix all of the glass was recrystallised to give a new phase, of composition $Nd_3Si_3Al_3(O,N)$, when annealed between 1000°C and 1350°C (see Figure IV.11.). No variation in composition or volume per cent present was found, whatever the annealing temperature, although the sample heat-treated at 1000°C had to be reheated for a further 5 hours for the transformation to become complete. This new solid solution phase retained the morphology of its parent glass, but unlike YAG in the yttrium sialons did not maintain the same orientation over large areas. What initially appeared to be single crystals contained segments which diffracted at different tilts (Figure IV.12). Also, the glass was fully recrystallised in the triple points. There was no evidence of the small traces of residual glass containing all the unwanted metallics at the β'/β''/crystal convergence points, a characteristic always seen in Syalon 201. Dark field imaging using diffracted beams from the new phase further revealed that the thin layers of glass sandwiched between adjacent grains had also been devitrified. This happens to some extent in the β'/YAG materials,

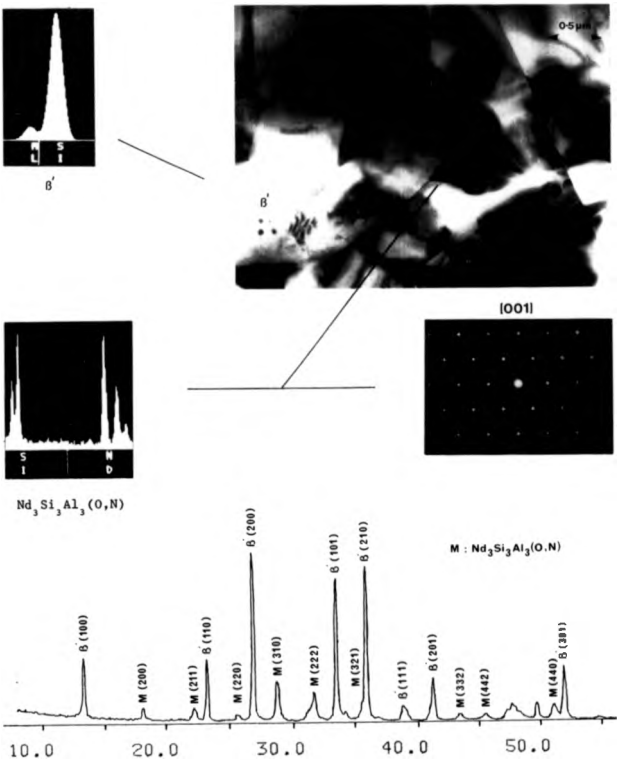

Figure IV.11 Microstructure of the annealed Nd Syalon 101-type material showing compositional analysis and X-ray spectra of the crystalline $Nd_3Si_3Al_3(O,N)$ matrix phase

A,B,C are individual crystals. Nucleation often appeared to stem from deformities such as indicated by arrows.

Triple point consisting of 4 individual crystals A,B,C,D.

Figure IV.12 Examples of segmentation within the $Nd_3Si_1Al_3(O,N)$ phase indicative of high free energy for nucleation

where the angle between the grains is not too acute and the radius of curvature of the precipitating YAG crystal front is not restricted from further growth by the adjoining β'/β' boundaries. In this material, however, all of the triple points appeared to be crystalline. Like yttrium, the neodymium atoms cannot be accommodated in the β' structure itself and, since there was no trace of any residual glass it seemed reasonable to assume that the composition of the new phase must be close to that of the original glass and certainly be able to absorb all of its constituents. The as-sintered glass was found to be very similar in composition to the recrystallised product but slightly more silicon rich, although this could have been due to the electron beam fluorescing surrounding β'-sialon grains (Figure IV.13). No shift in z-value of the β' phase was detected upon recrystallisation, as observed in similar circumstances when excess Si and N diffuse back into the β'-grains when the residual glass is devitrified to YAG in Syalon 201. Hence, any migration of Si and N out of the glass in this material must have been negligible. It follows that the final crystal composition must lie inside the glass forming region of the Nd-Si-Al-O-N system (see Figure IV.14). Multiple nucleation in the glassy triple points indicates that this recrystallisation at constant composition is easy to initiate and the process is well-advanced even after only a short anneal time. The energy threshold for nucleation must be low and the energy requirements for crystal growth must be relatively small involving only short range rearrangement or diffusion of the species rather than long range as in the YAG system.

From analysis of the XRD traces the $Nd_3Si_3Al_3(O,N)$ phase appeared to have a body-centred cubic crystal lattice with lattice parameter a = 9.756 Å. Liddell (1987) has recently prepared this

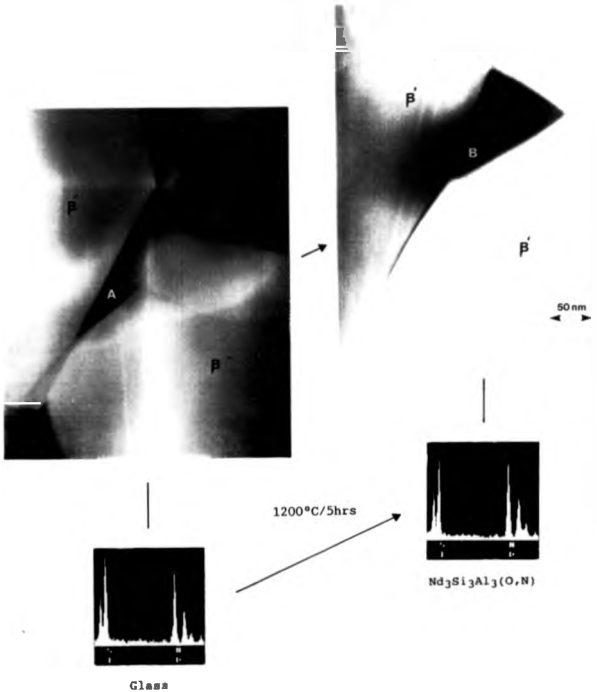

Figure IV.13 EDAX spectra from the glass in the as-sintered Nd Syalon 101-type material (A) and from the crystalline matrix in the heat-treated version (B) are similar which shows that recrystallization occurs at constant composition.

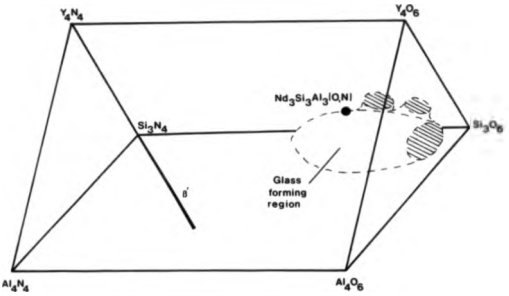

Figure IV.14 The Nd-Si-Al-O-N system, illustrating how the $Nd_3Si_3Al_3(O,N)$ composition must lie within the liquid forming region or be very close to the liquid boundary. (Liquid region outlined based on the Y-Si-Al-O-N liquid region, after Drew 1980, expanded towards the nitrogen end of the JÄnecke diagram)

phase in isolation and suggests that its structure is related to that of Y_2O_3 (cubic with a ~ 10Å) with some atomic sites equivalent and others being shared by the Nd and Al atoms: the level of sharing dependent upon the unit cell contents. When considering this formulation discrepancies arise because traces of the lines normally excluded by the crystallographic rules for body-centred cubic structures are visible on the Hägg-Guinier diffraction photographs, and the intensities of other lines are stronger than expected (Figure IV.15). In particular, the N = 28 and N = 60 lines (where $N = h^2 + k^2 + l^2$ and hkl are the Miller indices of the xyz co-ordinates of the plane) can clearly be seen in the spectrum from the single substance. Unfortunately in the sialon material this intergranular phase only occupies around 10 vol% and the N=28 line, which is already faint, is not visible. In addition, the N=60 line, if it is present, is masked by the much stronger β'(212) peak. The N=10, 30 and 42 lines though in both cases are stronger than expected. Fernie (1990) has now unequivocally shown this phase to be hexagonal with lattice parameters a = 7.987 Å, c = 4.874 Å by obtaining a series of electron diffraction patterns at set angles, tilting about the pole axis, and reconstructing the 3-D reciprocal lattice. Diffraction patterns obtained from localised areas in the present materials are in agreement with this hypothesis (Figure IV.16) and it now appears that the original BCC structure forms a larger sub-lattice.

Spacie et al. (1985) further claim that the phase is an oxide, rich in aluminium, probably a low temperature form of perovskite $NdAlO_3$. More recent work by Fernie et al. (1990) has shown that it contains a significant amount of nitrogen and establishes the composition as being $Nd_3Si_3Al_3O_{12}N_2$ (see Figure IV.17 for position in the Jänecke diagram). Accurate determination of the nitrogen content

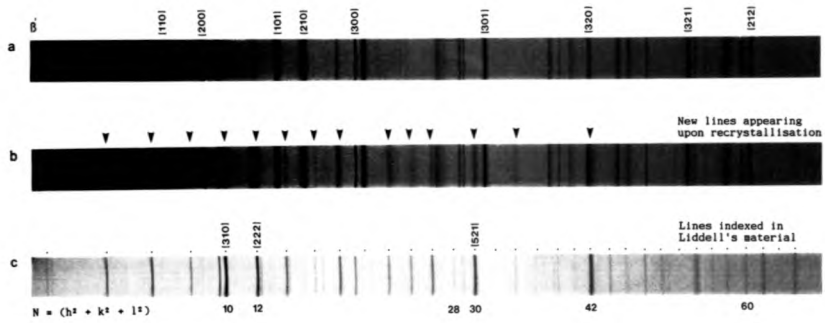

Figure IV.15 Hägg-Guinier spectra from a) the Nd Syalon 101-type composition before annealing b) after annealing and c) the $Nd_3Si_3Al_3(O,N)$ phase prepared in isolation by Liddell (1987), illustrating the relationship in crystallographic structure of the phase prepared by Liddell (1987) and the matrix phase devitrified 'in-situ' in the present work

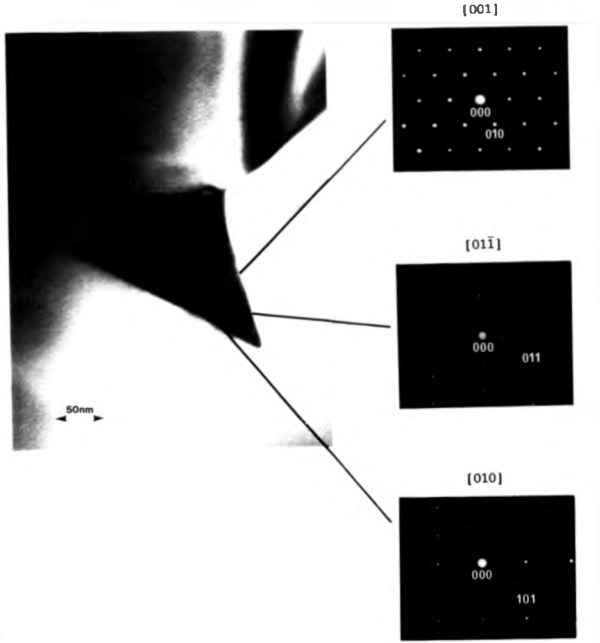

Figure IV.16 Diffraction patterns from the $Nd_3Si_3Al_3(O,N)$ phase, obtained at different tilts, consistent with the hexagonal crystallographic structure, $\underline{a}$ = 7.987 A $\underline{c}$ = 4.874 A, proposed by Fernie (1989)

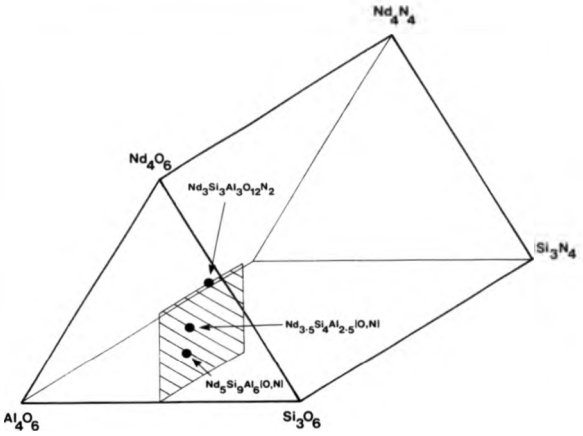

Figure IV.17 Position of the $Nd_3Si_3Al_3O_{12}N_2$, $Nd_{3.5}Si_4Al_{2.5}(O,N)$ and $Nd_5Si_9Al_6(O,N)$ phases within the Nd-Si-Al-O-N system. (after Fernie et al., 1990)

of this phase in the present work proved difficult because of having to locate areas large enough to probe without being influenced by nitrogen from the surrounding β'-grains, but all measurements did indicate a substantial amount.

The stability of this phase, up to 1320 - 1330°C, is remarkably high. Spacie (1984) reported similar phases in the yttrium and cerium Si-Al-O-N systems (designated Y and Ce U-phase respectively) upon annealing at 1050°C but these were only stable up to 1200°C. Unfortunately, these phases existed in such small quantities in Spacie's materials that full chemical analysis was impracticable, but again both were indexed as having BCC unit cell structure with a dimension approximately equal to 10 Å. From compositional make-up it was concluded that both were rich in aluminium and oxygen. Whilst the diffraction data obtained by Fernie (1990) and in the present work are consistent with the phase structures reported by Spacie (1984) and Spacie et al. (1985) the discrepancy over composition still remains unresolved. It is important to add here though that in the contradicting reports the phases were formed in an oxide glass environment rather than in-situ in a Si_3N_4-based ceramic fired in a nitrogen atmosphere. The new Nd-phase identified here has repeatedly been analysed as being of composition $Nd_3Si_3Al_3O_{12}N_2$ and hence clearly contains a significant amount of nitrogen.

Fernie et al. (1990) also report the existence of two other phases of approximate compositions, $Nd_{3.5}Si_4Al_{2.5}(O,N)$ and $Nd_5Si_3Al_6(O,N)$, lying within the Nd-Si-Al-O-N glass forming region (see Figure IV.17). Initial investigations have shown these phases to be stable to temperatures of 1150-1250°C. With a higher silicon content than the $Nd_3Si_3Al_3O_{12}N_2$ phase they are more likely to be recrystallised in an environment richer in silicon than with the

current $Nd_3Si_3Al_3O_{12}N_2$ parent glass. The traces of unidentified phase recrystallised in the zero polytypoid material upon annealing at 1150°C are probably associated with one of these compositions.

As with the zero polytypoid materials, heat-treatments above 1350°C gave localised areas of Nd-N-apatite, but this time small amounts of neodymium aluminate ($NdAlO_3$) were also present. If the sample was re-heated or allowed to cool slowly between 1350°C and 1000°C some of the new phase reappeared. Fernie and Leng-Ward (1989) have examined the stability of this phase in isolation and shown that it melts at approximately 1320°C; if allowed to cool naturally the majority (~ 90%) recrystallises; if rapidly quenched the 'melt' subsequently remains as a glass.

Samples from creep bars held at 1200°C under a tensile stress of 77 MPa for 70 hours were examined to see if there was any change in the microstructure. Figure IV.18 shows evidence of 'rounding' at the triple points and de-faceting of the contacted β'/β'/$Nd_3Si_3Al_3(O,N)$ boundaries. Lewis and Lumby (1983) first reported this kind of phenomena in connection with β'-YAG sialon ceramics after creep testing at 1277°C. Near the surface of the bar the non-stoichiometric metal ions diffuse out to the oxide layer leaving pure solid/solid interface contacts. To alleviate the imbalance in interfacial energies acting along the β'/β' and β'/YAG interfaces the YAG crystals are transformed to rounded, roughly equiaxed grains by diffusive rearrangement. (The mechanism is described in detail in Section V.5.) The process is slow, normally reaching the fully equilibrated 120° state over a period of a few hundred hours depending upon the ambient temperature. It would appear that a similar mechanism is prevalent here, but at 1200°C the rearrangement process is particularly slow. Even with fewer unwanted metallics (the Nd phase has absorbed most of

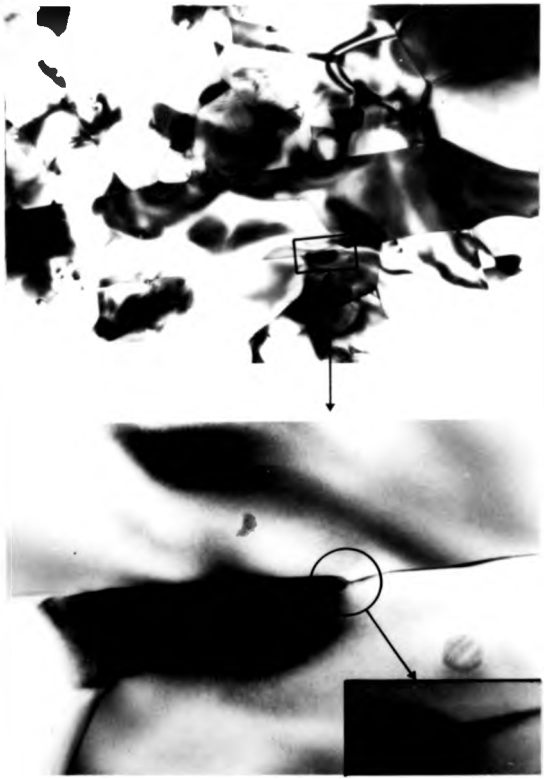

Figure IV.18 Morphological rearrangement of the triple points in the $Nd_3Si_3Al_3O_{12}N_2$ phase after 70 hrs exposure at 1200°C. 'Rounding' results from the increased solid/solid contact due to complete crystallisation and subsequent equilibriation of the interfacial energies

them) and consequently more solid/solid contact at the peripheries the rearrangement process has not progressed very far.

3.3 Microstructure of the annealed higher (6-9 wt%) polytype materials

As outlined in section IV.2 the majority of the higher polytypoid materials contained large amounts of Nd-N-melilite after sintering. This was considered unsuitable as a grain boundary phase, especially for a high temperature material, since Y-N-melilite becomes unstable and readily oxidises with an accompanying large volume expansion above 1300°C, oxidation of the Nd version produces a smaller volume expansion but the onset occurs at a lower temperature. Upon annealing, with the standardised Syalon 201 cycle, much of this melilite disappeared, but unfortunately, even with prolonged heat treatments most materials still contained significant amounts. In all cases, the mono-aluminate, $NdAlO_3$, was recrystallised instead, and in the absence of a YAG-type Nd_3Al_5 oxide phase this appeared to be the best refractory alternative. However, as discussed in Section II.6.2. Nd-N melilite dominates the β'-$NdAlO_3$ plane (see Figure IV.8) such that forming a pure 2-phase β'-$NdAlO_3$ ceramic free from melilite is impossible. In the present materials the original melilite must have decomposed or melted and re-formed a liquid once the anneal temperature was reached, from which the $NdAlO_3$ and new melilite was precipitated. All the materials contained some residual glass after annealing, even the ones which appeared to have insufficient liquid during sintering. For the 201 equivalent material in particular, which had no 'as-sintered' melilite, the overall glass composition must have just shifted towards the β'+melilite+liquid phase boundary

as the $NdAlO_3$ precipitated out, but at the same time stayed within the β'+liquid phase region (Figure IV.19).

Upon annealing the 201-type samples at different temperatures, it was found that small amounts of Nd-N-Q wollastonite were recrystallised after 5 hours at 1000°C. At 1100°C some of the $Nd_3Si_3Al_3O_{12}N_2$ phase was also precipitated and the two phases co-existed in roughly equal proportions, still with some residual glass, up to around 1350°C. Annealing at 1400°C followed by rapid cooling gave β'+$NdAlO_3$+glass only, whilst controlled cooling again allowed some of the new phase to re-form.

In trying to develop a high polytypoid material with a fully recrystallisable glass, a composition based on 10 wt% Nd_2O_3, 8 wt% 21R and zero Al_2O_3 fired for 5 hrs at 1800°C gave the most promising results (Composition 20, Table IV.1). Although this material contained some melilite after sintering, all of it had disappeared after annealing for 10 hours at 1350°C, and the subsequent matrix was found to be an approximate 50/50 mix of Nd-N-Q wollastonite and $NdAlO_3$ with very little residual glass (see Figure IV.20). Whilst the wollastonite would be the weak link, (its oxidation properties have still to be investigated), it should not undergo such catastrophic oxidation as the melilite phase. In the absence of a β'+$NdAlO_3$ material it was hoped that this 3-phase neodymium-based material could offer potential for use at elevated temperatures with properties comparable to yttrium Sialon 201.

4. Summary

With the exception of YAG, all of the yttrium phases in the Y-Si-Al-O-N system have an equivalent in the Nd-Si-Al-O-N system; with similar crystallographic structure but with expanded lattice

12H - 12H polytypoid
15R - 15R polytypoid
A - apatite
L - liquid
M - melilite
Y - Nd YAM
N - Nd_2O_3

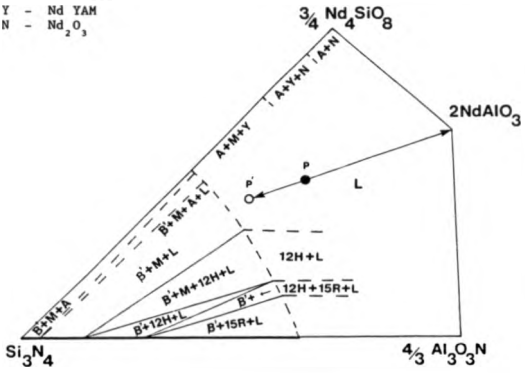

Figure IV.19 Illustration of how liquid compositions on the β' - $NdAlO_3$ plane may be partially devitrified to give β'+$NdAlO_3$+glass materials. Upon annealing, the average liquid composition P shifts to P' as $NdAlO_3$ precipitates out.

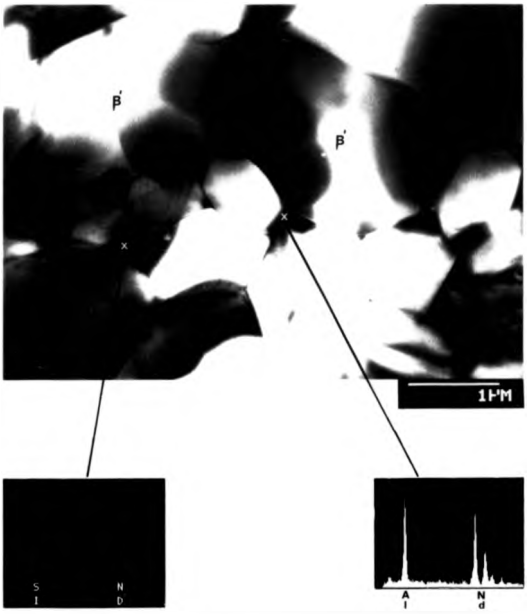

Figure IV.20 Microstructure of the annealed 10 wt.% Nd_2O_3, 8 wt.% 21R polytypoid, zero Al_2O_3 composition. Matrix phase consists of an approximate 50/50 mixture of $NdAlO_3$ and Nd N-α wollastonite

parameters. Whilst this may initially suggest that similar reactions occur in both systems, and hence that Nd_2O_3 can be directly substituted for Y_2O_3 in the preparation of pressureless sintered sialon ceramics, there are a number of significant differences:

1) The eutectic temperatures in the Nd-Si-Al-O-N system are generally 30-50°C below their yttrium counterparts.

2) Neodymium-glasses can accommodate a larger amount of dissolved nitrogen, consequently the Nd-glass forming region is more extensive that the Y-glass one.

3) Three new Nd phases, two with no analogy in the yttrium system, have been identified with compositions lying within this glass forming region. The most important of these has the composition $Nd_3Si_3Al_3O_{12}N_2$ and is stable to temperatures in excess of 1300°C.

In the absence of a phase equivalent to YAG, $NdAlO_3$ would appear to be the best alternative as a refractory matrix in Nd-sialon materials for use at elevated temperatures. Unfortunately Nd-N-melilite, which is unsuitable as a secondary phase, dominates this region of the phase diagram and the preparation of 2-phase β'+$NdAlO_3$ sialon ceramics, free from melilite, is impossible. Fully crystallised β'+$Nd_3Si_3Al_3O_{12}N_2$ and nearly fully crystallised β+$NdAlO_3$+Nd N-α wollastonite materials can be prepared and offer potential as improved grade neodymium ceramics for comparison with conventional yttrium based β'+YAG materials, such as Syalon 201.

CHAPTER V. YTTRIUM α'+β' SIALON CERAMICS

1. Background to recent developments

Oyama and Kamigaito (1971) and Jack and Wilson (1972) first noted that 'alloying' of the Al_2O_3 and AlN sintering additives with the α-Si_3N_4 powder in the hot-pressing of silicon nitride ceramics effectively reduced the final glass volume. The materials generated were essentially single phase β'-sialon materials with excellent high temperature properties.

It has been recognised for some time that in a similar way α'-sialon ceramics offer the potential of incorporating the sintering additives into the α-Si_3N_4 crystal structure upon densification in pressureless sintering. In this way essentially single phase α' materials can be envisaged with excellent mechanical and thermal properties, comparable to the hot-pressed materials, again due to the absence of any residual grain boundary glass. Unfortunately, detailed examination of the phase relationships in the Y-Si-Al-O-N system have shown that the region over which α' exists in equilibrium with a liquid is much smaller than that with β', and the preparation of dense single phase α' materials is further complicated by the higher viscosity of the liquid associated with α' precipitation. Jameel (1984) determined the extent of the α' region from the Si_3N_4-YAl_3N_4 join into the Y-α' plane (see Figure II.11) and concluded that the α' phase has very little solid solution out of the plane due to the discrepancy between the Al-N (1.87 Å) and Si-O (1.67 Å) bond lengths which prevents atomic rearrangement without change in crystallographic structure. The preparation of pure α' materials is thus extremely sensitive to oxygen/nitrogen balance and in practice the processing required imposes such stringent conditions upon composition.

homogeneity, and firing schedules that manufacturing such materials on a commercial basis is not feasible.

The preparation of pure α'+β' sialon composites allows little more flexibility. Walls (1986) examined the extent of the α'+β' phase field (Figure V.1) and concluded that even though the α'+β'+liquid region is somewhat larger than the α'+liquid region, the preparation of pure two phase materials is still extremely sensitive to O/N balance. In addition, the liquid has the dual role of aiding β' precipitation followed by absorption of the remainder to form α'. Unfortunately, both of these reactions occur simultaneously and compete for the available liquid, with the formation of α' beginning at a lower temperature than the formation of β'; the converse of what is desired. Generating a mixture in which the α → β', α → α' and β' → α' reactions occur uniformly throughout the bulk and finish together having absorbed all of the liquid is impractical and hence the restrictions on forming a pure di-phasic α'+β' material, free from localised pockets of residual glass and unreacted material, become virtually the same as for forming α' alone.

The best alternative is to form α'+β'+glass or α'+β'+YAG materials, absorbing most of the liquid as the reaction proceeds, without impeding the densification characteristics, and leaving as little residual glass as possible, which can then either be left untreated or again recrystallised to form YAG, but of a much reduced volume. To date no significant advantage has been foreseen in developing the latter since their upper operating temperature limit would not be expected to offer any improvement over that of conventional β'+YAG materials but α'+β'+glass ceramics have recently found use in the metal cutting industry where the increase in hardness and wear resistance afforded by inclusion of the α' species leads to

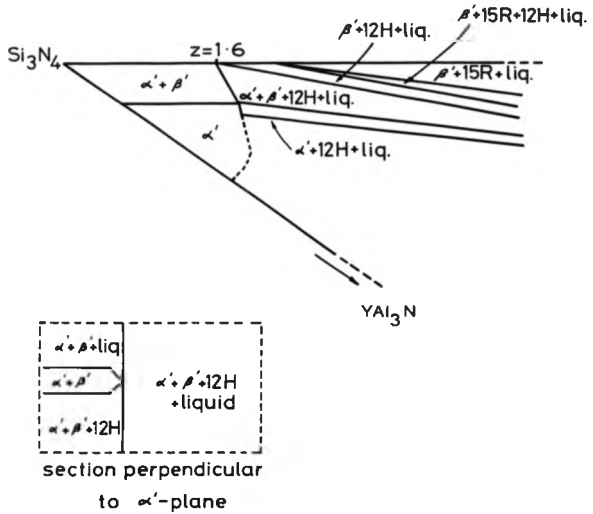

Figure V.1 Phase relationships in the α-sialon plane and perpendicular to the α'+β' region (after Wallls, 1986)

higher productivity ('longer-lasting' Kennametal Kyon 3000* tool tips for example).

Forming an α'+β'+glass or α'+β'+YAG material is relatively easy; Syalon 201 typically contains 6-8 vol.% α' after sintering. Lewis et al. (1980) demonstrated that to achieve a perfect β'+YAG material upon annealing necessitates having a residual matrix glass enriched with nitrogen so that its composition lies near the β'-YAG tie-line (see Figure II.10). This allows it to partition and form the yttrium-aluminium-oxygen containing phase with the remainder having the correct proportion of constituents to precipitate as more, or dilute the existing, β'. Glasses with insufficient nitrogen have compositions away from the β'-YAG tie-line and tend to form additional phases, such as yttrium disilicate, upon devitrification. In the case of Syalon 201, instead of starting with a perfectly balanced composition, the mixture prepared is slightly nitrogen rich (by adding additional 21R polytypoid) to ensure that no silicate phases, which would have a deleterious effect upon high temperature properties, will be recrystallised. When the polytypoid dissolves into the liquid in the early stages of the sintering process this excess causes it to become nitrogen saturated. Its composition shifts to the α'+β'+glass phase field and to alleviate this α' is evolved. The emergence of α' during sintering is thus taken as an indication of nitrogen saturation.

With the continued refinement of β'+YAG and α'+β'+glass materials over the past few years, the performance of pressureless

---

* Kyon 3000 is a registered trademark of Kennametal Inc. Pennsylvania

sintered sialon ceramics has been pushed nearer to the limits dictated by the intrinsic properties of Si_3N_4 itself, but the retention of even a small amount of phase derived from the sintering liquid still remains the primary factor inhibiting prolonged use at extreme temperatures. Inevitably, the YAG phase will always form a eutectic with SiO_2 produced in an oxidising environment, but by minimising the amount of YAG present initially the processes of oxidation and creep degradation should be correspondingly diminished.

2. Composition Variations

Having observed the evolution of α' in the sintering of Syalon 201, compositions were prepared with small perturbations from the base starting mix (82 wt.% Si_3N_4, 8 wt.% 21R polytypoid, 6 wt.% Y_2O_3, 4 wt.% Al_2O_3). The overall objective was to increase the nitrogen content of the sintering liquid, to generate more α' precipitation and thereby reduce the final glass volume. Favourable compositions were pursued further to determine whether similar results could be achieved when starting with smaller proportions of the liquid forming additives.

The changes in composition were carried out empirically. Initially, the 21R polytypoid content was increased solely at the expense of silicon nitride. This was repeated with no Al_2O_3 added to the starting mix. Finally, the Y_2O_3 content was varied in selected compositions to ascertain what effect this had upon densification kinetics and recrystallisation products. The compositions prepared, densities after sintering, and crystalline reaction products after annealing are listed in Table V.1. Cookson silicon nitride (grade 1002) was used for all compositions although some were reproduced using Kennametal powder. The difference in final density between

Table V.1 The yttrium based compositions investigated

Comp No.	Wt.% Constituents				Density	Crystalline Reaction Products		
	Si_3N_4	21R	Y_2O_3	Al_2O_3	g cm^{-3}	α' %	β' %	Other
1	84	6	6	4	3.25	-	100	YAG + wollastonite (tr)
2	82	8	6	4	3.25	8	92	YAG + wollastonite (tr)
3	80	10	6	4	3.25	10	90	YAG + wollastonite (tr)
4	78	12	6	4	3.26	16	84	YAG + wollastonite (tr)
5	76	14	6	4	3.26	17	83	YAG + wollastonite (tr)
6	74	16	6	4	3.28	24	76	YAG + wollastonite (tr)
7	88	6	6	0	3.25	12	88	YAG + wollastonite
8	86	8	6	0	3.25	16	84	YAG + wollastonite
9	84	10	6	0	3.25	30	70	YAG + wollastonite
10	82	12	6	0	3.25	43	57	YAG + wollastonite
11	80	14	6	0	3.25	52	48	YAG + wollastonite
12	78	16	6	0	3.25	57	43	YAG + wollastonite
13	76	18	6	0	3.27	55	45	YAG + wollastonite
14	74	20	6	0	3.23	55	45	YAG + wollastonite + AlN (tr)
15	72	22	6	0	3.18	54	46	YAG + wollastonite + AlN (tr +)
16	80	16	4	0	3.16	31	69	YAG + wollastonite
17	79	16	5	0	3.20	36	64	YAG + wollastonite
18	76	16	8	0	3.28	51	49	YAG + wollastonite
19	74	16	10	0	3.31	53	47	YAG + wollastonite
20	72	18	10	0	3.31	49	51	YAG + wollastonite
21	70	20	10	0	3.32	52	48	YAG + wollastonite

tr indicates trace

equivalent compositions was negligible and the reaction products were virtually the same except for small traces of iron silicide normally encountered with Kennametal silicon nitride-based materials.

For all the compositions with added Al_2O_3 the sintering cycle used was the standard cycle for normal Syalon 201 (1600°C/2 hrs, 1750°C/5 hrs) (see Figure III.1). For the materials with no added Al_2O_3 the second stage of the firing cycle was raised to 1800°C/5 hrs. It was found that this greatly improved the final density. In sialon materials in which the only Al_2O_3 present occurs as a surface impurity oxide film on the 21R polytypoid, the liquid which would normally be formed when the SiO_2-Al_2O_3-Y_2O_3 eutectic temperature is reached is almost entirely absent. Instead the main bulk of the liquid does not appear until the polytypoid reactions start which are usually associated with the onset of α-Si_3N_4 solution and β'-sialon precipitation. The $\alpha \rightarrow \beta'$ reaction proceeds fairly slowly at 1750°C; presumably with very little Al_2O_3 present the liquid is more viscous than for normal Syalon 201, but the reaction can be speeded up, to give completion in a reasonable time, by heating to 1800°C.

Increasing the polytypoid content generally gave rise to a higher density product. Most of the density measurements showed good correlation with the maximum theoretical values calculated using the method of mixtures. With the increased polytypoid zero Al_2O_3 series of materials the density reached a maximum of 3.29 g cm^{-3} with 18 wt.% polytypoid added to the starting mix. As the polytypoid content was increased further the density decreased sharply, and the material produced contained proportionately larger amounts of AlN. It would appear that with 18 wt.% the polytypoid addition has reached a critical level; below which an excess of liquid remains after

sintering, and above which the liquid produced is absorbed before full reaction and densification can take place.

The composition based on 16 wt.% polytypoid, 6 wt.% Y_2O_3, zero Al_2O_3 (composition 12 Table V.1) gave the highest α' containing material, saturating at 57% α' relative to β', (using the X-ray diffractometry technique), with only a minor amount of residual glass. When annealed the recrystallisation products were roughly equal proportions of YAG and N-α wollastonite rather than mostly YAG as evidenced with Syalon 201. This is believed to result partly from localised differences in the residual glass composition after sintering and from local inhomogeneities due to the preferential absorption of yttrium by the α' species. This behaviour is discussed in detail in Section V.4.

Increasing the Y_2O_3 content gave materials with higher densities which again showed good correlation with the theoretical values calculated from the method of mixtures. The final α'/β' ratios and the type of phases recrystallised were unchanged although increased amounts of glass remained after sintering. EDAX analysis showed that the α' phase was slightly more rich in yttrium in these higher Y_2O_3-containing materials.

Decreasing the Y_2O_3 content with a constant 16 wt.% polytypoid, zero Al_2O_3 material resulted in incomplete densification and subsequently lower amounts of α' evolution.

3. Reaction Sequences in the Formation of Yttrium α'+β' Sialon Ceramics

The sequence of reactions leading to the formation of yttrium α'+β' sialon materials was investigated by firing compacted compositions at temperatures between 1000-1800°C, in 50°C intervals,

with a duration of 5 hours at temperature. This firing period, although rather lengthy, allowed a more accurate determination of which reactions contribute most to the densification process than had previously been covered (Sun et al. 1985; Walls, 1986). For the α'+β' phase evolution study the composition based on 16 wt.% 21R polytypoid, 6 wt.% Y_2O_3, and zero Al_2O_3 was investigated since this had produced the most α' in earlier tests. Samples of Syalon 101 and Syalon 201 were included in the sintering runs for comparison to verify the role played by increased polytypoid additions and because the reaction chemistry of their formation is reasonably well understood. In an effort to investigate the β → α' and β' → α' transformations compacts with the same composition as for the α'+β' experiments, but made up with β-type silicon nitride as the starting powder (supplied by Denka; grade SS: > 90% β, < 10% α, see Table III.1), were also included. The compositions prepared, densities, and relative proportions of crystalline phases identified after sintering are listed in Table V.2. Schematic representations of density versus temperature, in conjunction with phase evolution for the α-Si_3N_4 and β-Si_3N_4 based compositions respectively are shown in Figures V.2 and V.3, and representations of the Syalon 101 and 201 systems are presented in Figures V.4 and V.5.

In examining the reaction sequences in the formation of the α'+β' materials the sintering cycle can be split into 3 distinct regimes:-

(i) An initial stage upto around 1300°C where various phases are formed mainly by solid state diffusion reactions between the sintering additives.

Table V.2 Reaction sequences in the formation of yttrium α'+β' sialon ceramics - Compositions investigated

Composition Description	Wt.% constituents					As pressed density (20,000 psi) g cm^{-3}
	Si_3N_4	Supplier/ Grade	ZrO$_2$	Y_2O_3	Al_2O_3	
α-Si_3N_4 based	78.0	Kennametal	16.0	6.0	0	1.66
β-Si_3N_4 based	78.0	Denka BS	16.0	6.0	0	1.76
Syalon 101	85.3	Starck LC 10	3.0	7.7	4.0	1.92
Syalon 201	82.0	Kennametal	8.0	6.0	4.0	1.68

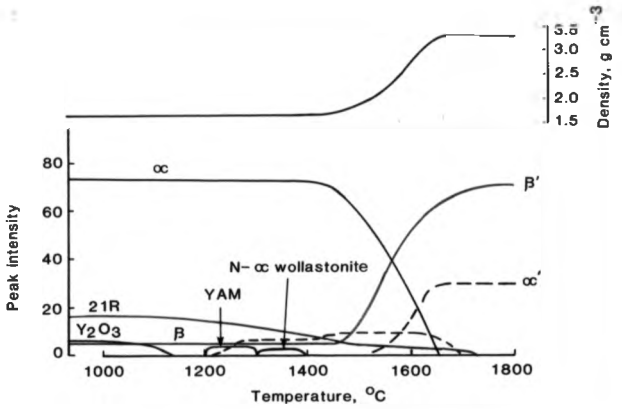

FIG. V. 2 REACTION SEQUENCES IN THE SINTERING OF THE α-Si_3N_4 BASED COMPOSITION vs. DENSIFICATION

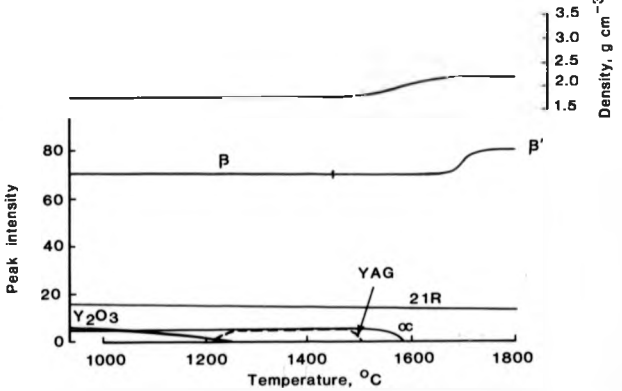

FIG. V.3 REACTION SEQUENCES IN THE SINTERING OF THE β- Si_3N_4 BASED COMPOSITION vs. DENSIFICATION

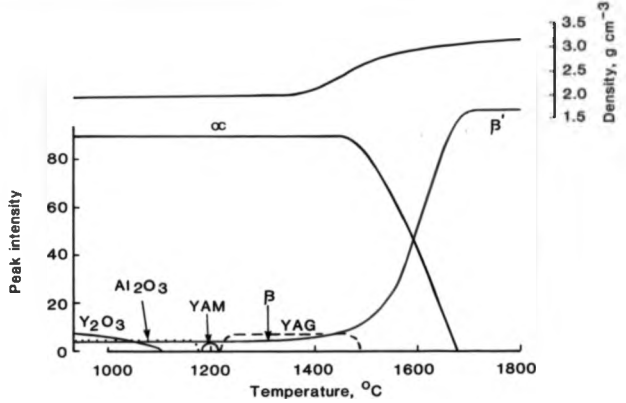

FIG. V. 4 REACTION SEQUENCES IN THE SINTERING OF SYALON 101 vs. DENSIFICATION

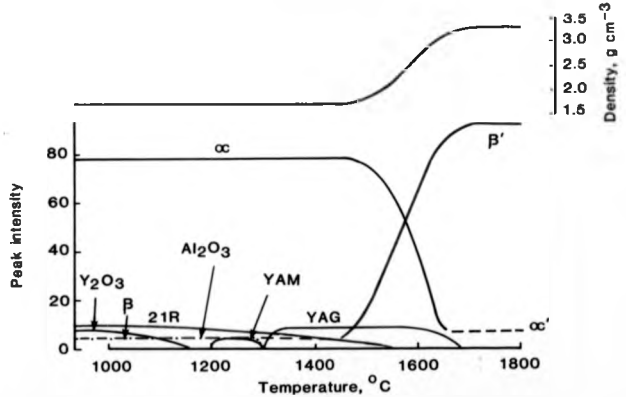

FIG. V. 5 REACTION SEQUENCES IN THE SINTERING OF SYALON 201 vs. DENSIFICATION

(ii) An intermediate stage from 1300°C to 1550°C involving liquid formation coinciding with dissolution of the additive phases and accompanied by the onset of the bulk Si_3N_4 solution/reprecipitation mechanisms.

(iii) The latter stage of the sintering cycle 1550 to 1800°C where the competing reactions of α' and β'-sialon precipitation, together with an overall reduction in liquid volume, tend towards equilibrium.

3.1 Reaction Sequences up to 1300°C

From 1200°C to 1300°C, in the α'+β' composition, YAM ($Y_4Al_2O_9$) was formed, and from 1250°C onwards a significant amount of YAG was also much in evidence. It is unlikely that there was any liquid in the system at this stage since the Y_2O_3-Al_2O_3-SiO_2 eutectic lies at ~1350°C (Bondar and Galakhov, 1963) so it seems plausible that these phases result from solid state diffusion reaction between the Y_2O_3 and the Al_2O_3 on the surface of the polytypoid powder. It is interesting that the intensity of the Y_2O_3 peaks on the diffractometer traces steadily decreased between 1000-1150°C and had completely disappeared before any YAM or YAG precipitated. There was no measurable increase in density, reinforcing the argument for no significant liquid formation, and the only other change which was discernable was a very minor decrease in the intensity of the polytypoid peaks. It is difficult to explain the underlying mechanisms of the decrease in Y_2O_3 peak intensities but it seems reasonable to suggest that the Y_2O_3 does form some small volume of liquid with the impurities in the other powders. It is unlikely that the Y_2O_3 becomes amorphous, and, since yttrium has a high scatter factor it is doubtful that it could form

some crystalline product by solid state mechanisms which could not be detected by X-ray diffractometry. It is strange however that no other researchers have reported similar observations, although little work has been carried out firing these materials at temperatures between 1000-1300°C for long periods.

Similar phenomena were observed with both Syalon 201 and Syalon 101. With 201, the emergence of YAM mirrored the behaviour of the α'+β' composition. From the intensity of the peaks on the diffractometer traces it appeared that the added Al_2O_3 played no part in the reaction. With the 101 composition hardly any YAM was produced even though the Y_2O_3 disappeared as before. This composition contained very little polytypoid and again the Al_2O_3 peaks appeared unaltered. It must be concluded that the Al_2O_3 for the YAM formation comes solely from the polytypoid. It must be more reactive than the added Al_2O_3, probably because it is present as an inhomogeneous surface film which is weakly bonded and very likely contains a higher proportion of impurities.

With the β-Si_3N_4 based composition no YAM was precipitated, and, unlike the other materials, small traces of Y_2O_3 still remained after firing for 5 hours at 1250°C even though there was a substantial amount of polytypoid, and hence surface Al_2O_3, present. This suggests that the α-type starting powder somehow influences the solid state reaction process between the Y_2O_3 and Al_2O_3. At this temperature it is unlikely that the Si_3N_4 itself plays an active role. The phenomenon is more probably related to the difference in surface oxide (ie. SiO_2) content of the α and β powders (manufacturers claim < 1.0% O for the β compared with 2-2.5% for the α) although the underlying mechanism by which this may occur is unclear.

With the Syalon 101 and 201 compositions the YAM and YAG never existed together. The evolution of YAG was particularly abrupt and coincided with an equally abrupt reduction in the intensity of the peaks of the added Al_2O_3. With the 201 composition in particular the initial emergence of YAG also clearly coincided with the disappearance of the YAM just below 1300°C (see Figure V.5). The total volume of YAG evolved, ~ 8 vol.%, indicates that the constituents of the YAM contributed to its formation.

In summary, it appears that YAM generally forms at a lower temperature than YAG, but some YAG may be precipitated when there is sufficient Al_2O_3 present on the surface of the 21R polytypoid. The bulk of the YAG formation during warm-up occurs when sufficient energy is supplied for activation of the reaction between the Y_2O_3 and added Al_2O_3 powder. This also coincides with the dissociation of any YAM which may have formed earlier.

3.2. Reaction Sequences from 1300°C to 1550°C

After firing the α'+β' composition for 5 hours at 1300°C, all of the YAM had disappeared and small traces of N-α wollastonite ($YSiO_2N$) had precipitated. These persisted upto 1400°C before dissociating and dissolving into the liquid. At temperatures up to 1350°C there was no detectable increase in density. With no Al_2O_3 added to the starting mix there would be very little liquid formed when the Y_2O_3-SiO_2-Al_2O_3 eutectic temperature was reached.

The Syalon 201 composition behaved in a similar way. After firing at 1350°C there were no signs of densification, even though the starting mix contained the same proportions of Y_2O_3 and Al_2O_3 sintering additives as the Syalon 101 composition which showed a 12% increase in density over the same temperature cycle. The liquid

formed in the 201 system is more rich in nitrogen and consequently has a higher viscosity. At 1350°C the viscosity must be so high that the mobility for particle rearrangement is negligible.

The onset of positive densification in both α'+β' and Syalon 201 compositions occurred around 1450°C. This was highlighted by a reduction in the amount of α-Si_3N_4 present and the evolution of the first few β'-crystals. Clearly, the sintering liquid had become much more fluid and the process of solution-reprecipitation had commenced. In the Syalon 101 and β-Si_3N_4 based compositions this densification threshold also coincided with dissolution of the YAG which had formed earlier.

The emergence of β'-sialon corresponding with the initial major increase in densification is in direct contrast to Walls (1986) who recorded the precipitation of α'-sialon first as low as 1400°C. Walls also concluded that the α' thus generated had largely expanded unit cell dimensions, indicating high cation substitution, which probably resulted from formation in an Al_2O_3 rich liquid. (Walls used AlN in the preparation of his compositions rather than 21R polytype (6AlN.SiO_2). To achieve the same O/N balance more Al_2O_3 had to be added). As the reaction process proceeded the solution of the Si_3N_4 phase caused further diffusion to take place and at equilibrium the α' phase had reverted to a lower substituted state. In the present study α' precipitation did not begin until above 1500°C and was characterised by a significant reduction in the amount of polytypoid present. No large lattice expansion was evident. Presumably, enough polytypoid had dissolved into the liquid at this point to give nitrogen saturation which then triggered the α' formation. As discussed in Section II.2 the precipitation of α' rather than β' is favoured from a nitrogen saturated glass but there has to be a

suitable concentration of modifier cations, in this case Y^{3+}, for this to occur. In the present material α' precipitation occurred from a convenient nitrogen containing liquid, from which some Al and O had been removed (by the precipitation of β'), rather than from an Al and O enriched nitrogen saturated liquid as in Walls' case. Hence the α' structure formed in the present material avoided the interim 'high-lattice' substituted state.

3.3. Reaction Sequences Above 1550°C

Between 1550-1650°C the α/α' peaks appeared as doublets on the diffractometer traces, particularly at high 2θ angles, increasing the temperature giving higher α' intensities and correspondingly lower α ones. With all compositions, after 5 hours at 1600°C virtually all of the original α-Si_3N_4 starting powder had disappeared and, with the exception of the β-Si_3N_4 based material, densities of over 98% theoretical had been attained. Upon firing above 1650°C these materials became fully dense and no other products were precipitated.

With the β-Si_3N_4 based composition the polytypoid level remained almost constant throughout; ~ 14 wt.% remained after firing for 5 hours at 1800°C compared with 16 wt.% added initially. The bulk of densification occurred between 1450°C and 1650°C, as with the other materials, but the maximum density achieved, 2.31 g cm^{-3}, was still only 71% of theoretical. The β was converted to β' above 1450°C almost certainly by inter-diffusion of aluminium from the small amount of polytypoid and surface impurity Al_2O_3 which had gone into solution, and some oxygen from the Y_2O_3 dominated liquid. The small volume of α-Si_3N_4 present in the Denka powder was converted to more β'-sialon at 1600°C and above. Apart from transformation of this small amount of α-Si_3N_4 there was no other evidence that solution-reprecipitation had

occurred within this composition. The intensity of the β and β' peaks during the β → β' transition remained constant and the low densities attained further emphasize that particle rearrangement was the principal densification method.

With conventional sialon materials α-Si_3N_4 has long been recognised the essential pre-requisite in obtaining good densities with pressureless sintering. Full densification has only been achieved with β-Si_3N_4 based materials by incorporating a step involving some hot-pressing. The driving force for rearrangement is derived from the inter-particle capilliary attraction when the liquid is formed. When this is the only densification process, and there is insufficient liquid to fill all the voids, the material does not fully densify. Hot-pressing provides the necessary additional driving force by compacting the particles into closer proximity.

In a normal Syalon sintering process the temperature is ramped up to 1600°C as quickly as possible taking care to avoid cracking the components by forming excessive thermal gradients. The temperature is then held for 2 hours to allow the mix to homogenise before ramping upto 1750°C and completing the firing cycle. In the current study rapid heating was expected to suppress the formation of some of the YAG and the other intermediate species and leave more liquid available for α' formation. At 1600°C the rate of α' evolution was greater than the rate of precipitation of β' (see Figure V.2) so including this hold ought to have allowed more α'-sialon to form. This was found to be the case. The α'+β' material prepared by firing for 2 hrs at 1600°C followed by 5 hrs at 1750°C had an α':β' peak ratio of 55:45 compared with 30:70 when fired for 5 hrs at 1750°C alone.

In practice the evolution of the α' and β' phases is not as simple as described above. At temperatures in excess of 1550°C the

$\alpha \rightarrow \alpha'$, $\alpha \rightarrow \beta$, $\beta \rightarrow \alpha'$ and $\beta \rightarrow \beta'$ reactions all compete for the available liquid, but more importantly the reactions which dominate depend on the composition of the liquid, and this varies throughout the firing cycle. In the material in the present study the $\alpha \rightarrow \beta'$ reaction is dominant until sufficient nitrogen has dissolved into the liquid then the $\alpha \rightarrow \alpha'$ reaction takes over. Even though no α' was precipitated in the β-Si_3N_4 based composition the $\beta' \rightarrow \alpha'$ transformation may take place (Walls, 1986). It is possible that once the evolution of α' has reached a certain level which leaves the liquid depleted of Al or O some of the β' may redissolve to give more liquid which could then provide additional 'stock' for further α' precipitation, either by direct crystallisation or by dilution of the existing α'-sialon phase. The α' and β' reactions are thus synergetic dependent upon both liquid composition and temperature. Equilibrium is only achieved during sintering when all the solution-reprecipitation transformations have reached a balanced accord.

Extending the dwell times at 1750°C had very little influence on the $\alpha':\beta'$ peak ratios. Re-firing or raising the final temperature to an 1800°C hold left the material unchanged except for a minor increment in density. It appears that the standard sintering cycle for Syalon 101 (i.e. 1600°C/2 hrs followed by 1750°C/5 hrs) is sufficient to take the reactions in this material to completion.

4. Microstructure of the As-sintered Materials

In evaluating the microstructure of the current $\alpha'+\beta'$ sialon compositions it was considered advantageous to prepare samples of materials in accordance with the directions outlined in U.K. Patent Application No. GB 2118927A (Kennametal Inc., 1983), the groundwork for the development of Kyon 3000 ($\alpha'+\beta'$+glass material) for

comparison. 17 example compositions are described in this report but only the two nearest in composition to the material under consideration in the present study (78 wt.% Si_3N_4, 16 wt.% 21R polytypoid and 6 wt.% Y_2O_3) were prepared. Table V.3 lists the initial formulation, processing stages and percentage of phases identified after sintering. Results published in the Kennametal patent and from the $\alpha'+\beta'$ material currently being investigated are also included for comparison. Essentially, the main differences in processing are the firing temperature and hold times. Kennametal fire for short times (~ 1 hr) at very high temperatures, close to the dissociation temperature of the silicon nitride itself. They also maintain that all of the products contain 0.1 - 10 wt.% residual glass after firing. In practise the densities obtained were below 98% of the values quoted and in both cases less than 30% α' had been precipitated compared with over 55% claimed.

The microstructures of both of the Kennametal materials were similar and resembled that of Syalon 101 in terms of grain sizes and apparent glass volume, although, instead of ~ 85 vol% acicular β'-sialon grains set in glass matrix, approximately 1/3 were α'-sialon, which generally tended to have a more plate-like rather than needle-like structure, and were less well defined in terms of geometrical shape (Figure V.6). A simple point count and analysis of back-scattered SEM images, utilising a black and white TV monitor fitted with an electronic filter capable of detecting the amount of signal contributing to the various 'grey levels', confirmed that both Kennametal samples contained 10-15 vol.% residual glass. By contrast, this is almost twice the figure that Kennametal report since they refer to weight % rather than volume % present and the glass:β' weight ratio is approximately 5:3. The discrepancy in results probably

Table V.3 Comparison between the present process specifications involved in the preparation of α'+β' sialon materials and those outlined Kennametal in UK Patent Application No. GB 2118927A (1983)

Composition Description	Wt % Constituents				Mill Time (hrs)	Sintering Cycle (°C)	Density (g cm^{-3})	Phases present after sintering		Other
	Si_3N_4	21R polytypoid	Y_2O_3	Al_2O_3				α'	β'	
Kennametal Pat Comp No. 8 (claimed)	81.35	12.11	6.54	0	48	1830/50 mins	3.276	55.7 (relative to each other)	34.2	Y-glass <10 wt.%
Kennametal Pat Comp No. 8 (actual)	81.35	12.11	6.54	0	48	1830/50 mins	3.19	28.5	72.5	~14 vol.% glass
Kennametal Pat Comp No. 16 (claimed)	78.7	13.89	6.48	0.93	72	1780/40 mins 1830/25 mins	3.27	58.5 (relative to each other)	31.5	No other phases present
Kennametal Pat Comp No. 16 (actual)	78.7	13.89	6.48	0.93	72	1780/40 mins 1830/25 mins	3.20	30.2	69.8	~12 vol.% glass
Current α'+β' material	78.0	16.0	6.0	0	72	1600/2 hrs 1750/4 hrs	3.27	55	45	<4 vol.% resid. glass

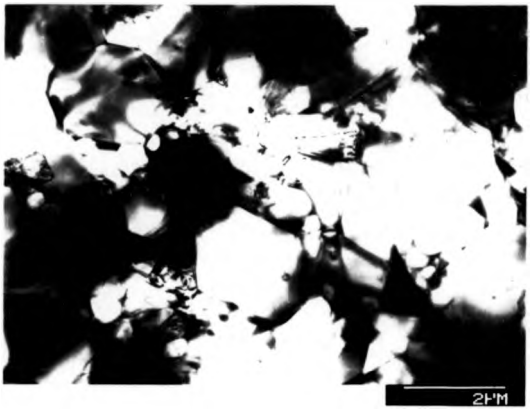

Figure V.6 TEM micrograph of the $\alpha'+\beta'$ sialon material prepared as outlined in UK Patent Application No. GB2118927A (Kennametal Inc., 1983) illustrating the glassy nature (dark areas) of the microstructure rather than full crystallinity as claimed.

partly stems from the different sources of silicon nitride used in make up. The Kennametal patent specifies Elkem* silicon nitride, but because this was unavailable Kennametal's own Si_3N_4, modelled on the same nitriding process route and claimed to have similar levels of impurities and particle size as the Elkem powder, was used instead. This ought to have behaved in a similar way and in practise it seems unlikely that Kennametal would purchase a similar grade powder for their tool tips from another company when they manufacture their own. Presumably, once development of their cutting tool ceramics was complete Kennametal began to generate their own raw materials to reduce production costs.

The 16 wt.% polytype α'+β' material in the present study exhibited an even less well faceted microstructure than the Kennametal compositions and the average grain size was slightly larger. (Figure V.7). The α' species appeared to occupy 70-80 vol.% which is in direct contrast to the 55-57 % value determined using the peak intensity calculation method. It is possible that with the X-ray technique there is some attenuation through internal scattering of the diffracted beam. Clearly the technique described by Grand et al. (1979) is not accurate with high α' content. Repeated tests using the same TV image analysis technique outlined above indicated approximately 3-4 vol.% residual glass. With a lower glass volume there was more sialon grain to grain contact and a much greater abundance of contact flattening. The adjoining interfaces had a high degree of stress related flaws, particularly in the form of dislocations, and tilting in the TEM showed a high concentration of stress patterns associated with such deformities.

---

* Elkem Metals, Norway

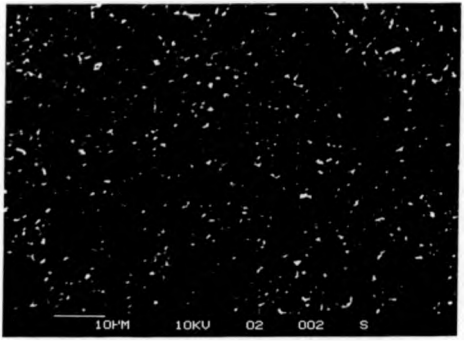

Figure V.7 General microstructure of the 'as-sintered' α'+β' material

Dark elongated needles represent the β'-sialon grains, mid-grey areas are the α'-sialon phase and bright areas are the residual glass.

In the series of materials with increased polytypoid additions and 4 wt.% Al_2O_3 the glass volume decreased as expected: from ~ 14 vol.% remaining with no polytypoid in the starting mix to ~ 7-8 vol.% with 18 wt.% polytypoid added. The α'-sialon platelet content increased from zero to ~ 35 vol.% with the X-ray technique over the same polytypoid addition scale.

With the increasing polytypoid, zero Al_2O_3 series of materials, the decrease in final glass volume was much more apparent. In the compositions with over 14 wt.% polytypoid added to the starting mix the volume of glass remaining after sintering was so reduced that measurement became complicated by uncertainty in the point at which the glass edge (very light grey phase on the TV monitor) merged with the α' boundary (mid-grey) (see Figure V.8). Clearly in trying to distinguish such low levels of minor phase the maximum resolution of the equipment had been reached. The 3-4 vol.% figure for the residual glass content in the α'+β' material is the best estimate from a number of measurements.

The increase in the amount of α' present was more abrupt and visually even more dramatic than the corresponding reduction in residual glass volume. In going from 8 to 12 wt.% polytypoid added the α' content increased almost fourfold giving the materials a much less faceted, less well-ordered, appearance especially in the SEM images.

The compositions with over 18 wt.% polytypoid added still contained small pockets of residual glass even though the XRD traces showed some unreacted α. X-ray diffractometry using the Hagg-Guinier camera also showed small traces of unreacted AlN but these could not be identified with the electron microscopes.

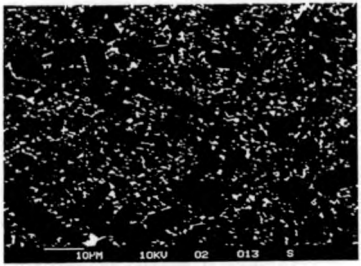

TV monitor image

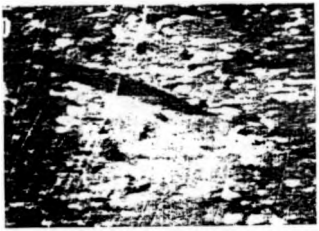

(Poor quality results from having to take polaroid image from TV screen. Unfortunately this was the only system available)

Image with the signal contributing to the secondary phase removed indicating 3 vol.% present

Figure V.8 General microstructure of the 'as-sintered' $\alpha'+\beta'$ material illustrating the technique for evaluating the residual phase volume and the difficulty in distinguishing between the various grey levels

The materials with low residual glass volumes often contained small traces of YAG after sintering. It is unlikely that these formed during the firing cycle but crystallised at favoured nucleation sites, for example points of high stress or discontinuities associated with increased grain contact, upon cooling.

5. Microstructure of the Annealed α'+β' Material

The bulk microstructure of the annealed α'+β' material (starting composition 16 wt.% polytypoid, 6 wt.% Y_2O_3, zero Al_2O_3) was distinct from that of any other sintered sialon or silicon nitride. Whilst similar in appearance to the early hot-pressed silicon nitride materials, instead of mainly single-phase β-Si_3N_4 crystals bonded together with a minor glass residue, this material consisted primarily of plate-like α' sialon grains interspersed with secondary acicular β' grains and small isolated equiaxed crystals of YAG, with curved rather than straight facets, at some of the triple points (Figure V.9). High resolution lattice imaging showed that there was no film of residual glass sandwiched between the sialon grain interfaces, as seen with the hot-pressed materials (Figure V.10), and dark field imaging, using diffracted beams from the YAG phase only, revealed that small numbers of YAG crystals in close proximity with each other diffracted at tilts which differed by no more than 1 or 2 degrees (Figure V.11). This phenomenon is synonymous with the similar long range orientation seen in the annealed β'+YAG materials but here the linearity only extended 3-4 μm rather than 200-300 μm.

As outlined in Section IV.3.2 Lewis and Lumby (1983) first described a similar granular microstructure near the surface of β'+YAG materials after hundreds of hours exposure in a highly oxidising environment. It was concluded here that the non-stoichiometric

α'+β' sialon with isolated pockets of YAG

Single crystals of β'-sialon with virtually no residual phase

Mainly β'-sialon grains with interconnected secondary YAG

Figure V.9 Comparison of sialon ceramic microstructures

a) The current annealed α'+β' sialon material
b) Typical hot-pressed sialon
c) Typical β'+YAG sialon

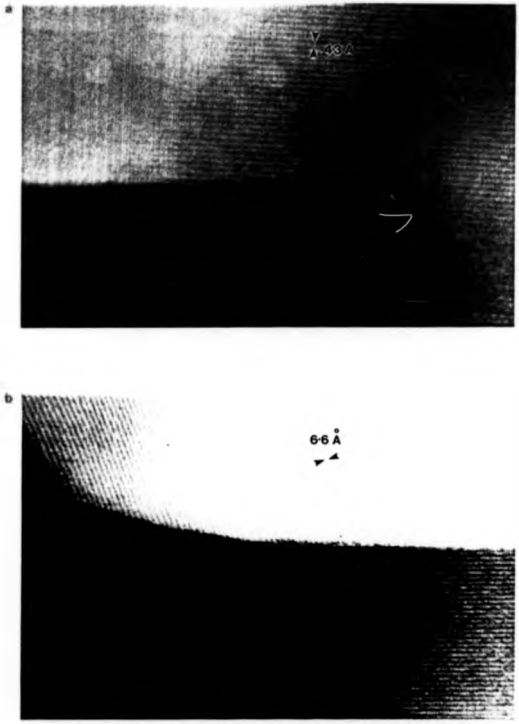

Figure V.10 High resolution lattice images of adjacent grain boundary interfaces in the α' + β' + isolated YAG (a) and Syalon 201 (b) materials, illustrating the receptiveness to the non-stoichiometric metallic ions of the α' phase and the consequent removal of the residual elements at the grain boundaries. The residual layer in b) is no more than a few atoms thick.

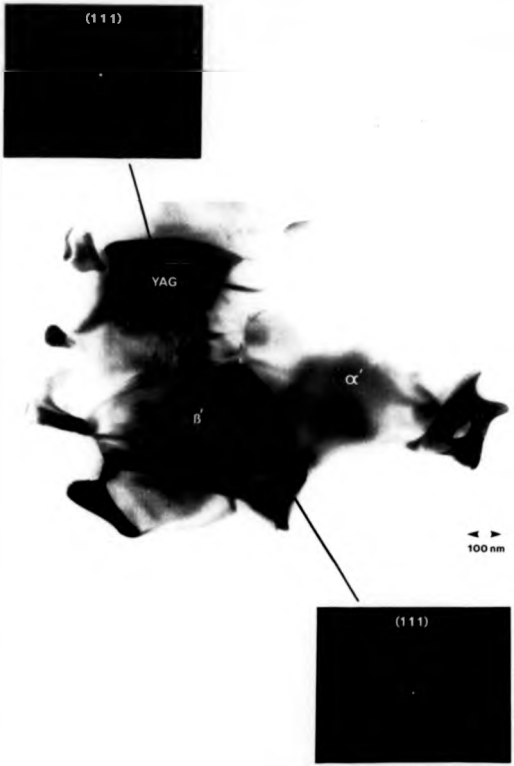

Figure V.11 Micrograph of the annealed α′+β′ material illustrating the small volume of recrystallised YAG present with adjacent crystals diffracting at similar tilts

metallic elements had migrated out to the surface oxide layer leaving a greater degree of solid/solid contact. To alleviate the imbalance in surface tension energies acting along the β'/YAG and β'/β' interfaces the YAG crystals had been transformed by diffusive rearrangement to a more rounded equiaxed grain configuration (Figure V.12).

In the present material the transformation had occurred throughout the bulk. The α' phase must have acted as an effective sink for the non-stoichiometric metallics to give the necessary grain to grain contact. (In the β'+YAG material the Y^{3+} ions cannot be accommodated within the β' structure, hence proper grain boundary contact could only occur when these ions were removed by some other process i.e. oxidation). Full transformation was rapid, occurring over a few hours, compared with hundreds of hours for the surface oxidation activated route, indicating how complete the absorption process must be. It is unlikely that the interfacial energy associated with α'/YAG and α'/β solid/solid contact is very different from that associated with β'/YAG, and β'/β', and since the energy difference between β'/β' and β'/YAG solid contact is considered to be negligible, the overall driving force for the rearrangement process should be similar. The impetus for such a rapid transformation must be derived solely from the requirement to balance the surface energies acting along the grain interfaces. In a fully crystalline medium it is energetically favourable for the interface energies acting towards a point to adopt a more isotropic configuration. Figure V.13 shows a schematic representation of how the bulk transformation is believed to occur. After sintering, the liquid fills the grain junction channels and there is a high degree of energy anisotropy (the individual sialon grains having a highly faceted morphology). Upon annealing, the

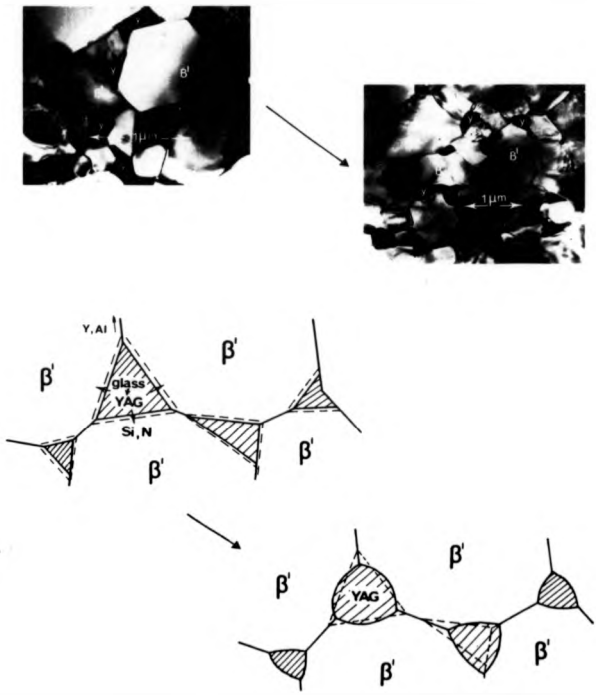

Figure V.12 Illustration of the change in microstructural morphology near the surface of β'+YAG materials following long term exposure in an oxidising environment. Excess Si and N diffuse into the β', and Y and Al migrate out to the surface oxide layer leaving increased solid/solid contact. The interfacial energy anisotropy is reduced with the consequential rearrangement of the YAG to a more isolated granular form.
(after Lewis et al. 1984)

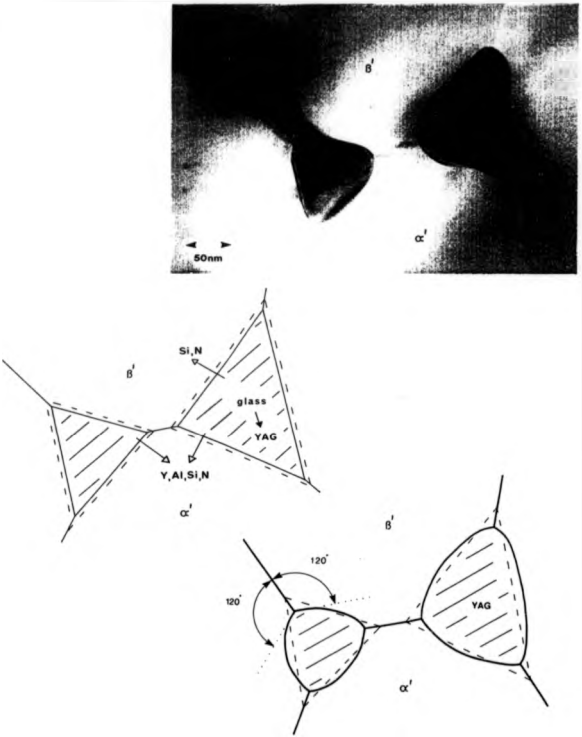

Figure V.13 Illustration of the bulk mechanisms involved in change of YAG morphology in the α'+β' material. Upon crystallisation excess Si and N diffuse into the sialon grains but the α' phase is also receptive to the other non-stoichiometric metallic ions which results in increased solid/solid contact throughout the bulk. To equilibriate the imbalance in interfacial energies the YAG crystals are rearranged to a more isolated granular form

interfacial contact energies try to balance each other by effecting realignment. In trying to adopt a more isotropic morphology and achieve the balanced 120° equilibrium position the faceting is relaxed in favour of more curved boundary configurations.

The short range similar crystal orientation suggests that after sintering localised pockets of glass are interconnected via thin films sandwiched between the sialon grains (as in Syalon 201 after sintering). The YAG must nucleate at the contact points and grow rapidly during the early stages of the anneal cycle, partially encapsulating the sialon grains which each crystal spans. The unwanted metallics are probably simultaneously absorbed by the α' phase and then the YAG is transformed to the equiaxed shape with adjacent crystals, which once formed part of a larger single crystal, then having similar lattice orientations.

For good homogeneity and to achieve complete transformation the ideal material should contain at least 50% α' to ensure that the non-stoichiometric elements trapped at the interfaces are in contact with an α' grain and hence have somewhere to diffuse to.

The XRD traces indicated that N-α wollastonite typically constituted upto 15% of the products precipitated upon devitrification. By contrast Syalon 201 typically contains upto 5 vol.% N-α wollastonite. (In a 5 component system upto 5 phases may exist at equilibrium). Due to the small volume and microstructural nature of the minor phases it was difficult to distinguish between the wollastonite crystals and those of YAG by electron diffraction. EDAX analysis allowed some differentiation between the two phases but here the results were unreliable because repeated analysis indicated that some of the YAG crystals contained significant amounts of silicon (Figure V.14).

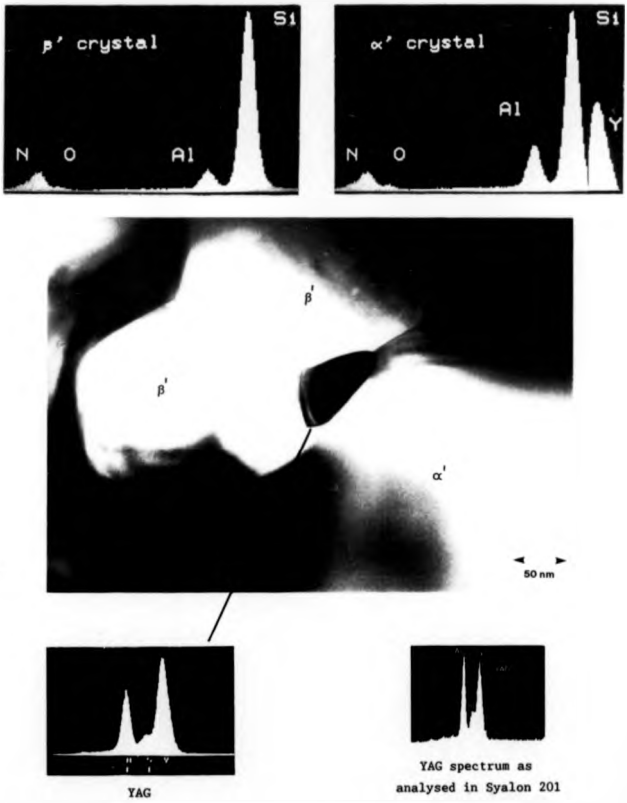

Figure V.14 Microstructure of α'+β'+isolated YAG material. EDAX analysis of the YAG crystals indicating reduction in the aluminium content and significant silicon solution

Sun et al. (1988) recently presented evidence for a small range of silicon solid solubility in YAG. Some silicon is normally observed when analysing YAG in sialon materials due to the inevitable fluorescence of silicon from the surrounding β'-grains, but in the present material the levels detected were much higher than that normally expected and the relative intensities of the Al k peaks were reduced in proportion. Hardly any nitrogen was detected with the low atomic number element detector adding further support for some Si solid solution.

The precipitation of N-α wollastonite rather than just YAG is probably partly due to the small excess of oxygen in the starting composition and to local variations in the glass composition after sintering. Extensive analysis tended to indicate that the triple points in which wollastonite had crystallised were bounded mainly by α'-sialon grains, but the results were speculative because contact could only be established in two dimensions rather than three. It seems possible that once crystal growth has isolated small areas of liquid during the sintering process, prolonged heating could encourage some preferential removal of particular elements by diffusion into the surrounding grains. This would then leave small encapsulated areas of glass, of slightly different composition from the remainder, from which wollastonite precipitation could be formed upon annealing. The α' phase is more receptive to absorption of the metallic cations than the β', and where the liquid is bounded solely by the crystallisation fronts of growing α'-grains, the preferential removal of these particular elements may cause the remaining liquid to achieve a composition which is Al deficient and from which further α' precipitation cannot take place. Upon annealing the composition of the resultant glass may favour N-α wollastonite crystallisation rather than YAG.

EDAX analysis of the level of aluminium substitution in the β'-sialon phase gave a measured average z-value of 0.97. The value calculated from the d-spacings observed with the Hagg-Guinier camera was z = 1.2. Both values are in good agreement with the range of z-values, obtained by Walls (1986), over which α' and β' may co-exist.

6. Summary

The formation of α' in the preparation of sialon materials offers the potential of incorporating the sintering additives into the Si_3N_4 structure upon densification. The fabrication of pure α' or α'+β' sialon materials is extremely composition sensitive and impractical on a commercial basis.

The preparation of α'+β'+glass materials allows more compositional freedom and greater flexibility. Such materials are increasingly finding use in the metal cutting industry where the additional advantage of increased hardness afforded by inclusion of the α' species leads to greater surface cutting speeds and improved durability.

By careful control of the starting composition it is possible to generate a material with a minimal amount of residual glass which may be fully recrystallised with a post sintering heat treatment to give essentially an α'+β'+YAG ceramic. During the devitrification of such small volumes of glass the α' phase absorbs the non-stoichiometric elements and the YAG crystals produced undergo diffusive rearrangement to equilibrate the imbalance in energies acting along the solid/solid interfaces. The YAG crystals adopt to an isolated equiaxed granular morphology and with no residual phase between the sialon grains this material is expected to offer improved high temperature capabilities compared with conventional β'+YAG ceramics.

CHAPTER VI. MATERIAL PROPERTIES

1. Physical Properties

1.1 Appearance

The physical appearance of the Nd_2O_3 - substituted materials was similar to that of their yttrium counterparts except that highly polished surfaces generally tended to show a darker charcoal grey colouration. Polished surfaces of the $\alpha'+\beta'+$isolated YAG material were also darker grey in colour (Figure VI.1).

The variation in colour and opaqueness of sialon materials has been attributed mainly to the volume of secondary phases present. Silicon nitride has an associated light-energy absorption band-width and pure materials are generally black in appearance. Increasing the volume of secondary phases present increases the reflectivity which results from a shift in the overall absorption band-width to generate the lighter grey colour. To interpret the difference in colouration between similar materials, such as the equivalent Nd and Y β'+glass sialons, other factors must be taken into consideration. Mitomo et al. (1982a, 1982b) have attributed some minor variations in colour and reflectivity to the specific transition ions present in the sialon glass and to the inherent levels of porosity. Since the materials under examination in the present work are considered to be fully dense the former description most probably forms the basis for the variation.

1.2 Density

With full densification, compositions based on a Nd_2O_3, rather than Y_2O_3, sintering additive had a higher density. Nd_2O_3 has a higher molecular weight than Y_2O_3 so from the method of mixtures,

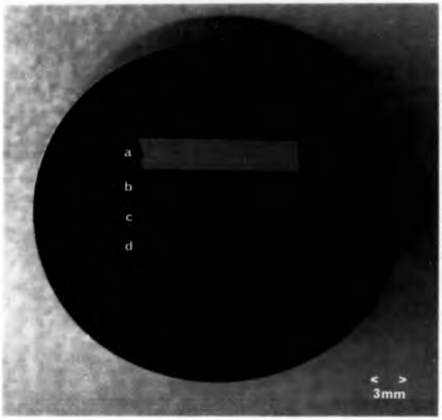

Figure VI.1 Illustration of the variation in colour of the sialon materials investigated

a) Syalon 101

b) Syalon 201

c) $\alpha' + \beta' +$ isolated YAG

d) $\beta' + Nd_3Si_3Al_3O_{12}N_3$

assuming that similar reactions take place, some increase was predicted. The molecular weight of Nd_2O_3 equates to 7.24 g cm^{-3} compared with 5.01 g cm^{-3} for Y_2O_3, and fully densified Nd_2O_3-fluxed materials had a typical density of 3.37 - 3.38 g cm^{-3} compared with 3.25 - 3.26 g cm^{-3} for equivalent Y_2O_3-based versions.

For the α'+β'+isolated YAG material full density was increased from 3.25 - 3.26 g cm^{-3} to 3.27 g cm^{-3}.

2. Mechanical Properties

2.1 Fracture Toughness

The results of the fracture toughness measurements on the materials generated are listed in Table VI.1. The values for Syalon 101 and Syalon 201 are included for comparison.

The toughening mechanisms relating the empirical fracture toughness properties to the underlying ceramic microstructures are well understood (see Section II.7). At low temperatures, in materials consisting of an array of acicular β'-sialon grains set in a minor matrix phase, the mechanisms of crack tip deflection toughening, micro-cracking, and pull-out or crack bridging in the wake of an advancing crack-front are predominant. These processes are fairly insensitive to temperature upto the transition temperature (T_g) of any glass present, whereupon the effects of creep cavitation and viscous flow become the determining factors.

The Nd_2O_3 substituted materials achieved similar microstructures to the pressureless-sintered yttrium sialons and hence exhibited similar property characteristics. The measured fracture properties can be interpreted in the same way according to the toughening mechanisms outlined above. The actual K_{IC} values were marginally higher which is probably due to the slight increase in number and size

Table VI.1 Results of the fracture toughness measurements

Material	Measured K_Ic value MPa $m^{½}$
Syalon 101	7.7 ± 0.2
Nd-based Syalon 101 equivalent	7.8
Syalon 201	5.5
Nd-based Syalon 201 equivalent	5.6
β′+$Nd_3Si_3Al_3O_{12}N_2$ (anneal 1200°C/5hr)	6.1
β′+50/50 $NdAlO_3$/Nd N-α wollastonite	5.1

Table VI.2 Summary of the modulus of rupture measurements

Material	Modulus of Rupture Value MPa (Weibull modulus indicated in brackets)					
Temp °C	20	1000	1100	1200	1300	1400
Syalon 101	945 (11)	760	210	-	-	-
Nd Syalon 101 equiv.	1053 (10)	570	197	-	-	-
Syalon 201	725 (8)	695	-	600	-	500
Nd Syalon 201 equiv.	792 (14)	821	-	614	499	267
β′+$Nd_3Si_3Al_3O_{12}N_2$	909 (10)	850	773	574	355	123
β′+50/50 $NdAlO_3$ / Nd-N-α wollastonite	717 (11)	742	-	654	676	598
α′+β′+isolated YAG	788 (8)	-	-	669	596	622

All values have standard error typically ± 10%

of the elongated β' grains. It appears that having Nd rather than Y ions in the sintering liquid enhances this anisotropic grain growth behaviour although the chemistry by which this occurs is not yet fully understood. The difference in liquid viscosity between equivalent Nd and Y containing glasses at the same temperature is probably partly responsible as is the inhomogeneous nature of early liquid formation resulting from agglomeration of the Nd_2O_3 powder particles during the preparation stage.

The α'+β'+isolated YAG material exhibited fracture toughness properties which were approximately 20% higher than for conventional β'+YAG ceramics. This was rather surprising since the microstructure consisted of a much more isotropic grain morphology and from the formulation above the mechanisms of crack deflection, pull-out, and crack bridging were expected to be less effective. This improvement in resistance to crack propagation is likely to derive from an inherently higher cohesive energy between adjacent sialon grains. The removal of the mono-layers of residual phase sandwiched in the grain junction channels results in an increase in solid/solid contact which may have a higher associated bond energy. Some improvement may be afforded by the increased grain size - the mechanism of internal micro-cracking is determined by average facet size. In addition, in conventional β'+YAG materials there is a minor volume expansion as the glass is devitrified to YAG which generates internal stresses within the material. In the present α'+β' material devitrification is accompanied by the YAG rearrangement process which is seen to alleviate much of this internal stressing which may contribute to the propagation of a crack front.

2.2 Modulus of Rupture

The results of the modulus of rupture tests are summarised in Table VI.2. For fully dense materials MOR is dictated primarily by K_{Ic} via the relationship

$$MOR \propto K_{Ic} \qquad (VI.1)$$

(see equation II.iv). In correlation with the measured fracture toughness properties the Nd-based materials exhibited similar room temperature characteristics to their more conventional yttrium variants. Again the actual values for the Nd_2O_3-substituted materials were marginally higher due to the minor increments in resistance to crack propagation.

At elevated temperatures the mechanism of creep cavitation becomes strength determining. The results from the high temperature MOR tests are presented schematically in Figure VI.2. As with the yttrium Syalon 101 β'+glass material the mechanical strength of the Nd version diminished rapidly above 1000°C once the glass began to soften. When the glass transition temperature is reached the reduction in interfacial cohesive energy results in rapid grain boundary shear. Cavity formation in the triple points resulting from the hydrostatic tension generated there then becomes catastrophic.

The Nd Syalon 201 equivalent material contained less residual glass than the Syalon 101 version and hence exhibited a more gradual reduction in strength between 1000°C and 1400°C, although its performance was significantly poorer than that of conventional Syalon 201.

The β'+$Nd_3Si_3Al_3O_{12}N_2$ material exhibited good strength retention up to 1300°C. This material is fully crystalline and the problems of

Fig VI.2 MOR Degradation of the Nd-based Materials with Temperature

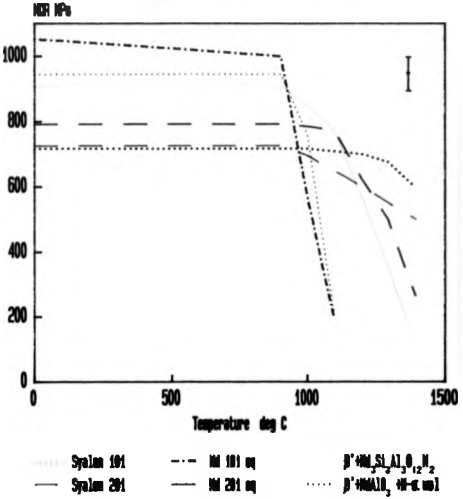

cavitation did not occur until the melting or dissociation of the secondary phase began.

The β'-sialon material with a matrix phase consisting of an approximate 50/50 mix of Nd N-α wollastonite and $NdAlO_3$ showed improved properties up to 1400°C indicating the stability of the secondary phases up to this temperature and a lower volume of intrinsic residual glass compared to Syalon 201.

The results of the MOR measurements on the α'+β'+isolated YAG material are illustrated schematically in Figure VI.3. In accordance with the K_{Ic} dependence, and the improvements in fracture toughness over Syalon 201, the modulus of rupture values at room temperature were also superior. At elevated temperatures this material retained proportionately more strength as the temperature was raised further again reaffirming the importance of achieving full crystallinity to inhibit creep cavitation mechanisms.

2.3. Hardness

The results of the hardness measurements are listed in Table VI.3. The values on the Rockwell A scale are converted to approximate Vickers hardness (kg mm^{-2}) for ease of assessment. Values for mild steel and tungsten carbide are included for comparison.

The values from materials prepared with Nd_2O_3 as the sintering additive were similar to those from materials prepared with Y_2O_3.

With the Y_2O_3 sintered materials the hardness depended upon the polytypoid addition in the starting composition and was proportional to the amount of α'-sialon precipitated. Hardness is determined by the volume of plastic deformation beneath an indentor which is dictated by the resistance to dislocation motion parallel to the

Fig VI.3 MOR Results from the α'+β'+YAG
Material at Elevated Temperatures

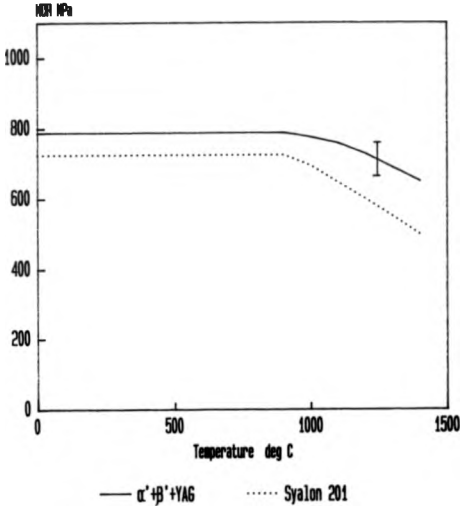

Table VI.3 Results of the hardness measurements

Material	Rockwell Hardness A scale	Equivalent Vickers Micro-hardness Kg/mm^2
Syalon 101	91.1 ± 0.1	1340 ± 5
Nd Syalon 101 equiv.	91.4	1400
Syalon 201	92.4	1595
Nd Syalon 201 equiv.	92.8	1675
β'+$Nd_1Si_1Al_1O_{12}N_2$	92.4	1596
β'+50/50 $NdAlO_3$ / Nd-N-α wollastonite	92.7	1655
α'+β'+isolated YAG	94.5	2010
Mild steel	-	180
Tungsten carbide	92.1	1540

applied stress. Clearly, the greater the resistance, the smaller the affected volume for a given indentation load and hence the higher the hardness. In conventional β'-sialon materials the hardness is governed by the β' species, which normally accounts for over 85 vol.% of the bulk. The hardness is determined by the Burgers vector associated with dislocations through lattice-friction stresses in the c axis direction. Since the c axis dimension, ($c_{\beta'}$-2.91Å) is smaller than the a dimension (a_{β}-7.60Å) the corresponding Burgers vector is smaller and dislocations in this direction are favoured (see Figure II.1). The c axis dimension of the α' species ($c_{\alpha'}$-5.62Å) is not so dissimilar from that of the a dimension. The associated Burgers vector is correspondingly higher and hence the resistance to dislocation motion in the c axis direction is increased. In a mixed phase α'+β' sialon the overall effect is to increase the average Burgers vector and hence the hardness. The measurements on the α'+β'+isolated YAG material represent a 26% improvement in Vickers hardness over Syalon 201 and a 50% improvement over Syalon 101.

VI.3 Creep

The results from the creep tests on the Nd-based materials at 1227°C are presented in Figure VI.4. At this temperature the creep resistance of the β'+50/50 N-α wollastonite/$NdAlO_3$ material was comparable to that of Syalon 201. All of the curves demonstrated the characteristic geometry indicative of the underlying mechanisms of an initial transient stage followed by more steady state deformation after long periods.

The results from the creep tests on the β'+$Nd_3Si_3Al_3O_{12}N_2$ material at different temperatures are illustrated in Figure VI.5. Up to 1300°C the overall strain and steady state strain-rate increased

Fig VI.4 Creep Test Results from the
Nd-based Materials 1277°C 77MPa

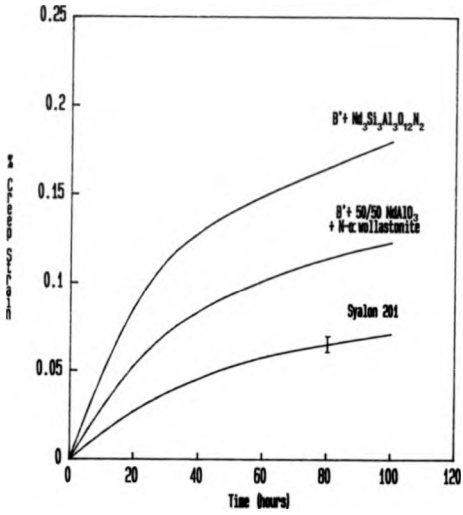

Fig VI.5 Creep Test Results from the $\beta'' + Nd_3Si_3Al_3O_{12}N_2$ material

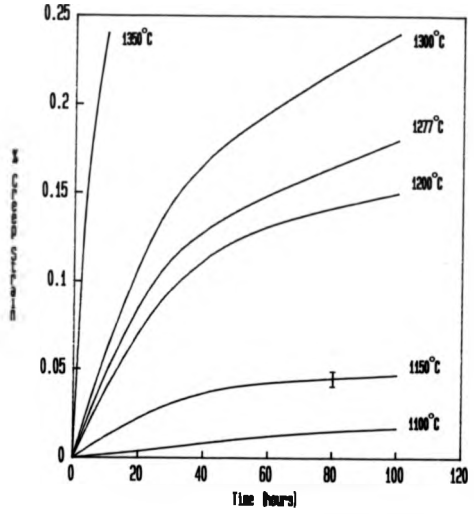

with temperature. Above 1327°C the secondary phase reverted back to a liquid and the mechanisms of creep cavitation and viscous flow became catastrophic.

The results from the creep tests on the increased polytypoid series of materials, with 4 wt.% Al_2O_3 added to the starting composition tested at 1277°C, and without Al_2O_3 tested at 1327°C, are presented in Figures VI.6 and VI.7 respectively. Increased polytypoid additions resulted in enhanced creep resistance which stemmed from the reduction in secondary phase volume. This was most evident with no added Al_2O_3. With both series of materials the creep properties were improved with upto 18 wt.% polytypoid content. Above this level the creep resistance became progressively poor - a reflection of the incomplete densification and presence of some unreacted species.

The α'+β'+isolated YAG material contained no residual glass and after 100 hours at 1277°C, load 77 MPa, the measured creep strain was negligible. After 100 hours at 1327°C the creep deformation was less than 4% of that normally seen with Syalon 201 when tested at the same temperature. Clearly full crystallinity is essential to ensure good creep resistance, but the microstructural morphology forms the underlying rate determining factor. In the steady state, creep is controlled by the rate of material transport. In the conventional β'+YAG ceramics the monolayers of residual glass sandwiched between adjacent grains provide a route for relatively easy diffusional transport of material (see Figure VI.8). In the α'+β'+isolated YAG material there is no residual glass and the bonding between adjacent grains is stronger. Material being transported has to negotiate a much more tortuous path. In addition the diffusion path lengths are longer because the YAG crystals have retreated into the triple points. The strain rate for grain boundary diffusional creep is proportional

Fig VI.6 Creep Test Results 1277°C 77MPa
Effect of increasing 21R (4wt% alumina)

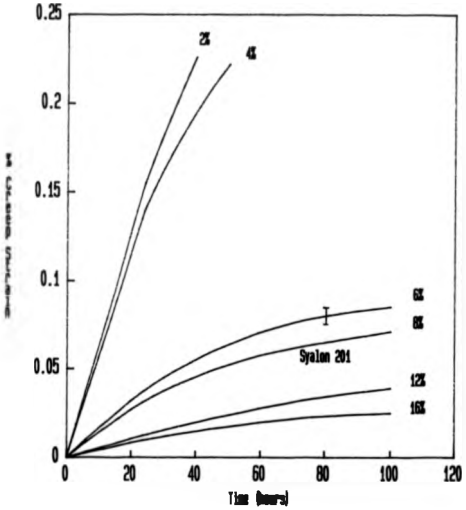

Fig VI.7 Creep Test Results 1327°C 77MPa
Effect of increasing 21A (zero alumina)

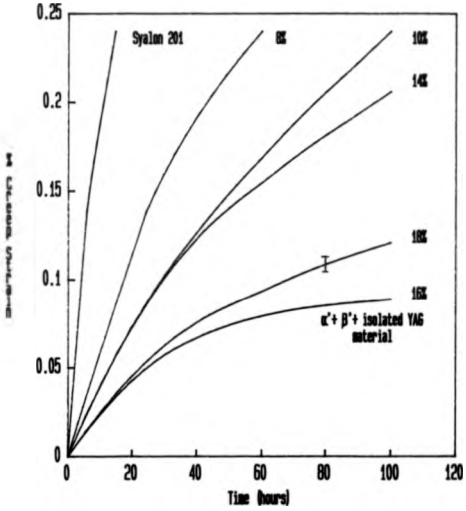

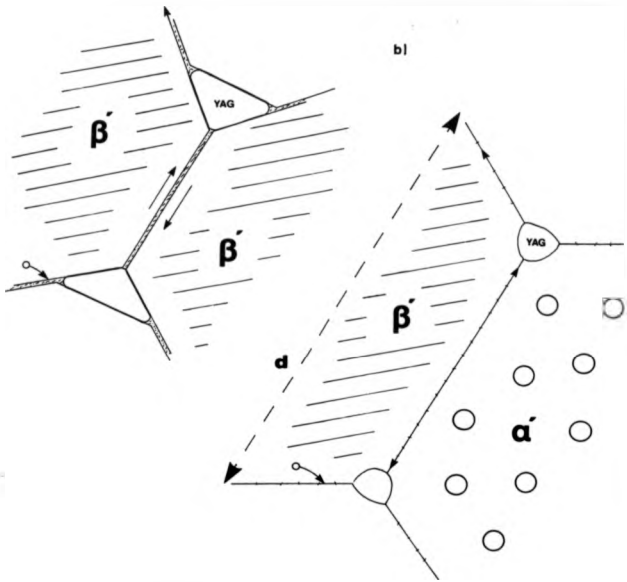

Figure VI.8 Illustration of the underlying mechanisms for the improvement in creep and oxidation resistance of the α′+β′+isolated YAG material. In conventional β′+YAG ceramics (a) the residual glass provides a path for material transport. The α′+β′+isolated YAG sialon ceramic (b) contains no residual glass and material transport is further inhibited by stronger interfacial bonding, larger grain sizes, and longer diffusion path lengths

to $1/d^3$ where d is the grain size and the larger average grain size of the α'+β'+isolated YAG material further enhances its resistance to creep deformation.

4. Oxidation Resistance

The difference in oxidation characteristics between the α'+β'+isolated YAG and Syalon 201 (β'+YAG) materials is illustrated in Figure VI.9. After 50 hours exposure in an oxidising environment at 1300°C the 201 material had developed an oxide layer 30-40μm thick compared with a layer less than 10μm on the α+β'+YAG material.

The whole oxidation process is in accordance with the series of mechanisms outlined by Babini et al. (1984) (see Section II.7 and Figure II.18). In the initial stages, layer formation starts with oxidation of the exposed sialon faces, with rapid metallic ion transport from adjacent YAG crystals also open to the atmosphere at the material surface. The α'+β' material contains less secondary phase for metallic ion feedstock and after only 5 hours the amount of oxide formed is visibly reduced. The initial layer is discontinuous in nature but the oxide areas grow and form a more complete surface film as the oxidation reactions proceed. At 1300°C the layer is not protective; bubbles consistent with nitrogen gas evolution are clearly visible in the micrographs. As the metallic ions diffuse from the bulk into the SiO_2 dominated layer its viscosity is reduced and the increase in concentration of metallics at the outer surfaces encourages the precipitation of more complex oxides. With reduced viscosity the mechanisms proceed more rapidly. The nitrogen bubbles evolve until they burst, disrupting the oxide layer and exposing fresh surfaces for renewed attack. The oxidation process thus progresses into the material with the rate of diffusion of the oxygen and

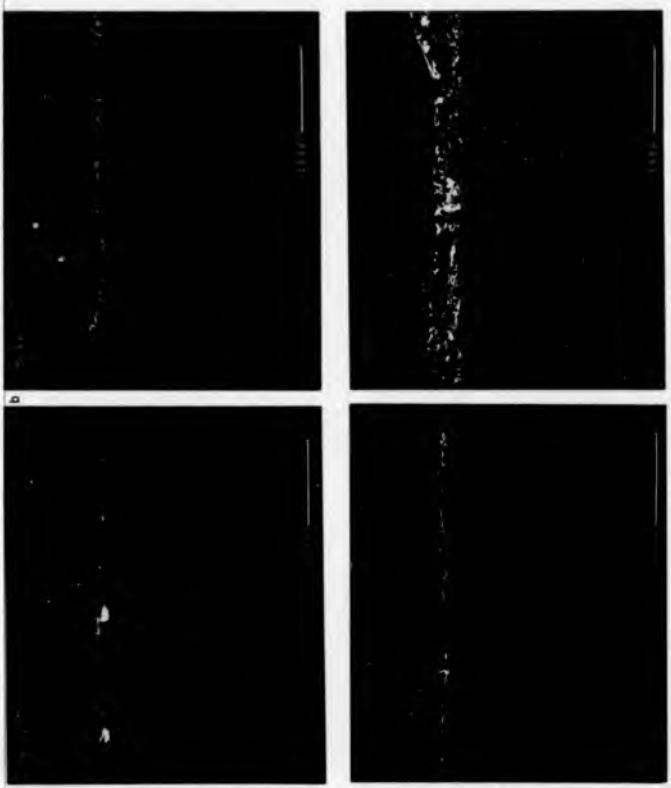

Figure VI.9 Comparison of the formation of an oxide layer on the $\alpha' + \beta' +$ imolated YAG (a) and Syalon 201 (b) materials at 1300°C. Disruption in the oxide layers after 50 hours exposure is consistent with nitrogen bubble evolution

metallic ions determining the rate of ingress. After 50 hours the difference in diffusion rate between the two materials is reflected by a metallic ion depleted layer approximately 60 μm deep in the Syalon 201 materials compared with only 10μm in the α'+β'. Clearly at this temperature the α'+β'+isolated YAG material exhibits superior oxidation resistance to the conventional β'+YAG materials. Again, this can be attributed to the transient liquid phase sintering and consequential removal of the residual grain boundary glass upon annealing, and hence the large reservoir of metallic ions which decrease the oxide layer viscosity and enhance diffusion.

At temperatures much in excess of 1300°C it appears unlikely that the α'+β'+YAG material will demonstrate such significant improvements. At around 1350°C the YAG forms a eutectic with the SiO_2 and the reversion back to a liquid is expected to be catastrophic as with the conventional β'+YAG materials. In addition when the α' species itself oxidises or dissolves into the reformed liquid the release of a significant proportion of metallic ions would further reduce the liquid viscosity and enhance the oxidation process.

5. Summary

The mechanical response of the materials generated within the present research can be interpreted by reference to their physical microstructure and to the underlying mechanisms for property enhancement. The neodymium sialon materials have similar microstructures to their yttrium counterparts and hence exhibit similar property characteristics. The development of Nd materials with a fully recrystallisable glass to give an alternative stable matrix phase has allowed the formulation of high temperature Nd-based

materials with properties comparable to the conventional β'+YAG ceramics.

The yttrium α'+β'+isolated YAG material exhibits superior high temperature properties compared to the conventional β'+YAG ceramics. The removal of all of the residual grain boundary glass and absorption of the non-stoichiometric metallic ion by the α' species upon annealing is essential to minimise degradation through diffusion controlled mechanisms. In achieving an isolated YAG morphology this material behaves in a similar way to a hot-pressed silicon nitride whilst maintaining the enhanced strength characteristics of pressureless-sintered sialon materials. In addition inclusion of the α' species affords this material increased hardness properties.

CHAPTER VII. APPLICATIONS AND PERFORMANCE

1. Introduction to Field Trials

To evaluate the performance of the α'+β' material components were fabricated and tested in applications where Syalon 101 and 201 are fairly well established. These were mainly comparative tests of metal cutting capability and measurement of component life-times in hot metal extrusion. Components were also prepared and tested in applications where the increase in hardness and wear resistance of the α'+β' material was expected to be beneficial in the hope of opening up new markets and generating new business. These were primarily high wear applications involved in cold forming processes, such as metal drawing, and in the transport of abrasive material, for example with shot blast nozzles. A number of field trials were carried out, but many of the components fabricated were still in service after the time-frame of this research and the results could not be fully collated by the time of writing.

1.1 Tool Tips

10 squares of material 12.5 x 12.5 x 4.75 mm were cut from billets of Syalon 101, Syalon 201 and the α'+β'+isolated YAG sialon material and forwarded to De Beers, Ascot for final shaping into tool tips (Figure VII.1). Cutting trials were carried out on cast iron.

The initial results indicated that the α'+β' material exhibited superior cutting properties to those of Syalon 201 which in turn was preferable to Syalon 101. Unfortunately, the data could not be quantified due to the scatter of the results and the time needed to examine and optimise the cutting conditions, i.e. maximum face cut speed and applied cutting force or rate of cut, but the tests did

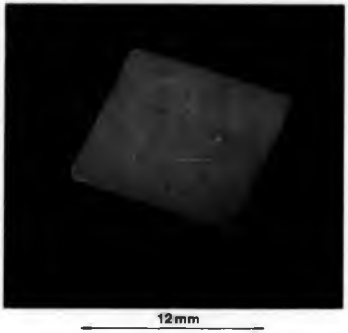

Figure VII.1 Design of the tool tips for the metal machining trials

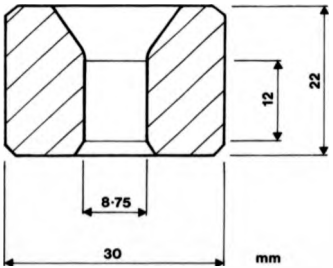

Figure VII.2 Cross-section showing design of the extrusion dies

indicate that if excessive pressure was applied the leading edge of the α'+β' tip was prone to chipping or spalling. This effect was worse with the Syalon 201 material and was believed to be derived from 'snagging' of the metal and from thermal stresses generated by friction at the cutting face. The problem could be partially alleviated by increasing the flow of the cutting fluid which probably improved the cutting performance by reducing the contact friction and by providing additional cooling.

1.2 Extrusion Dies

Hot metal extrusion trials were conducted by Eaton Automotive Spa, Michigan. 3 extrusion dies were supplied in steel support sleeves (Figure VII.2). (It is normal practice to support the die during the metal extrusion operation to ensure that the material is under compression rather than tension which causes failure through 'bursting'.) To maintain their competitive advantage the company would give no specific information regarding their extrusion process except that the dies were used for extruding a standard brass at temperatures typically between 600-900°C. In continuous service normal Syalon dies last 12 to 15 weeks with this process. The die life is defined as the time up until the diameter of the product becomes over tolerance i.e. for these particular dies when the bore size has increased from 8.75 mm dia to 8.90 mm. At the time of writing the dies were still in service having successfully operated for 10 weeks with 'little signs of wear'. Eaton Automotive also indicted that the extruded bar had a superior surface finish.

1.3 Drawing Dies

The α'+β' material was evaluated in cold drawing applications with the full co-operation of Delta Rods Ltd, West Bromwich. Delta Rods are extensive users of Syalon materials for extrusion purposes, but were particularly interested in more durable drawing dies tominimise down-time during their replacement. Syalon 101 and 201 dies had been tested on previous occasions but their performance was only comparable with the more traditional tungsten carbide dies and did not justify the additional cost.

A single die fabricated from the α'+β' material was initially supplied shrunk fit in a steel (H13) case (nominal interference fit 0.4%)(Figure VII.3). Dies fabricated from Syalon 101, 201 and 501 were also supplied for comparative tests in conjunction with the standard tungsten carbide equivalents.

Coils of pre-extruded brass (DIN CuZn 36% Pb 1.5%, 150 kg each), for electrical accessories and lighting fittings, were pulled through the dies, without lubrication, in the configuration illustrated in Figure VII.4. During pulling the temperature of the die typically reached 270-350°C due to the friction generated. The pull rate was approximately 0.35 ms^{-1} and the feed stock size was 6.72 mm dia. pulling down to a start draw size of 6.30 mm dia., i.e. a reduction ratio of 12%. The product became over tolerance and the die had to be replaced when the insert bore size reached 6.35 mm dia. The results for the different materials are illustrated in Figure VII.5.

Clearly the Syalon 501 material was inferior and was not well-suited to this particular application. With extrapolation it can be seen that the Syalon 101 and 201 material exhibited similar lifetimes to the conventional tungsten carbide dies allowing a maximum

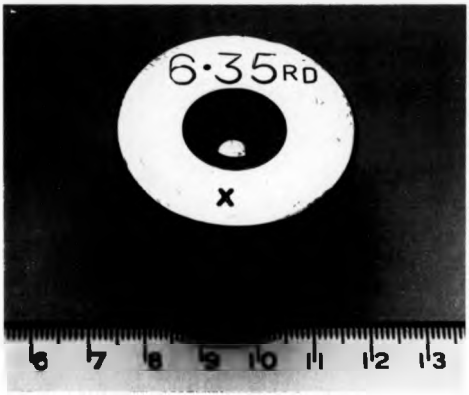

Figure VII.3 The $\alpha'+\beta'$-isolated YAG drawing die shrunk fit in its support case

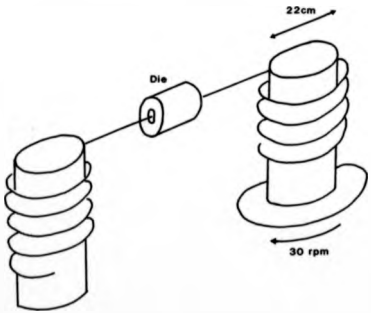

Figure VII.4 Configuration of the brass rod drawing operation

Fig. VII.5 Results from the Brass Drawing Trials

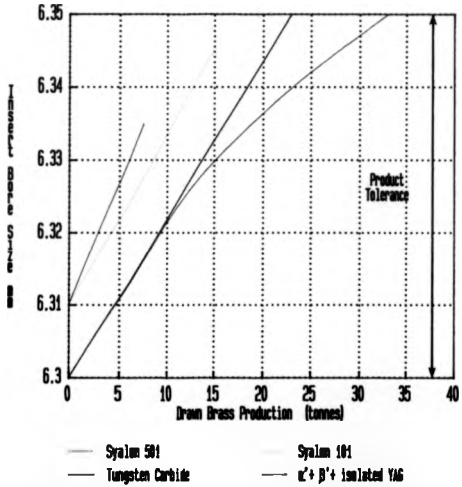

pull of typically 153 coils, 23 tonnes of feed stock material. The α'+β' material exhibited a different wear pattern to the other materials; more parabolic rather than linear. In the early stages material erosion was higher but this became relaxed and the die went on to allow a pull of 220 coils, 33 tonnes of stock before becoming over tolerance, representing an improvement of 43% over the conventional carbide dies. The surface finish was reported as very good from the beginning to the end of the run.

Delta Rods are currently carrying out further trials to substantiate the advantages of the material and to examine the possibility of faster pull rates.

1.4 Other Applications

Additional work is currently being undertaken to explore the use of the α'+β' material in other high wear applications. These include trials with shot blast nozzles for directing high pressure jets of Al_2O_3 grit for metal surface cleaning purposes. Initial tests have been described as encouraging although the improvements have yet to be quantified. Other areas of interest include tools for forming car engine valves and tappet shims via metal pressing, forging or stamping operations, and as material for replacement valves and tappet discs themselves for use in high performance vehicle engines. Components are also being tested for increased wear and corrosion resistance in the preparation of Nickel-Cadmium household batteries.

2. Overall Performance

In all of the field trials the new α'+β'+isolated YAG material performed at least as well as the conventional Sialon 101 and 201 materials. In many applications the performance demonstrated was

far superior. In environments involving exposure to highly erosive wear mechanisms the incorporation of this new material was particularly effective. The increase in hardness afforded by the inclusion of the α'-sialon species was primarily responsible for the improvements rather than an increase in mechanical strength. The reduction in residual phase volume was believed to have a minor effect on the material's strength and hardness properties but in operations at elevated temperatures this reduction was envisaged to be particularly beneficial. Unfortunately, it was not possible, within the scope of this research to fully examine this formulation by testing the material in more appropriate applications such as in gas turbine engines.

CHAPTER VIII. OVERVIEW

A good understanding of the phase relationships which occur within a particular system and a knowledge of how the reaction chemistry may be controlled or manipulated to obtain a desired or idealised microstructure has allowed improved materials, with enhanced properties, to be developed for use in more demanding environments. Materials in the M-Si-Al-O-N systems are fairly well advanced but they are expensive and their use is limited at extreme temperatures because they retain residues from the processes involved in their formulation. This research work illustrates a method of producing cheaper sialon materials and demonstrates a mechanism for incorporating the majority of the densification additives into the bulk microstructure of the product and modifying the remainder to generate materials with improved high temperature characteristics.

The main conclusions of this work are that:

1. Nd_2O_3, which is currently less than one fifth of the price of Y_2O_3, may be substituted for the latter in the preparation of β'+glass sialon materials provided that special care is taken to prevent hydrolysis of the raw Nd_2O_3 powder during preparation. These neodymium-based materials exhibit similar mechanical properties to their Yttrium counterparts.

2. The absence of a phase equivalent to YAG in the Nd-Si-Al-O-N system complicates the formation of materials in which the residual glass may be fully recrystallised to generate a ceramic for use at elevated temperatures. By careful control

of the starting composition it is possible to achieve a glass which can be devitrified to give a mixture of $NdAlO_3$+NdN-α wollastonite to generate a material with high temperature mechanical properties comparable to those of the conventional β+YAG sialons. The eutectic temperatures in the Nd-Si-Al-O-N system are typically 30-50°C lower than for the corresponding yttrium variants, hence the Nd versions of materials of equivalent composition generally exhibit slightly inferior creep and oxidation properties at elevated temperatures.

3. The glass forming region in the Nd-Si-Al-O-N system is far more extensive than in the yttrium system. Nd-sialon glasses can accommodate up to 30 equiv. % nitrogen compared with ~20 equiv. % for yttrium. A number of new Nd-phases, with no synonym in the yttrium system, have been identified within this expanded glass region and these offer potential as alternative devitrification products upon annealing. In particular a β' sialon material has been prepared with a crystalline matrix of composition $Nd_3Si_3Al_3O_{12}N_2$. The glass devitrifies at constant composition and undergoes full recrystallisation. This new sialon material is stable upto the melting or decomposition temperature of this new phase (~1325°C) and the phase reforms if the temperature is lowered sufficiently slowly. Up to approximately 1250°C this new material exhibits similar property characteristics to the conventional β'+YAG materials.

4. The preparation of pure α' and α'+β' sialon materials is extremely composition sensitive. α'+β' materials which

contain a very minor amount of residual glass can be prepared much more easily. By control of the starting composition this small volume of glass may be devitrified to form mainly YAG. Upon annealing, the α' species is particularly receptive to the non-stoichiometric elements which results in increased solid/solid contact following absorption. To alleviate the interfacial energy anisotropy the YAG crystals are transformed by diffusive rearrangment to an isolated equiaxed granular morphology.

5. The reduction in secondary phase volume and subsequent removal of residual grain boundary glass and YAG crystal segregation gives this material substantially improved high temperature properties. The diffusion controlled mechanisms of oxidation and creep degradation are diminished due to a high diffusion coefficient resulting from the lack of an easy transport path.

6. The increase in hardness afforded by inclusion of the α' species allows demonstrable improvements in wear resistance.

The improvements which have been demonstrated with this new range of materials are illustrated in Figure VIII.1. Clearly the materials developed in this work have gained some ground in extending the existing range towards the ceramic development objective outlined in the 1970's (see section II.8 and Figure II.19).

Over the past few months component field trials have been carried out which highlight the advantages of having a harder sialon

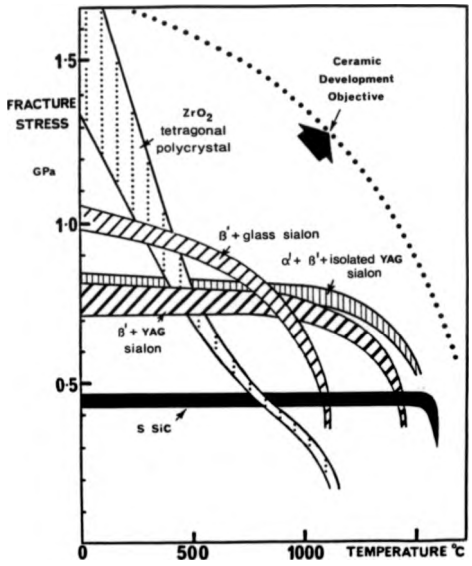

Figure VIII.1 The ceramic development objectives outlined in the 1970's illustrating how the $\alpha'+\beta'+$isolated YAG material pushes the limitations nearer to the development goals

material with a much reduced and modified residual phase volume. This has led to higher productivity and expansion of sialon sales into areas otherwise untapped by ceramic materials. The α'+β'+insolated YAG materials developed in the present work have exhibited such significant improvements in performance to warrant worldwide protection and this new generic range of sialon materials is currently subject to British Patent Application No. GB 8809052.7 (1989). The particular grade of material developed within this research programme is now being marketed by Vesuvius Zyalons Midlands Ltd. (formerly Lucas Cookson Syalon Ltd.) as Syalon CM 200. Increased efforts are being undertaken to optimise the operating conditions for this new sialon material, to understand its behaviour and maximise its performance in specific applications, with the ultimate aim of fully realising its potential within the market place.

REFERENCES

ASM Engineered Materials Reference Book, ASM International, Ohio ISBN 0-87170-350-5

Babini, G.N., Bellosi A., and Vincenzini P., 1984, J. Mat. Sci. 19, 3487.

Bondar, I.A., and Galakhov, F., Ya., 1963, Izv. Akad. Nauk. SSSR, Ser. Khim, 7, 1325.

British Standards Institution, 1989, BS 1902, Section 3.8: ISO, 5017, 1988, Methods of Testing Refractory Materials, Part 3, General and Textural Properties.

Brown, F.W. Jr., and Srawley, J.E., 1966, ASTM STP, 410, 12-14.

Brook, R.J., Carruthers, T.G., Bowen, L.J. and Weston, R.J., 1977, 'Nitrogen Ceramics', (Ed. Riley, F.L.) Pub. Noordhoff, (Leyden), 383.

Buang, K.B., 1979, PhD Thesis, University of Newcastle-upon-Tyne.

Coble, R.L., 1963, J. Appl. Phys. 34, 1678.

Coble, R.L., 1970, J. Appl. Phys. 41, 4798.

Colquhoun, I., Thompson, D.P., Wilson, W.I., Grievesson, P., and Jack, K.H., 1973, Proc. Brit. Ceram. Soc. 22, 181.

Deeley, G.G., Herbert, J.M., and Moore, N.C., 1961, Powder Met. 8, 145.

Dodsworth, J., 1980, PhD Thesis, University of Newcastle-upon-Tyne.

Drew, R.A.L., 1980, PhD Thesis, University of Newcastle-upon-Tyne.

Drew, P., and Lewis, M.H., 1974, J. Mat. Sci. 9, 1833.

Faber, K.T. and Evans, A.G., 1983, Acta. Metall. 31, 565.

Faber, K.T. and Evans, A.G., 1984, J. Am. Ceram. Soc. 67, 225.

Fernie, J.A., 1990, PhD Thesis, University of Wrawick.

Fernie, J.A., and Leng-Ward, G., 1989, Personal Communication.

Fernie, J.A., Lewis, M.H., and Leng-Ward, G., 1990, to be published in J. Mat. Sci. Lett.

Funke, V.F., and Samsonov, G.V., 1958, Zhur. Obshch. Khim., 28 (90), 267.

Gaukler, L.J., Hohnke, H., and Tien, T.Y., 1980, J. Amer. Ceram. Soc. 63, 35.

Gaukler, L.J., Lukas, H.L., and Petzow, G., 1975, J. Amer. Ceram. Soc. 58, 346.

Gazza, G.E., 1975, Bull. Amer. Ceram. Soc. 54, 778.

Grand, G., Demit, J., Rust, J., and Torre, J.P., 1979, J. Mat. Sci. Letters 14, 1749.

Hampshire, S., 1980, PhD Thesis, University of Newcastle-upon-Tyne.

Hampshire, S., Park, H.K., Thompson, D.P., and Jack, K.H., 1978, Nature 274, 880.

Hardie, D., and Jack, K.H., 1957, Nature 180, 332.

Hohnke, H., and Tien, T.Y., 1983, Progress in Nitrogen Ceramics (Ed. Riley, F.L.) Pub. Nijhoff, N., 101.

Huseby, I.C., and Petzow, G., 1974, Powder Met. 6, 17.

Ito, J. and Johnson, H., 1968, Amer. Min. 53, 1940.

Jack, K.H., 1973, Trans. J. Brit. Ceram. Soc. 72, 376.

Jack, K.H., 1976, J. Mat. Sci. 11, 1135.

Jack, K.H., 1978, 'Phase Diagrams', Mat. Sci. & Tech. 4, (Ed. Alper, A.M.), publ. Academic Press, 241.

Jack, K.H., 1981, Science of Ceramics, 11, 125.

Jack, K.H., 1983, 'Progress in Nitrogen Ceramics', (Ed. Riley, F.L.), pub. Nijhoff (Hague), 45.

Jack, K.H., and Wilson, W.I., 1972, Nature 238, 28-29.

Jama, S.A.B., Thompson, D.P., and Jack, K.H., 1975, Proc. Brit. Ceram. Soc. 'Special Ceramics 6', (Ed. Popper, P.), 299.

Jameel, N.S., 1984, PhD Thesis, University of Newcastle-upon-Tyne.

Janecke, E., 1907, Z. Anorg. Chem. 53, 319.

JCPDS, 1975, Joint Committee of Powder Diffraction Standards, Pub. International Centre for Diffraction Data, Pennsylvania, USA.

Kato, K., Inowe, Z., Kijima, K., Kawada, H., and Yamane, T., 1975, J. Amer. Ceram. Soc. 58, 90.

Kingery, W.D., 1959, J. Appl. Phys. 30, 301.

Kingery, W.D., Bowen, H.K. and Uhlmann, D.R., 1960, 'Introduction to Ceramics', Wiley, 704.

Kohatsu, I., and McCauley, J.W., 1974, Mater. Res. Bull. 9, 917.

Korgul, P., Hendry, A., and Thompson, D.P., 1983, 'Progress in Nitrogen Ceramics', (Ed. Riley, F.L.) Pub. Nijhoff, 375.

Lange, F.F., Singhal, S.C. and Kuznicki, R.C., 1977, J. Amer. Ceram. Soc. 60, 249.

Layden, G.K., 1976, 'Process development for pressureless sintering of sialon ceramic components', Final Report, Naval Air Systems Command, Contract N 00019-75-C-0232.

Lenel, F.V., 1948, Trans. Amer. Inst. Min. Engrs., 175, 878.

Lewis, M.H., 1987, New Materials and their Applications, (Ed. Burnay, S.G.), pub. IOP., 41-51.

Lewis, M.H. and Bernard, P., 1980, J. Mat. Sci., 15, 443.

Lewis, M.H., Bhatti, A.R., Lumby, R.J., and North, B., 1980, J. Mat. Sci. 15, 103.

Lewis, M.H., Leng-Ward, G., and Jasper, C., 1988, Sintering additive chemistry in controlling microstructure and properties of nitride ceramics, in Messing, Fuller and Hausner (eds.), Ceramic Transactions I, Amer. Ceram. Soc. Inc., 1019-1033.

Lewis, M.H., and Lumby, R.J., 1983, Powder Met. 26, No. 2., 73

Liddell, K., 1986, Private communications reported in Walls, P.A., 1986, PhD Thesis, and Slasor, S., 1989, PhD Thesis.

Liddell, K., 1987, Internal progress report, Wolfson Laboratory for High Strength Materials, University of Newcastle-upon-Tyne.

Liddell, K. and Thompson, D.P., 1986, Br. Ceram. Trans. J. 85, 17.

Lumby, R.J., and Coe, R.F., 1970, Proc. Brit. Ceram. Soc. 15, 91.

Lumby, R.J., North, B. and Taylor, A.J., 1975, 'Special Ceramics 6', (Ed. Popper, P.), 283.

Marchand, R., 1976, C.R. Acad. Sci., Paris, 282, Ser. C. 329-331.

Morgan, P.E.D., and Carroll, P.J., 1977, Mat. Res. Bull. 12, 251.

Mitomo, M., Moriyoshi, Y., Sakai, T., Onzaka, T., and Kobayashi, M., 1982a: J. Mat. Sci. 1, 25-26.

Mitomo, M., Moriyoshi, Y., and Suzuki, J., 1982b: Proceedings of the 5th CIMTEC Symposium, June 1982, Pub. Elsevier Science Publishers, Netherlands.

Oyama, Y. and Kamigaito, O, 1971, Jap. J. App. Phys. 10, 1637.

Price, G.H.S., Smithells, C.J., and Williams, S.V., 1938, J. Inst. Metals, 6, 239.

Rae, A.W.J.M., 1976, PhD Thesis, University of Newcastle-upon-Tyne.

Rae, A.W.J.M., Thompson, D.P., Pipkin, N.J., and Jack, K.H., 1975, 'Special Ceramics 6', (Ed. Popper, P.), 347.

Ramsdell, L.S., 1947, Amer. Min. 32, 64.

Roebuck, P.H.A.R., 1978, PhD Thesis, University of Newcastle-upon-Tyne.

Roebuck, P.H.A.R., and Thompson, D.P., 1977, 'High Temperature Chemistry of Inorganic and Ceramic Materials', (Ed. Glasser, E.P. and Potter, P.E.), The Chemical Soc., London, 222.

Slasor, S., 1985, Internal Report, Wolfson Laboratory for High Strength Materials, University of Newcastle-upon-Tyne.

Slasor, S., 1988, PhD Thesis, University of Newcastle-upon-Tyne.

Spacie, C.J., 1984, PhD Thesis, University of Newcastle-upon-Tyne.

Spacie, C.J., Liddell, K., and Thompson, D.P., 1985, J. Mat. Sci. Letters, 7, 95.

Srinavasan, M., and Seshadri, S.G., 1981, 'Fracture Mechanical Methods for Ceramics Rock and Concrete', ASTM, 745, (Eds. Freeman, S.W., and Fuller, E.R.), Amer. Soc. for Testing Materials, 46.

Sun, W.Y., Oli, Xiaqtin, Litai, M.A., and Yen, T.S., 1988, Translation: 'Solubility of Si in YAG', Microstructure and Properties of Ceramic Materials, Proc. of 1st China-US Bilateral Seminar on Inorganic Materials Research, held at Shanghai, 17-21 May 1983, (Ed. Yen, T.S., and Pask, J.A.), Beijing Science Press, 1984, 501.

Sun, W.Y., Walls, P.A., and Thompson, D.P., 1985, 'Non-Oxide Technical and Engineering Ceramics', (Ed. Hampshire, S.) pub. Elsevier, 105-117.

Tanaka, H., Hasegawa, Y., and Inomata, Y., 1979, Proc. Int. Symp. on Factors in Densification and Sintering of Oxide and Non-Oxide Ceramics (Eds. Somiya, S. and Saito, S.) Japan, 458.

Terwilliger, G.R., and Lange, F.F., 1974, J. Am. Ceram. Soc. 22, 197.

Thompson, D.P., 1977, J. Mat. Sci., 12, 2344.

Toropov, N.A., 1960a, Trans. Intern. Ceram. Congr. 7th, London, 440.

Toropov, N.A., 1960b, Trans. Intern. Ceram. Congr. 7th, London, 438.

Toropov, N.A., Bondar, I.A., Galakhov, F., Ya, Nikogosyan, K.S., and Vinogradova, N.V., 1964, Izv. Akad. Nauk. SSSR, Ser. Khim. No. 7, 1162.

Toropov, N.A., and Kisseleva, T.P., 1961, Zh. Neorgan. Khim. 6, No. 10, 2353, Russ. J. Inorg. Chem. (English Transl.), 1193.

Tsuge, A., Nishida, K., and Komatsu, M., 1975, J. Am. Ceram. Soc. 58, 323.

U.K. Patent Application, 1983, No. GB 2118927A, Kennametal Inc.

U.K. Patent Application, 1989, No. GB 8809052.7, Vesuvius Zyalons Midlands Ltd.

Walls, P.A., 1986, PhD Thesis, University of Newcastle-upon-Tyne.

Walls, P.A., and Slasor, S., 1984, Internal Report, Wolfson Laboratory for High Strength Materials, University of Newcastle-upon-Tyne (Reported in Walls, P.A., 1986, PhD Thesis).

Wild, S., Grieveson, P. and Jack, K.H., 1972a, 'Special Ceramics 5', (Ed. Popper, P.), Brit. Ceram. Res. Assn. (Stoke on Trent), 289.

Wild, S., Grieveson, P., Jack, K.H., and Latimer, M.J., 1972b, 'Special Ceramics 5', (Ed. Popper, P.), Brit. Ceram. Res. Assn. (Stoke on Trent), 377.

Zernicke, J., 1955, 'Chemical Phase Theory', Kluwer Publ. Co. Ltd. (Deventer, Netherlands).